The Role of Salt Tectonics in the Hydrocarbon Potential of the Post-Salt Deposits (Albian to Recent), Offshore Gabon

Marvel M.H. Makhubele

Supervisors:

Dr. Emese Bordy (University of Cape Town, South Africa)

Dr. Alexei Milkov (SASOL Petroleum International, South Africa)

Duncan Barkwith (SASOL Petroleum International, London)

2014

A thesis submitted in partial fulfilment of the requirements for the degree of **Master of Science** (Petroleum Geoscience Programme) in the Department of Earth Sciences, University of the Western Cape, South Africa

PLAGIARISM DECLARATION

1. I know that plagiarism is wrong. Plagiarism is using another's work and to pretend that it is one's own.

2. I have used the Harvard referencing style as the convention for citation and referencing. Each significant contribution to, and quotation in this thesis from the work, or works of other people has been attributed and has cited and referenced.

3. I have not allowed, and will not allow, anyone to copy my work with the intention of passing it off as his or her own work.

4. I acknowledge that copying someone else's work or parts of it is wrong, and declare that this is my own work.

SIGNATURE: ____  _____

DATE: __01/04/14_____

ABSTRACT

Following successful discovery and production of hydrocarbons, Gabon is one of the key hydrocarbon target countries in Africa. Located in the Lower Congo Basin, the study area is based in Etame Marin Permit (EMP), which is licensed to VAALCO Energy Inc., and has been producing hydrocarbons since 2002. The currently explored and producing reservoirs are in the pre-salt sandstones of the Aptian Gamba Formation, charged with hydrocarbons sourced from the syn-rift lacustrine shale of the pre-Aptian Melania Formation. With the aim of finding potential petroleum plays in the post-salt successions and by using 3D prestack depth migration (PSDM) seismic sections and wireline logs, a detailed study of the post-Aptian stratigraphy and salt tectonics of the EMP was undertaken. Eight distinct reflectors were identified based on gamma ray signatures, stratal terminations and isopach trends. Sediment distribution patterns and the relative sea level history of the succession were determined by applying principles of sequence stratigraphy and salt tectonics. Furthermore, two potential plays have been outlined in the post-salt carbonates of the Albian Madiela Formation as well as in sandstones of the Turonian Azile Formation. These reservoirs might have been charged with hydrocarbons from the pre-salt shale of the Melania Formation and/or potentially also enriched from the Albian and Cenomanian shales. For these post-salt hydrocarbon reservoirs to be charged by the pre-salt source rocks, windows within the extensive evaporitic sealing of the Aptian Ezanga Formation were required. 3D PSDM seismic sections attest that diapirism of the Aptian salt unit generated ample hydrocarbon migration pathways from the pre-salt source rocks to post-salt reservoirs. Five well-developed potential salt windows have been identified, two of which have good probability to have facilitated the upward migration of hydrocarbons, because these salt windows are located up dip of oil producing wells. However, even if hydrocarbons are found in the post-salt reservoirs, similarly to the Yombo Field (located offshore Congo, south of the EMP), these shallow reservoirs in the EMP are likely to produce heavy oils due to biodegradation.

ACKNOWLEDGEMENTS

First and foremost, I would like to thank my sponsors, SASOL Petroleum International (SPI), for the funding and also providing all dataset that made this work possible. My sincere gratitude to all the staff who gave me a helping hand while working at SPI over the December holidays. I would also like to thank Inkaba ye Africa, for the extra funding, which they provided to aid to my studies.

A huge thank you to my supervisors at SPI: Dr. Alexei Milkov, Mr Tahir Chaudhry and Mr Duncan Barkwith for all their guidance, wisdom and input in this thesis; it was well received, appreciated and I learnt a lot from you guys. I would like to thank Ms Donna Boyd for all her help in this work, and for being my "consultant". I would also like to thank Prof. Jan Van Bever Donker and Prof. Martin Jackson for all their academic assistance as well. My sincere gratitude to both Beth and Richards Kahle, who took some time out of their busy schedule to read my thesis.

An enormous thank you to my mother, sister, nephew, brothers and friends for being patient with me throughout the time I was working on this thesis; thank you so much for being my inspiration, for always believing in me and for your understanding, while I constantly moan about my thesis. A gigantic thank you to my good friend and ex-supervisor Prof. "Uncle" Dave Reid; your faith in me, and your encouragement is what kept me going throughout my studies, and thank you for building a solid foundation in me, which I will always use in life. I really miss our long non-academic talks.

Last but definitely not least, the one person who helped me made this project possible, my supervisor, Dr. Emese Bordy; words cannot begin to describe how grateful I am for you. You have been the pillar of my strength and the reason why I worked so hard in the last 11 months. I have so much love, respect for you, thank you for nurturing me academically, and yet giving me enough space to have my own independence and enabling me to think and write scientifically and produce work I am proud of. Thank you for agreeing to be my supervisor and for believing in me so much. I wish you all the success in life and good health for your family. Kea leboga (THANK YOU).

In loving memory of my baby brother Thabelo Funani Makhubele

Table of Contents

1 INTRODUCTION AND BACKGROUND

1.1 Introduction

Hydrocarbon exploration activities in Gabon started in the mid 1920's following the discovery of oil seeps onshore. This led to more exploration, resulting in the discovery of the onshore Ozouri Field, which started production in 1956. More discoveries were made in the pre-salt Ikassa Kongo-2B well, which was drilled in 1959 in southern Gabon. The discovery of a giant Anguille Marin oil field in 1962 made Gabon one of the hydrocarbon "hot spot" areas, grabbing the attention of large oil companies such as Shell, which started to explore the country in 1963. Since this discovery more companies have explored Gabon in search of hydrocarbons, and in recent years with improving technology, explorations and discovery have not only been onshore but moved offshore in deep waters as well. (C and C Reservoir reports, 2006)

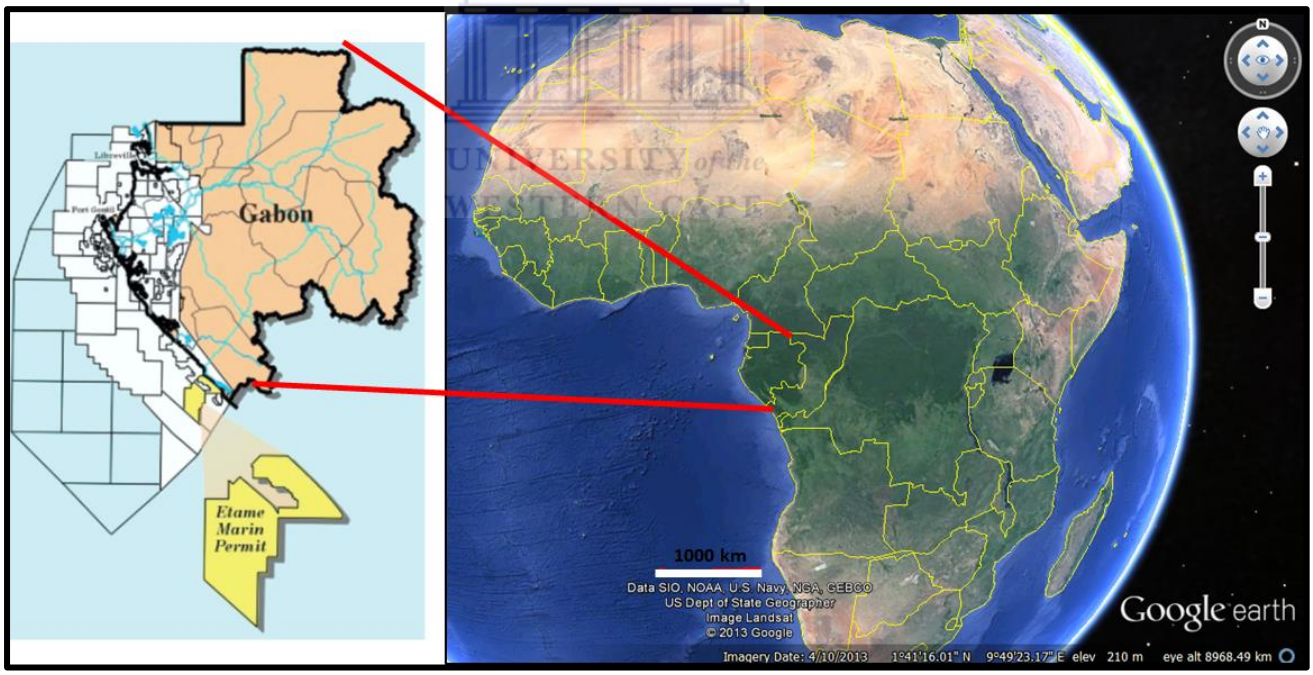

Figure 1.1: Geographical location of the EMP offshore Gabon (modified after Gill and Cameron, 2002; 2013 Google Earth Image).

Located at the northern part of the Lower Congo Basin, our study area is from the 3074 km^2 EMP (Figure 1.1), which has been licensed to VAALCO Gabon (Etame) Incorporated (28.073750%) since 1995 (Gill and Cameron, 2002). The licence is shared with the following key partners: Sasol Petroleum Etame Limited (27.75%), Addax Petroleum Etame

Incorporated (32.5%), Sojitz Etame Limited (2.983125%), PetroEnergy Resource (2.335625%) and Tullow Oil Gabon S.A (7.5%). Initial hydrocarbon discovery in the EMP was made in 1998 with the first oil production in September 2002 (Gerry, 2012). The Lower Congo and surrounding basins were formed in the Early Cretaceous, during the break-up of Gondwana, when South America and Africa began to rift-apart (Rasmussen, 1996; Hudec and Jackson, 2004; Dupre *et al.*, 2007; Jackson *et al.*, 2008; Beglinger *et al.*, 2012). The sedimentary record in offshore Gabon comprises the Lower Cretaceous syn-rift and Upper Cretaceous post-rift successions, separated by an Upper Aptian salt formation (Figure 1.2) (Gill and Cameron, 2002). Oil produced in the EMP is sourced from the Barremian shales of the Melania Formation and the main reservoirs are the sandstones of the Barremian Dentale Formation and the Aptian Gamba Formation. In the other oil fields in Gabon, reservoirs are the older sands of the Melania and Lucina Formations (Gill and Cameron, 2002). Both the source and the reservoir rocks are overlain by the extensive and thick Aptian salt deposits of the Ezanga Formation (Figure 1.3) (Gill and Cameron, 2002). These Aptian evaporites, with their extensive lateral and vertical dimensions, act as both seal and trap for hydrocarbon, restricting the hydrocarbon migration and sealing them in the pre-salt reservoirs (Gill and Cameron, 2002).

Post-depositional salt movement in the study area was primarily triggered by the burial effect of the Upper Cretaceous and Tertiary clastic sequences (Gill and Cameron, 2002; Beglinger *et al.*, 2012). Due to the movement of the salt, the latter successions have also been dragged basinwards in a down-slope gravitational mass movement process, and these might have created traps in the overlying sediments (Figure 1.2) (Beglinger *et al.*, 2012). For example, Gill and Cameron (2002) showed that the Albian carbonates Madiela Formation (Figure 1.2 and 1.3) and the overburden sediments have a rapid lateral variation in thickness which reflects the complexity of the gravitational mass movement processes and the resulting stratigraphic architecture in this area.

1.2 Objectives

Through detailed seismic and sequence stratigraphy, tectonics and salt tectonics studies, this thesis investigates a potential working post-salt petroleum system in Etame Marin Permit (EPM) in order to identify potential post-salt petroleum plays. Since pre-salt source rocks could have potentially charged these plays, this thesis furthermore investigates the potential windows in the Aptian salt (Ezanga Formation) that could have served as hydrocarbon migration pathways from the pre-salt source rocks to post-salt petroleum reservoirs. If such

windows do exist, at least one test well is recommended to be drilled in structural traps close to the windows and if successful, the focus of hydrocarbon exploration in the EMP can be extended beyond pre-salt sediments.

1.3 Geological Background

Located along the western margin of Africa, in the Pan-African zones of lithospheric weakness, the Mesozoic-Cenozoic Congo Basin formed as a result of rifting in the Barremian (~144 Ma) and subsequent drifting during Late Albian-Cenomanian (~105 Ma) of South America from Africa (Figure 1.2 and 1.3) (Binks and Fairhead, 1992; Dupre *et al.,* 2007; Gill and Cameron, 2002).

The Early Cretaceous rifting phase resulted in (a) crustal extension along the strike-slip and normal faults; (b) the formation of grabens and horsts and (c) deposition of a syn-rift fluvio-lacustrine succession (Binks and Fairhead, 1992; Dupre *et al.,* 2007). The Extension stage is marked by normal faults, which are sub-parallel to the strike of the shoreline (Dupre *et al.,* 2007).

The transition from rifting to drifting was accompanied by a restricted shallow marine environment in the Late Aptian that deposited the evaporites (Gill and Cameron, 2002; Dupre *et al.,* 2007). The onset of the subsequent drifting phase in the Aptian is associated with the opening of the south Central-Atlantic Ocean and formation of the passive continental margin of West Africa (Binks and Fairhead, 1992; Rasmussen, 1996).

The review of the lithostratigraphy and sedimentology of the study area in sections 1.3.1 to 1.3.3 is mainly based on the following references, unless or otherwise stated: Dupre *et al. (*2007); Gill and Cameron (2002) and Beglinger *et al.* (2012).

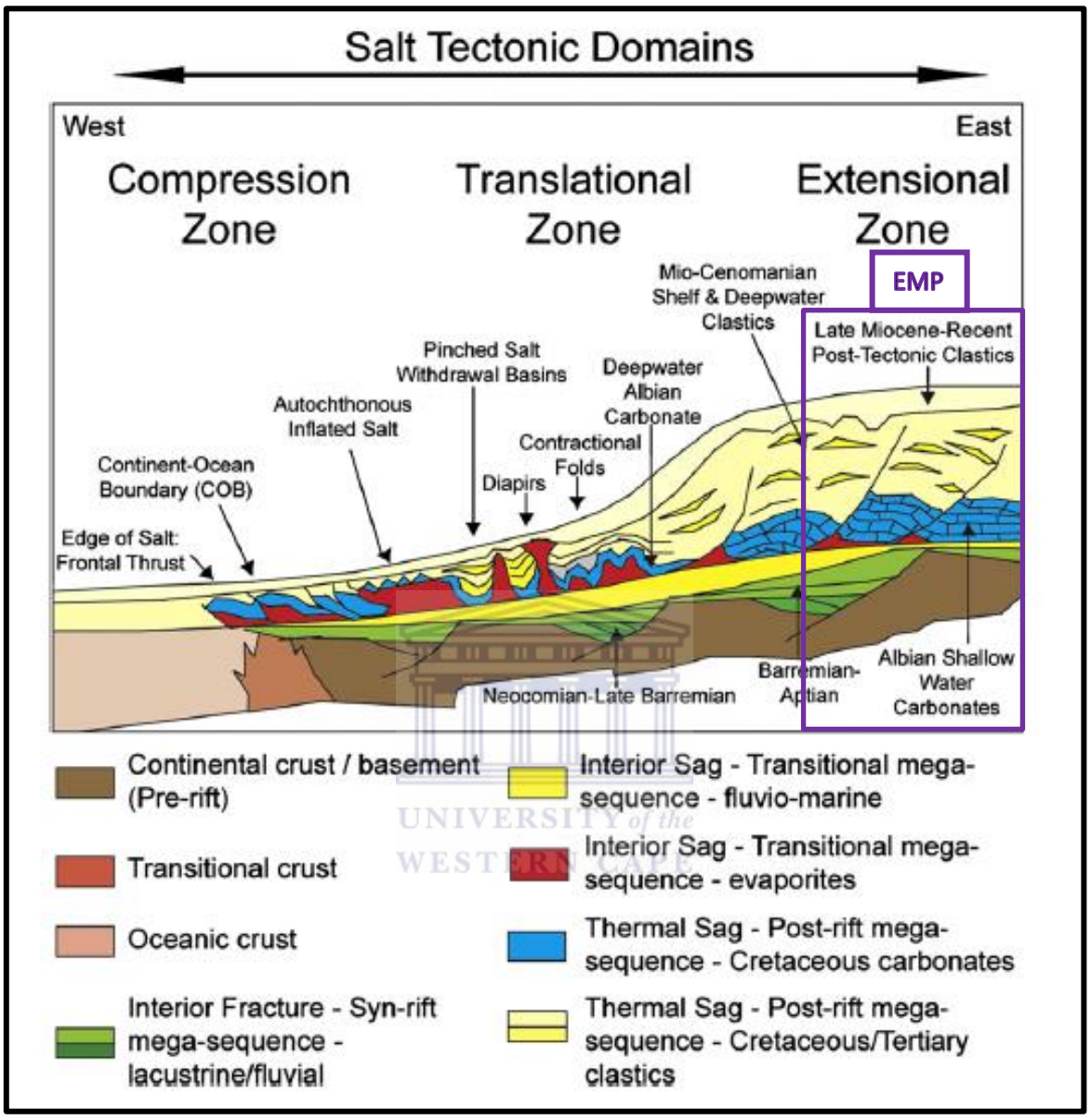

Figure 1.2: The regional geology of the study area offshore Gabon, showing the pre, syn and post-rift succession. (Source: Brownfield and Charpentier, 2006).

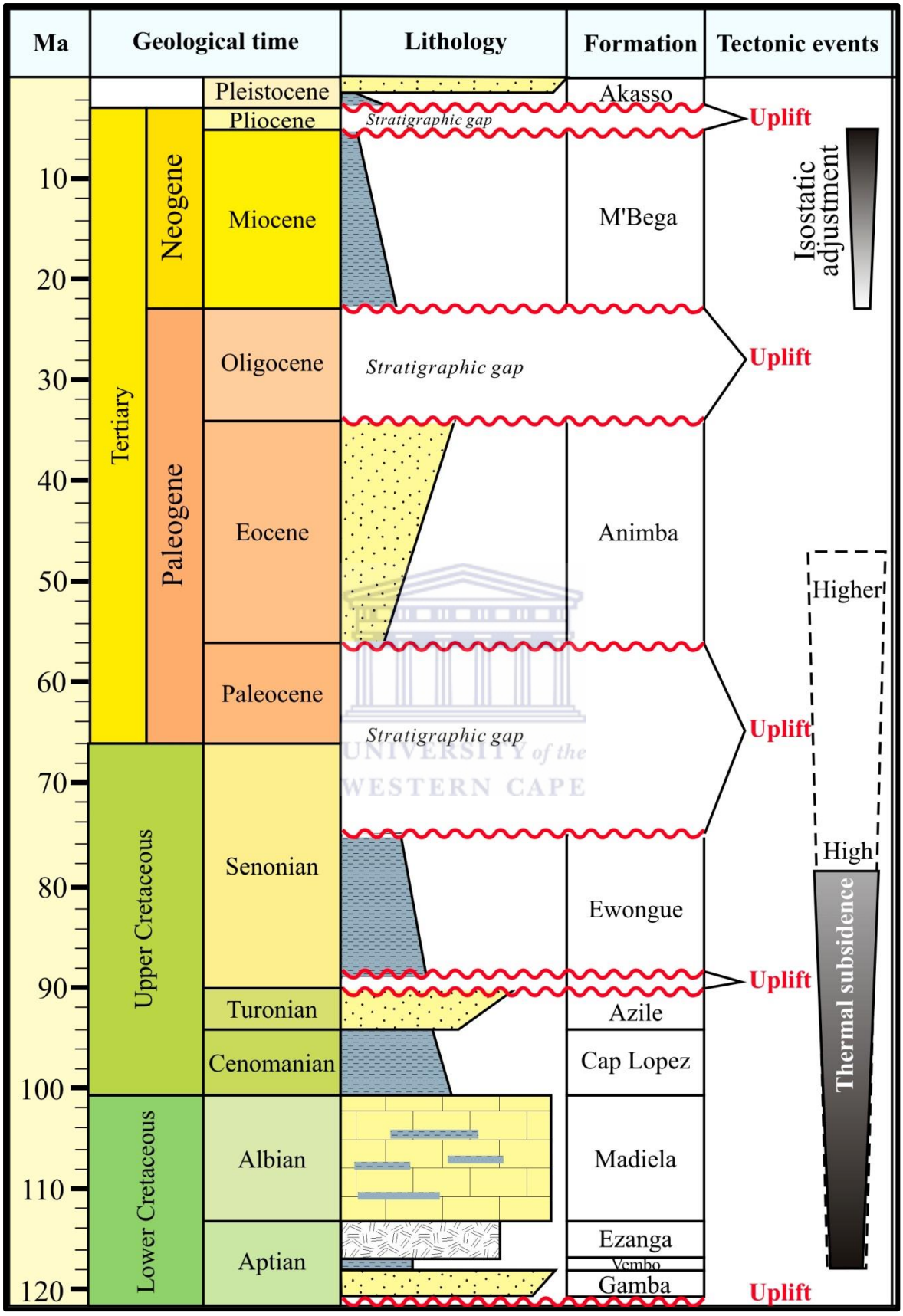

Figure 1.3: Simplified stratigraphic section of the Etame Marin Permit in offshore Gabon, showing the reservoir, source rock, seal and the tectonic evolution of our study area (Modified from Gill and Cameron, 2002).

1.3.1 Pre-Syn rift phase

Pre-rift and syn-rift basin fill geometry and sediments are generally poorly known in the study area, mainly because these successions are overlain by the extensive evaporites of the Ezanga Formation (Figure 1.3) which has strong acoustic impedance, and thus limit the seismic resolution of the older successions.

Pre-rift sediments, which mark the basement, are estimated to have been deposited in alluvial, fluvial and lacustrine environments between the Late Proterozoic to Jurassic. At the time of deposition of pre-rift sediments, subsidence and early extension resulted in the development of a sagging basin which is referred to as the Afro-Brazilian Basin/depression.. The syn-rift sediments include lacustrine turbidites and the organic-rich shales of the Melania Formation followed by fluvio-deltaic sediments (Figure 1.3). With total organic carbon content (TOC) of 5-6%, the lacustrine shales of the Lower Melania Formation are the main source rocks for hydrocarbons in the study area. During the Barremian – the Early Aptian, the rift was further filled by fluvial sandstones and the deltaic to lacustrine shales of the Dentale. In addition, Early Aptian was a period of erosion, which resulted in a regional unconformity that separates the syn-rift from the transitional-drift phase sediments (Figure 1.3).

1.3.2 Transitional to drift phase

The end of the rifting phase was marked by a restricted shallow marine environment in which, during a marine transgression, an unconformity and onlapping Early Aptian siliciclastics of the Gamba sandstone formed (Figure 1.3). During the transgression, at the end of the transitional phase, ~ 500 m of the Ezanga Formation evaporites were also deposited (Figure 1.3). They are commonly referred to as the "Aptian Salt", and their estimated age is ~116-114 Ma (Jackson *et al.*, 2000; Hudec and Jackson, 2004). The salt formation continued into the Early Albian.

Overlying the evaporites are the shallow marine, ramp/platform carbonates of the Madiela Formation (Figure 1.3) which were deposited during the drift phase from Late Aptian to Late Albian, ~114-99 Ma. Dupre *et al.* (2007) interpreted the half grabens with tilted blocks and

wedging units as being bounded by syn-depositional normal faults; because these faults appear to crosscut the platform carbonates and show evidence of faulting during deposition. Furthermore, they also demonstrated that the thin-skinned extension in the carbonates resulted from a syn-sedimentary gravity driven deformation. In the more proximal setting, titled blocks within the Madiela Formation were interpreted by Hudec and Jackson (2004); Dupre *et al.* (2007) as faults blocks which were isolated by extreme extension (i.e., 'pre-rafts').

The Upper Cretaceous clastic succession overlying the Madiela Formation, among others, comprises organic-rich shales (Cap Lopez Formation) (Figure 1.3) which were deposited when sedimentation rate was low under anoxic conditions (potential source rock?). Eventually, with the on-going drift, stable, open marine clastic sedimentation in water depths of 1-2 km was established. The last phase of deposition was during the Oligocene/Miocene to present, which started during the time of the submarine erosion of the ramp. This erosional event, according to Beglinger *et al.* (2012), removed ~500 m of sediments in the outer shelf region. This post-salt succession also contains several well-documented unconformities that are linked to the interplay between local tectonics and global sea level changes (i.e., relative sea level changes) in the region (Figure 1.3).

1.4 EMP petroleum system

1.4.1 Pre-salt stratigraphy

Current hydrocarbon exploration in the EMP is focused on the pre-salt plays due to the proven presence of good petroleum systems (i.e., Gamba sandstone Figures 1.2, 1.3, 1.4, 1.6 and 1.7) (Gill and Cameron, 2002). In the pre-salt succession, the petroleum system contains:

(a) The Melania shale as source rock, which is made up of mainly type I and intermediate type I-II kerogen, with TOC of 5-6%, and according to Martin *et al.* (2009) and Beglinger *et al.* (2012) these source rocks reached maturity and started generating hydrocarbons in Late Cretaceous;

(b) The Gamba and Dentale sandstones as oil-producing reservoirs which have high porosity (20-30%) and permeability (100 md to 5D) (Figures 1.5, 1.6 and 1.4), with hydrocarbons charged into the reservoirs during the Cenomanian (~100 Ma) (Gill and Cameron, 2002; Beglinger *et al.*, 2012) and;

(c) The Ezanga salt is an excellent seal and trap due to its impermeable and very extensive nature (Gill and Cameron, 2002; Beglinger *et al.*, 2012). Furthermore, the highly fractured Dentale sandstones and shales provide a good secondary migration path of the generated hydrocarbons (Figure 1.4) (Gill and Cameron, 2002).

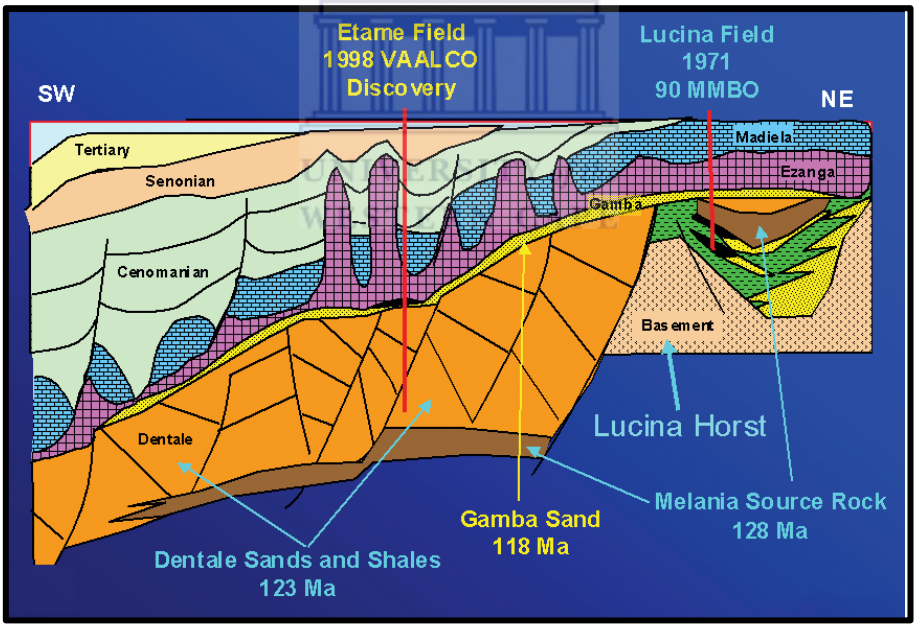

Figure 1.4: Simplified geological cross-section of the EMP, showing the lithologies of the Lower Congo Basin (Source: Gill and Cameron, 2002).

1.4.2 Post-salt stratigraphy

The extensive thickness of the Ezanga salt makes it difficult for hydrocarbons to migrate across the impermeable salt. However, post-salt stratigraphy has potential hydrocarbon plays,

because in certain areas, as the salt flows, it may form diapirs or allochthonous salt, which might detach from the main salt body (Hudec and Jackson, 2004; Dupre *et al.*, 2007). This detachment would create a window, thus allowing communication between the pre-salt and the post-salt sediments and serve as a pathway for hydrocarbons to migrate into the post-salt sediments (Figures 1.5 and 1.6) (Beglinger *et al.*, 2012). The petroleum plays in the post-rift sediments would potentially include: the Melania shale and potentially Upper Cretaceous shales as source rock, with Madiela carbonates and Turonian sands as reservoirs, and seal from Upper Cretaceous shales. The traps would be associated with the reported unconformities as well as faults and other salt tectonic structures.

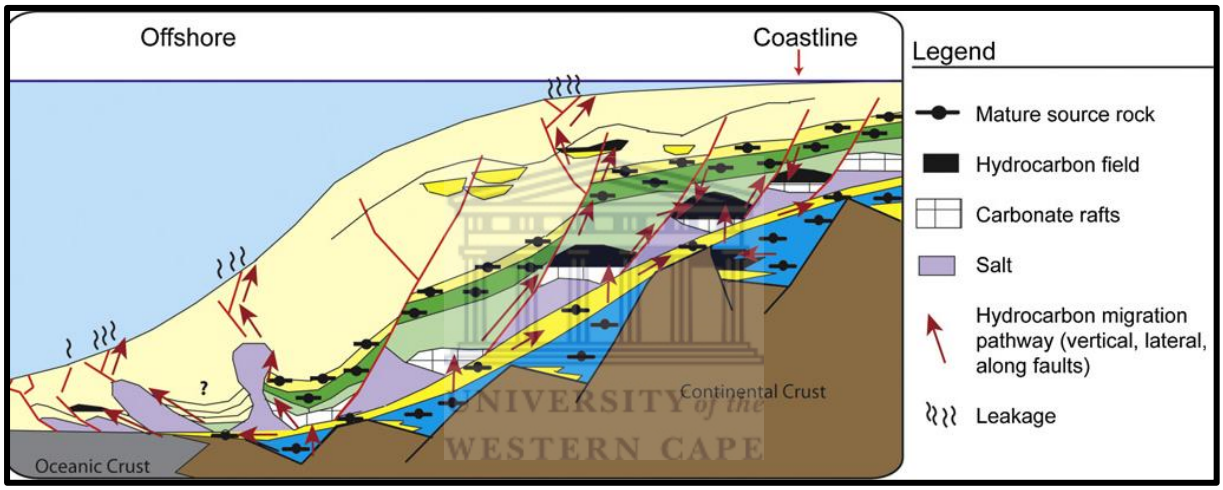

Figure 1.5: Geological cross-section from offshore West African margin. This model was adopted from Huc (2004), showing that there can be a window in the salt to let the hydrocarbons to migrate from the pre-salt to post-salt sediments (Source: Beglinger *et al.*, 2012).

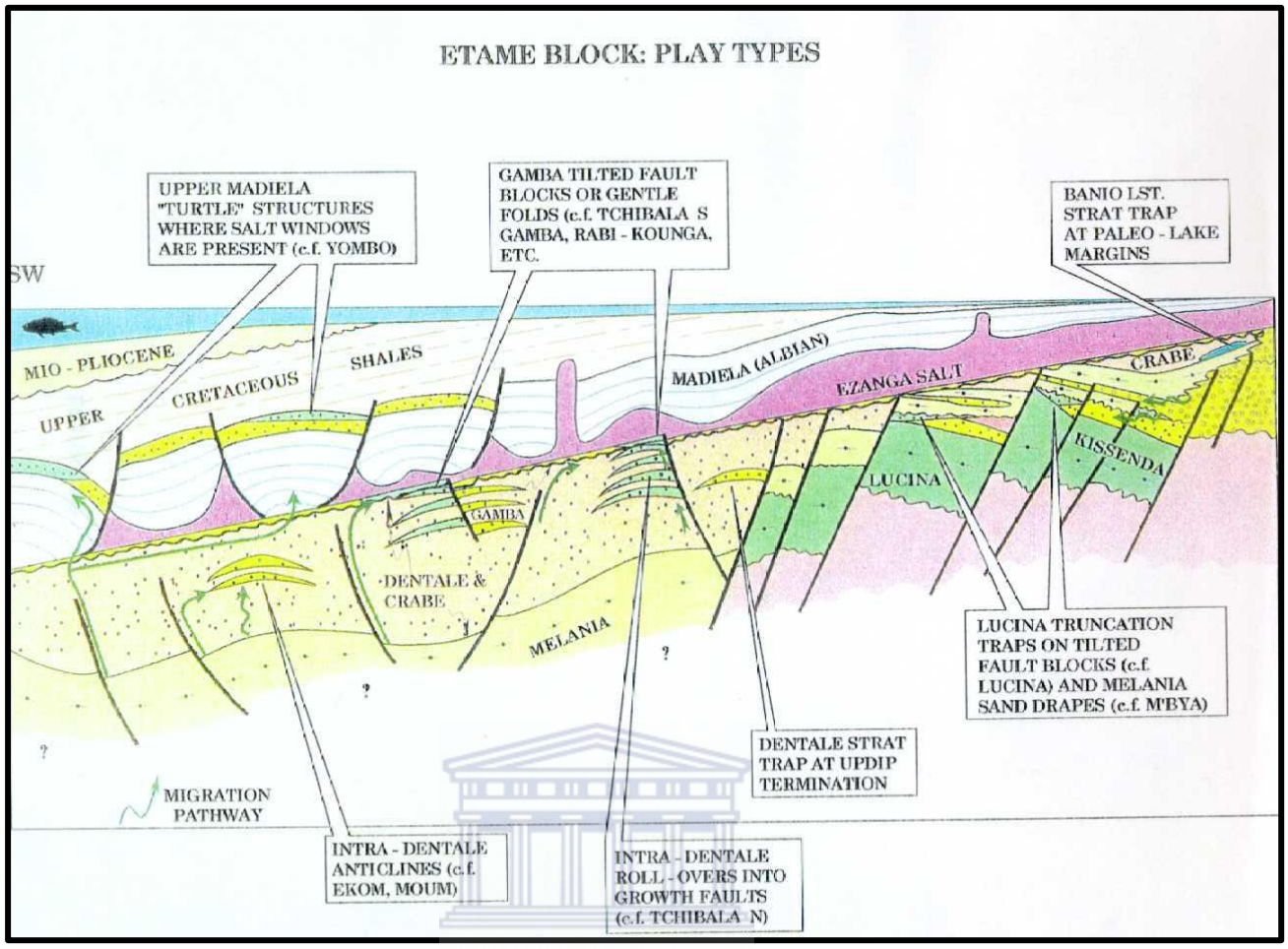

Figure 1.6: Petroleum play type in the EMP, also showing potential migration pathways from pre-salt to post salt deposits. (Source: Vaalco Energy reports, 2005).

Figure 1.6 shows the potential post-salt plays in the EMP, although there are no post-salt producing fields in the EMP at the moment. The Yombo Field which is located offshore the Republic of Congo in Marine I exploration Block, in the Lower Congo Basin, south of the EMP, is currently producing hydrocarbons from post-salt sediments (Figure 1.7) (Van Horn, 2001). According to Van Horn (2001), and as shown in Figure 1.7, the producing reservoirs in the Yombo field are the Cenomanian-age Tchaka Formation and the Albian-age Sendji Formation. In 2001, the estimated averaged production from the Yombo field was 16,000 barrels per day (b/d) (Van Horn, 2001). The producing reservoirs in the Yombo field have calculated recoveries greater than 100 million b/o (barrels of oil) and are very shallow, less than 200 m in depth (Van Horn, 2001). This field is evidence of a working potential post-salt petroleum system in the Lower Congo Basin.

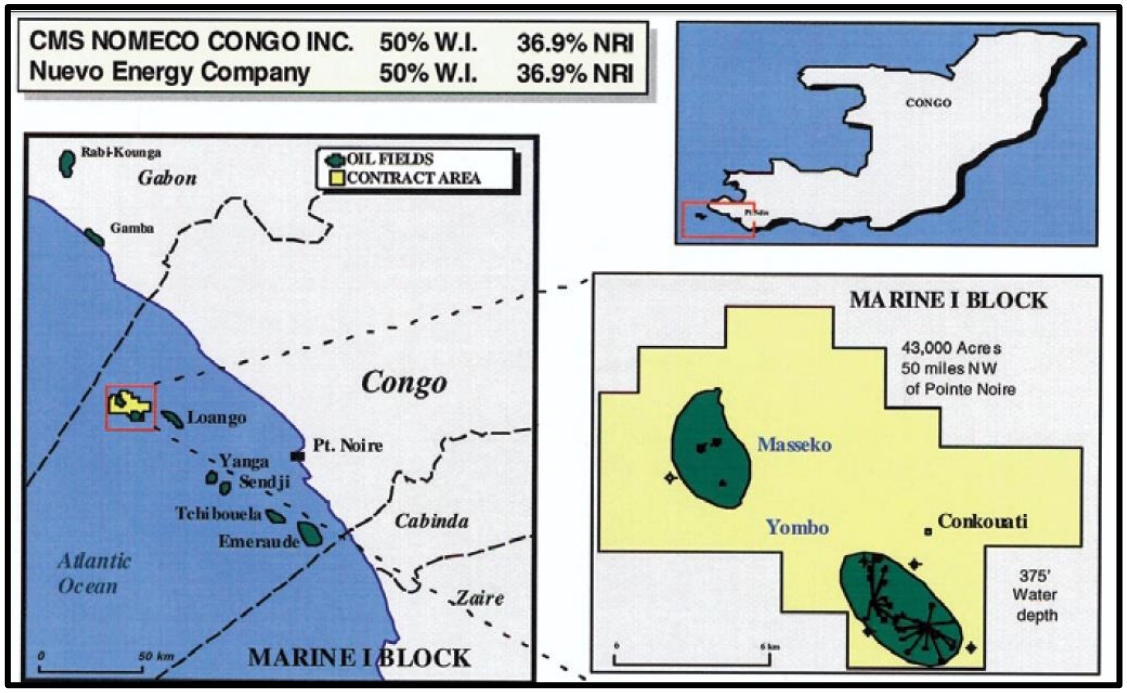

Figure 1.7: Location of the Yombo field which produces oil from the Cenomanian-age Tchaka Formation and the Albian-age Sendji Formation (Source: Van Horn, 2001).

2 EVAPORITES AND SALT TECTONICS

2.1 Evaporites

Common evaporites are gypsum ($CaSO_4 \cdot 2H_2O$), anhydrite ($CaSO_4$) and halite ($NaCl$); which form as precipitates from evaporating water bodies with high concentration of salt minerals in areas of high evaporation and limited precipitation, in marine or lacustrine environments (Reading, 1996, p. 283; Hudec and Jackson, 2007). Modern day examples of areas of active evaporite precipitation are the Dead Sea and the Great Salt Lake in Utah (Tucker, 2001, p. 166). Characteristically, lacustrine evaporites occur in association with deposits of inland sabkhas and saline mudflats (Tucker, 2001, p. 169). Most of the significant evaporites in the geological record are however marine in origin and were deposited during

the Phanerozoic (Reading, 1996, p. 281 and Hudec and Jackson, 2007). The distribution of known evaporites is shown in Figure 2.1, which also illustrates some of the largest salt deposits (e.g., the Messinian Mediterranean Evaporites: 2400 × 600 km – Reading, 1996, p. 281). Along the West African margin, evaporites are restricted to Mocamedes, Kwanza, Lower Congo, North and South Gabon, and Douala Basins, with the cut-off to the south restricted by the Walvis Ridge (Dupre *et al.*, 2007).

The main control on the deposition of evaporites within basins is the balance between the water influx into the basin and brine reflux out of the depositional basin (Kendall and Harwood, 1996, p. 124). According to Friedman *et al.* (1992), p. 308, in settings where there is a two-way flow of water, such as in the ocean, the deposition of evaporites will mainly be around the edges of the basin. Whereas in basins where there is a one-way flow, such as in lakes, precipitation of evaporites will mainly be in the centre of the basin.

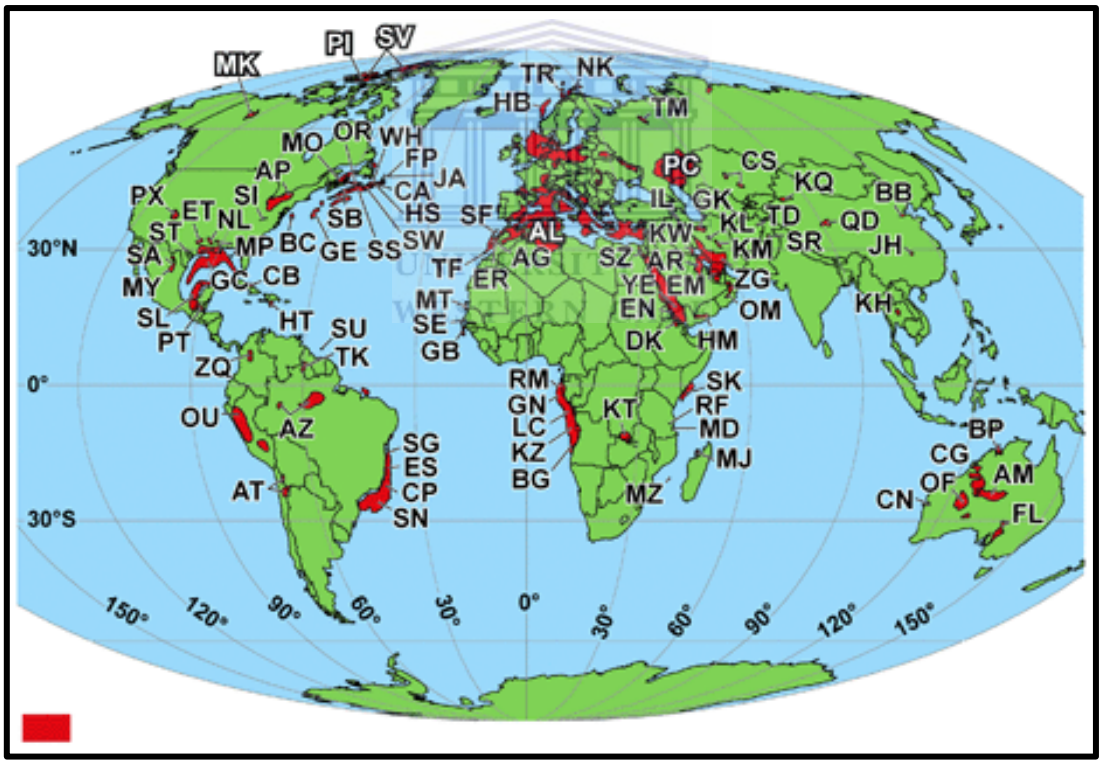

Figure 2.1: Salt basins of the world. Many salt basins (shown in red) are associated with large petroleum fields (Source: Hudec and Jackson, 2007).

The depositional setting of the Aptian salt basin during rifting of South America from Africa in the Late Cretaceous (125 to 110 Ma) is illustrated in Figure 2.2. The eight stages development of the Aptian salt basin (Figure 2.3) as reconstructed by Bryant *et al.* (2012) are:

(1) The extension between South America and Africa resulted in fresh water lakes forming;

(2) Fresh water lakes deepened due to subsidence from extension and continuous separation of the two continents;

(3) An increase in ocean water level resulted in oceanic water spilling into the lake, causing mixing of fresh water and salty seawater;

(4) Ocean level falls, and the continuous rifting causes fracturing in the ridge separating the ocean from the lake and hence allowing hydraulic communication between the ocean and the lake;

(5) As the water level in the lake drops, evaporation takes place;

(6) Increasing evaporation rates and a drop in water level in the lake result in the initiation of salt deposition;

(7) Deposition of evaporites continued until maximum deposition, at this stage, salt minerals stopped being produced, and a highly saline layer which is made up of insoluble sediments started to form (mostly anhydrites) and;

(8) The final stage in the deposition and preservation of the Aptian salt is the increase in ocean level, changing the depositional setting from lacustrine to marine environment.

Figure 2.2: The Aptian salt basin during the Early Cretaceous (Source: Bryant *et al.*, 2012).

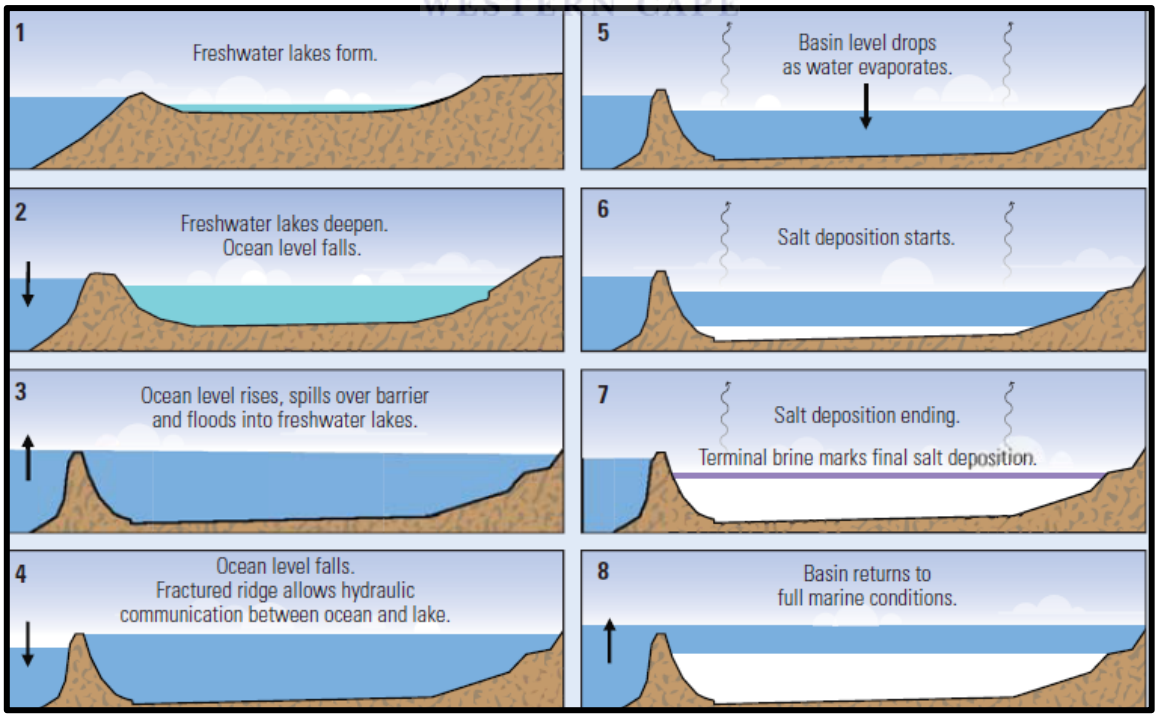

Figure 2.3: Stages in the development of the Ezanga salt Basin and its preservation (Source: Bryant *et al.*, 2012).

2.2 Salt tectonics

Evaporites behave differently from clastics and carbonates due to their different rheological (i.e., rock mechanical) characteristics (Hudec and Jackson, 2007). Evaporites are sensitive to tectonic stress and their deformation style will change to accommodate the stress imposed on them during tectonic events (Kendall and Harwood, 1996; Hudec and Jackson, 2007). Furthermore, evaporites deform by viscoelastic mechanism, unless in unusual areas which are associated with dyke intrusions and mining, where the salt might fracture (Kendall and Harwood, 1996; Hudec and Jackson, 2007). Salt is also a Newtonian fluid, which typically flows in the direction of less stress when pressure is applied by the overburden sediments (Quirk and Pilcher, 2012). Some additional characteristics of salt are: impermeability (hence excellent seal for hydrocarbons), high thermal conductivity; incompressibility and unique deformation mechanisms (e.g., wet diffusion and dislocation creep) (Fossen, 2010).

In other words, because salt is structurally weak, viscous and has a lower density (~2.16 g/cm^3) than most rocks, it will start to rise upwards due to buoyancy when buried at certain depth by younger sediments (Kendall and Harwood, 1996, p. 124; Fossen, 2010; Quirk and Pilcher, 2012). Figure 2.4 shows the different types of structures that can be formed by salt as it moves upwards.

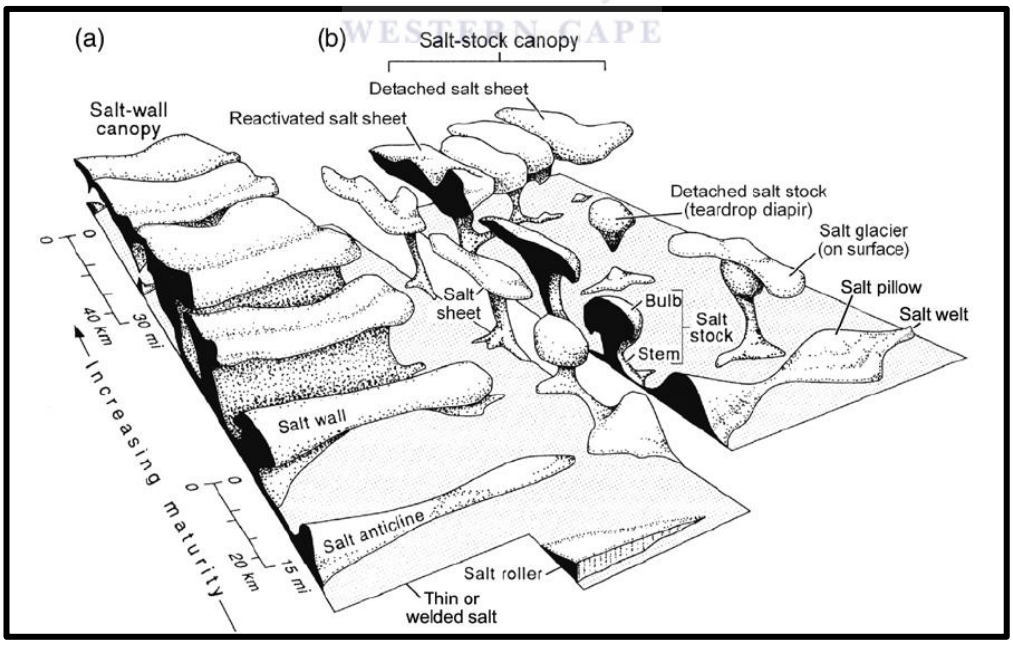

Figure 2.4: Salt can form different structures as it flows upwards or laterally, indicating some of the structure which results from salt movement. (Source: Hudec and Jackson 2007).

Salt can flow either (a) when movement is maximal in the centre with no displacement or movement along the margins of the salt body (Poiseulle flow – Figure 2.5a); or (b) when the overburden sediments move parallel to the base of the salt layer (Coeutte flow – Figure 2.5b) (Hudec and Jackson, 2007; Fossen, 2010). Thinning of the original salt layer and the growth of salt diapirs are mostly associated with Poiseulle flow (Fossen, 2010).

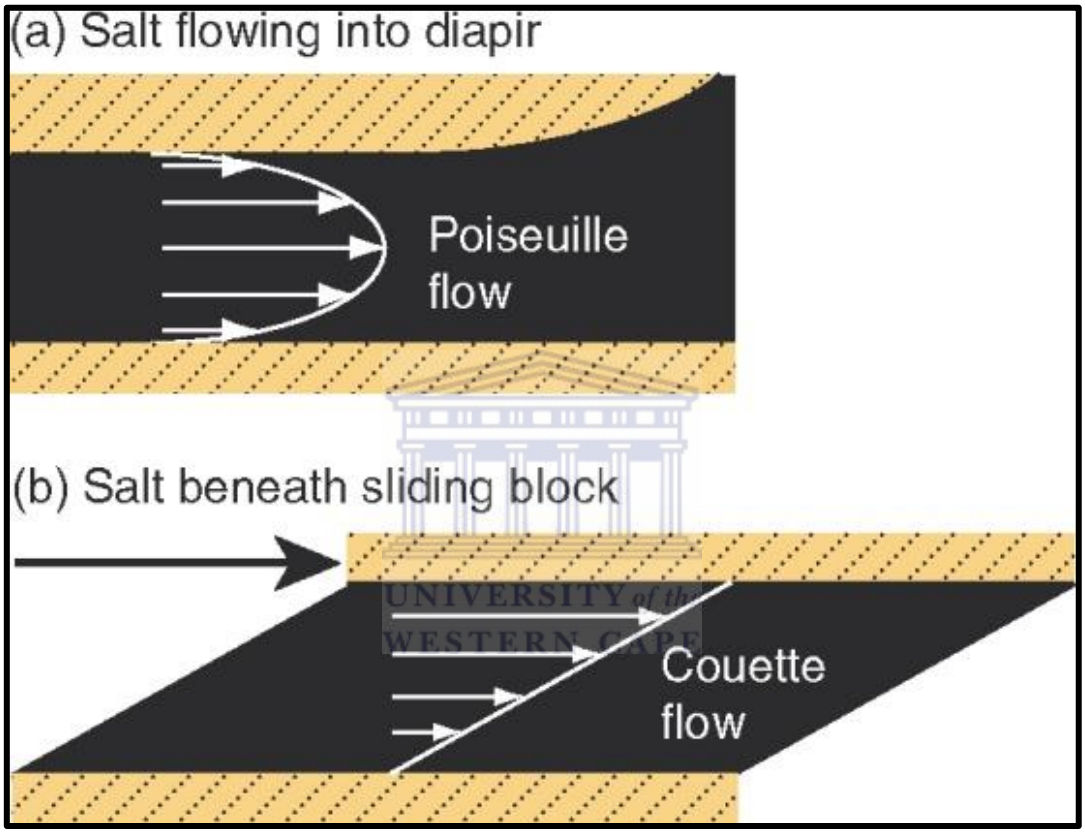

Figure 2.5: Poiseulle flow, where the flow is maximum at the centre and zero at margin, allowing the salt to flow upwards. Coeutte flow, where overlaying strata moves parallel to the salt (Source: Fossen, 2010. Also online http://www.cambridge.org/).

The strength of the overburden sediments that the salt must penetrate as it moves upwards and the friction along the boundaries of the salt are the main factors that restrict the flow (Hudec and Jackson, 2007; Fossen, 2010). The latter restriction occurs because the upper and the lower contacts that salt makes with the surrounding rocks imposes a frictional force against the salt as it moves (Hudec and Jackson, 2007; Fossen, 2010). The main forces that drive salt movements as stated in Fossen (2010) are:

a) Gravitational loading, where the load of the overlaying sediments is disproportionally distributed because of uneven density or thickness, as a result salt can start to flow (Figure 2.6a);

(b) Displacement loading which occurs during rifting or compression where salt will respond by flowing due to the tectonic stress as illustrated in Figure 2.6b and;

(c) Thermal loading where salt expands and becomes buoyant due to being exposed to heat (Figure 2.6c).

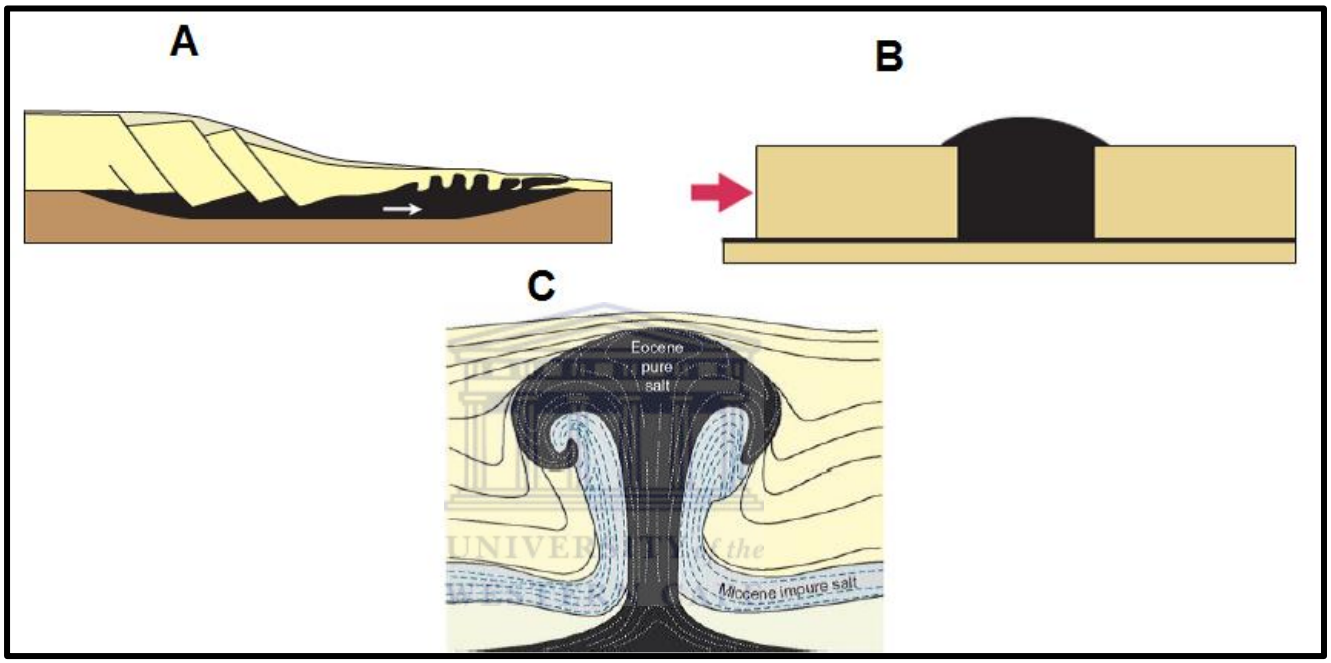

Figure 2.6: (a) Salt movement due to gravitational loading. (b) Salt movement due to shortening/contraction and (c) salt rising up due to thermal loading (Source: Fossen 2010, online http://www.cambridge.org/resources/emods/Chapter%2019/19%20Salt%20tec).

When salt rises upward, it forms diapirs that can be classified into:

1. Reactivation diapirs (Figure 2.7a) form as the response of salt to fracturing or faulting in the overburden sediments during extension. Some authors have also shown that normal faults play a crucial role in accommodating the movement of salt upward into the overlaying sediments (Hudec and Jackson, 2007; Fossen, 2010; Quirk and Pilcher, 2012).

2. Active diapirs (Figure 2.7b) form in both extension and compression settings. In extension setting, it is due to buoyancy, whereas in compression setting; it is driven by displacement loading (Hudec and Jackson, 2007; Fossen, 2010).

3. Thrust diapirs form in compressional settings where the salt movement is in the hanging wall of the fault, Figure 2.7d (Hudec and Jackson, 2007).

4. Passive diapirs (Figure 2.7f) form when the salt reaches the surface during sedimentation (Hudec and Jackson, 2007).

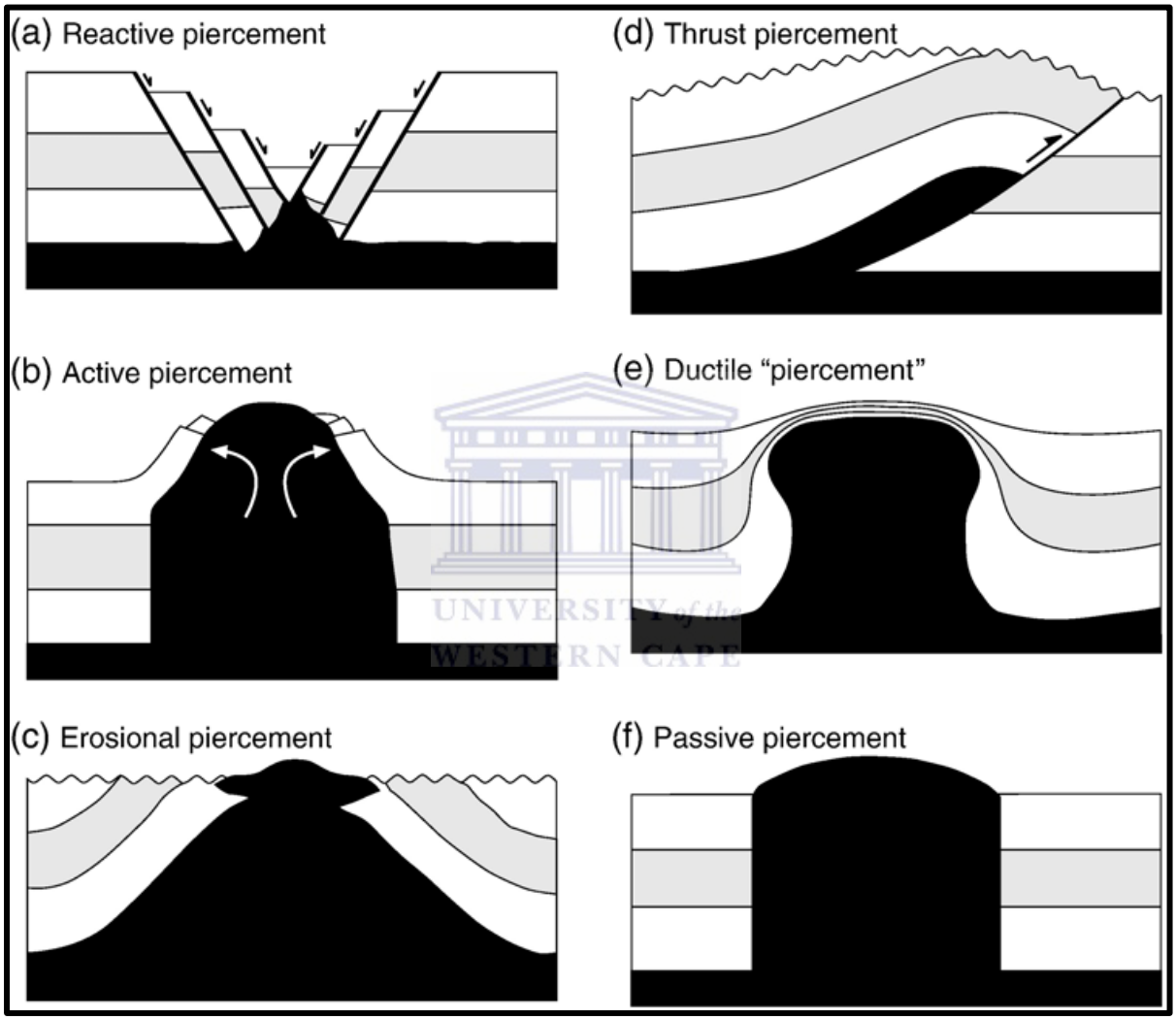

Figure 2.7: (a) Reactive diapir formed as a result of extension in the overburden. (b) Active diapir is formed by the rising diapir due to bouyancy. (c) Salt diapir protruding above the unconformity. (d) Rising salt due to thrusting, where the salt tend to be on the hanging wall. (e) Ductile piercement deforms the overburden sediments during salt flow. (f) Passive diapirforms when the diapir reaches the surface while "flowing" upwards (Source: Hudec and Jackson 2007).

During compression, as the salt is squeezed, parts of it can be detached from the main salt body as shown in Figure 2.8a. During this process, the salt is weaker than the overlying sedimentary rocks (Fossen, 2010). Sometimes during compression, salt is emplaced on top of the overburden of younger sediments and can start flowing laterally; this is referred to as

allochthonous salt (Figure 2.8b) (Hudec and Jackson, 2007; Fossen, 2010). In extensional settings (rifts), the process of salt reactivation may occur during passive stage, when the salt diapir reaches the surface and may even start to flow on the surface (Figure 2.8c) (Hudec and Jackson, 2007; Fossen, 2010). Occasionally, when the salt reaches the surface during rifting, it can collapse due to the overburden of the newly deposited sediments, which might result in the formation of a mini-basin (Figure 2.8d) (Fossen, 2010).

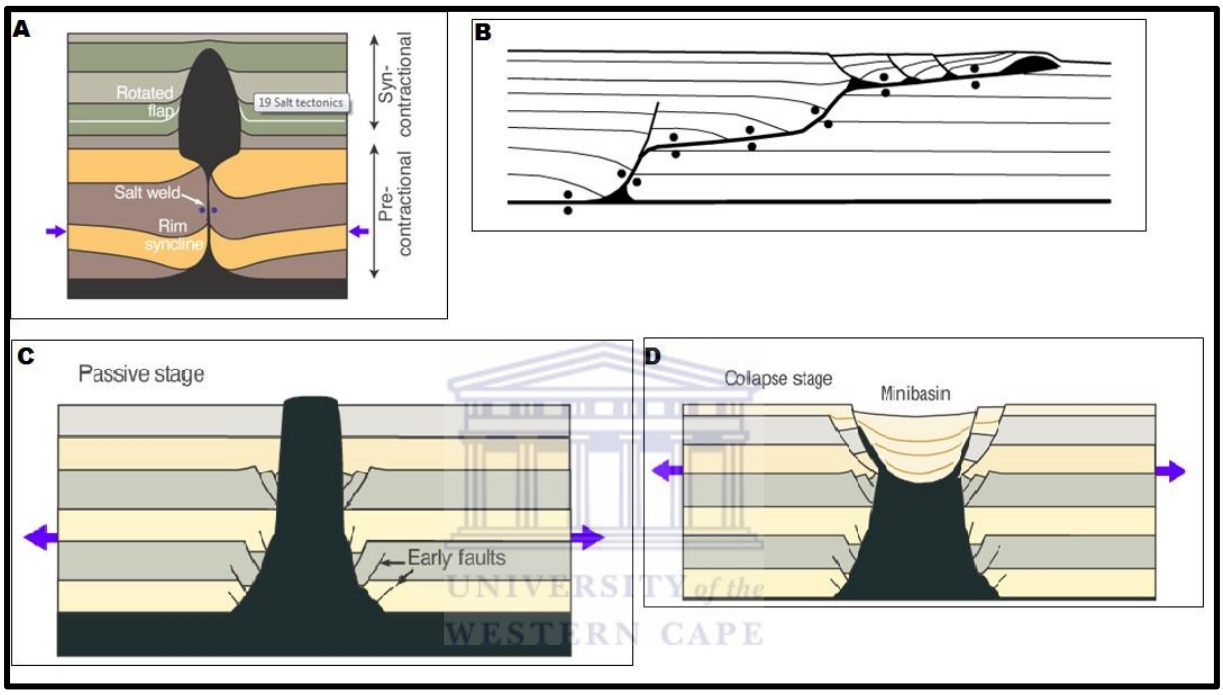

Figure 2.8: (a) The effect of shortening on the movement of salt. The weaker salt moves into the mechanically stronger overburden. (b) Allochthonous movement of the salt. (c) During extension the diapir can change from reactive-active-passive diapirism. (d) During rifting salt can reach the surface, because salt is weak, the sediment deposited over it will cause it to collapse to form a mini basin (Source: Fossen, 2010, modified from Hudec and Jackson, 2007).

3 PRINCIPLES AND CONCEPTS OF SEQUENCE STRATIGRAPHY AND SEA LEVEL CHANGE

3.1 Sea level change

Sea level can be classified into eustatic (global) or relative (local) sea levels (Figure 3.1) (Catuneanu, 2006, p. 5). According to Hart (1990), global sea level changes are controlled by (a) changes in the volume of the hydrosphere, which has remained the same for the past 1.5 Ga, (b) the change in the volume of ice on land, and (c) the change in the capacity of the ocean basin which changes through geological time during a supercontinent cycle (Figure 3.2).

The relative (local) sea level, often abbreviated as RSL and taken as synonym for base level changes, is a function of local tectonics (e.g., local isostacy, thermal or structural subsidence (or T)) and global sea level (or E), so the simple equation RSL = T + E applies (Catuneanu, 2006, p. 86). RSL changes can create or destroy accommodation, which is the amount of space that is available for sediments to accumulate (Figure 3.2). Accommodation can also be gradually destroyed by aggrading, prograding or retrograding sediments, or in other words, sedimentation can also consume accommodation (Catuneanu, 2006, p. 77). Furthermore, the combined effects of changes in relative sea level, global climate change, as well as global and local tectonics (Hart, 1990; Catuneanu, 2006, p. 74) control sediment supply and sediment distribution in a sedimentary basin.

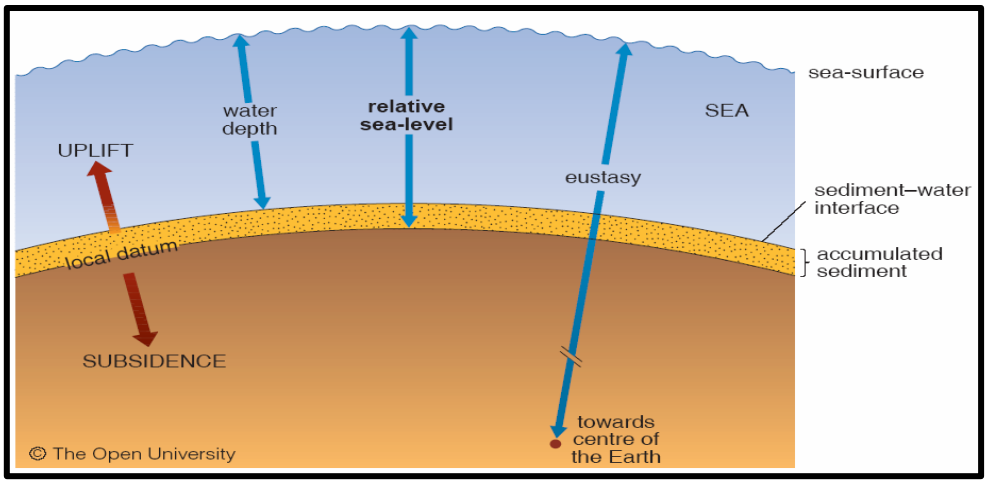

Figure 3.1: The relationship between relative sea-level, water depth, global (eustatic) sea-level, tectonics (uplift and subsidence), and accumulated sediment. Note that relative sea-level incorporates subsidence and/or uplift by referring to the position of sea-level with respect to the position of a datum at or near the sea-floor (e.g. basement rocks, top of previous sediment package) as well as eustasy (i.e. global sea-level) is the variation of sea-level with reference to

fixed datum, for example the centre of the Earth (Angela Coe, Copyright © 2003 The Open University).

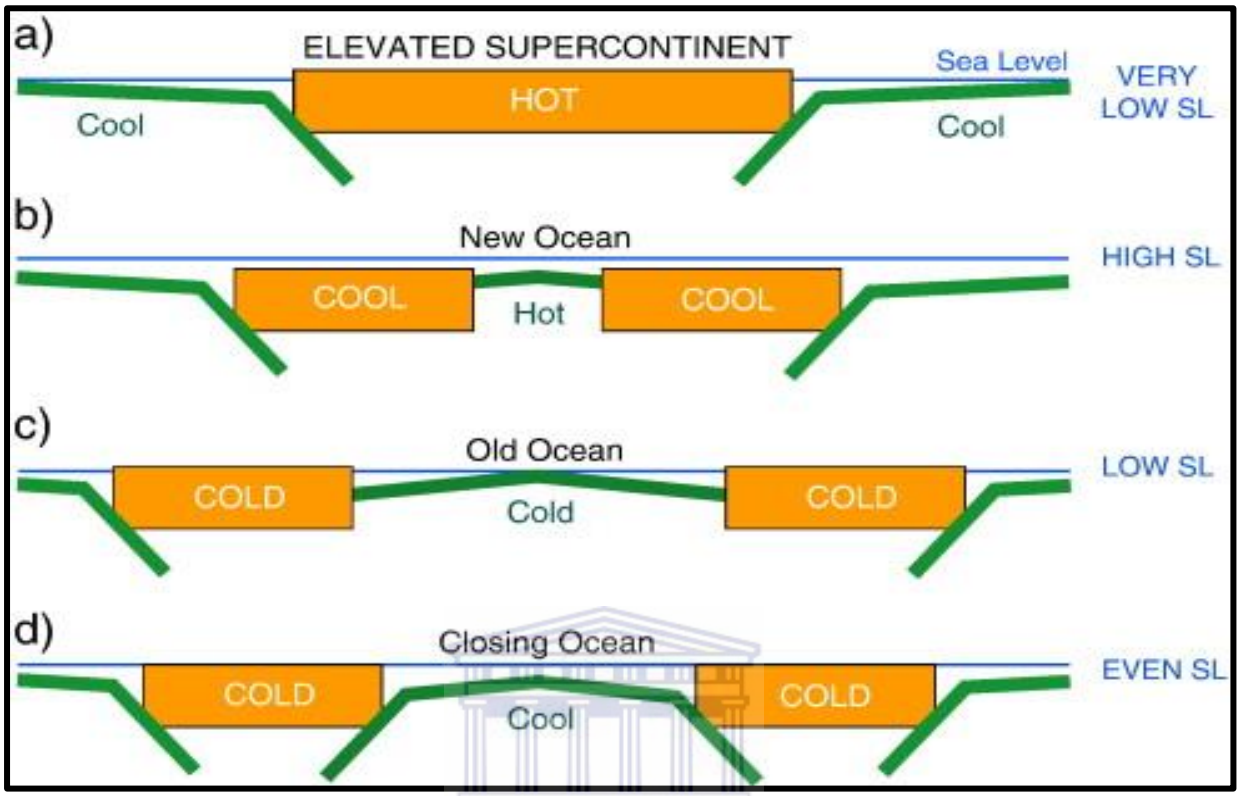

Figure 3.2: Effect of the supercontinent cycle on global sea level. (a) Supercontinents are epeirogenically elevated and so correspond to periods of low global sea level. (b) When they break up, the resulting continental fragments cool and subside as they separate so that global sea level rises. (c) In addition, the new oceans are floored by young, hot, shallow crust, so they cannot accommodate much seawater. (d) But as these oceans get older and colder, they become deeper, causing global sea levels to fall until the oceans start to close (Source: Nance *et al.* 2014).

Variation in RSL (or base level) and sedimentation together determine the evolution of shoreline trajectories through geological time which are referred as either transgressions or regressions (Catuneanu, 2006, p. 77). The former describes the landward movement of the shoreline, whereas the latter refers to the advancement of the shoreline towards the sea (Catuneanu, 2006). During transgression, a retrograding stacking pattern forms in which fine-grained sediments overlie coarse-grained sediments, while during regression, progradational stacking patterns form, where fine-grained sediments are overlain by coarse-grained sediments (Figure 3.3) (Catuneanu, 2006, p. 89). Regression can be subdivided into forced regression and normal regression (Catuneanu, 2006, p. 89). Forced regression is independent of sediment supply and occurs when a drop in RSL reduces the accommodation space, whereas normal regression occurs when the rate of sediment supply is greater than the rate of

relative sea level rise (Catuneanu, 2006, p. 90). All in all, the identification of depositional trends and stacking patterns in the rock record enable us to reconstruct shoreline shifts through geological time, and thus indirectly, determine changes in the major controlling factors of sedimentation (e.g., past changes in the global climate, global and regional tectonics). For instance, a major progradational event in the seismic-reflection data might imply either a large-scale global sea level fall or a major local uplift event in the nearshore to onshore areas, relative to the changes in the global sea levels. Similarly, retrogradation, which indicates transgression, might be simply linked to events of fast global sea level rise, but could also be due a period when the rate of global sea level fall was outpaced by the higher rates of local subsidence.

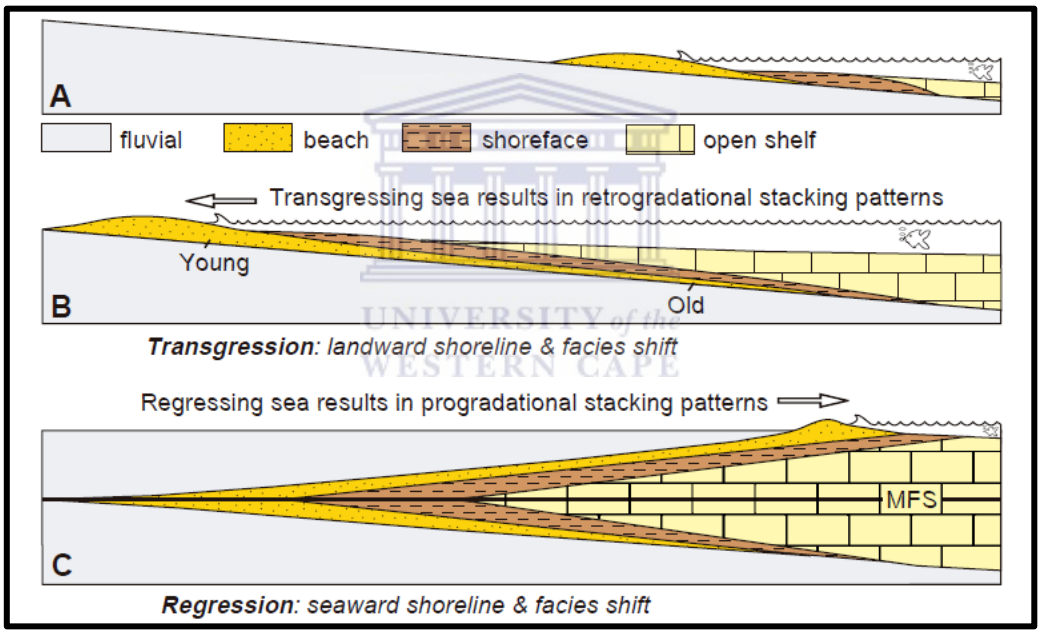

Figure 3.3: Shoreline shift models, showing that during transgression the shoreline shifts in a landward direction and retrogradation occurs, while during regression the shoreline shifts in a seaward direction and progradation occurs. The maximum flooding surface (MFS) separates retrogradational from overlying progradational stacking patterns (Source: Catuneanu, 2006, p. 90)

It is common practice to explain the shoreline shifts recorded in any continental margin succession of the Atlantic Ocean by the events predicted by the global sea level chart produced by Haq *et al.* (1987); Miller *et al.* (2005); Haq and Schutter (2008). However, Miall (2009) demonstrated the dangers of the uncritical application of this global sea level chart to relate depositional trends in a given study region to global events. Using fairly detailed Upper

Cretaceous data sets from tectonically unrelated basins ranging from New Zealand to Russia, Miall (2009) found that sea-level lowstands predicted from the global sea level chart most of the time occurred at different times in the stratigraphic record of the studied data sets. Miall (2009) thus critics the use of the eustatic chart to predict to explain the shoreline shifts recorded especially in the pre-Neogene stratigraphy, because the global eustasy chart of the pre-Neogene is inaccurate as it is derived from a geological record that is riddled by increasingly more frequent and larger time gaps (i.e., unconformities). This later concept, i.e., that the resolution and reliability of the geological record (and the details of the events captured in it) becomes less accurate with deep time, is a well-established concept in geology. What this means is that, since the stratigraphy of interest is Cretaceous in age, linking the shoreline shifts of Western Africa, the changes shown in eustatic sea level chart of Haq *et al.* (1987); Miller *et al.* (2005); Haq and Schutter (2008) is unsatisfactory even if the local tectonic history of the region would be better known . As such, for our interpretations of sea level fluctuations, RSL will be determined from what we see on the seismic section (i.e., stratal termination), rather than using the Haq *et al.* (1987) chart to infer eustatic sea level changes.

3.2 Seismic and sequence stratigraphy

Over the last 40 years petroleum companies have increasingly relied on seismic and, more recently on, sequence stratigraphy in locating natural resources in the rock record, because this stratigraphic method allows a fairly accurate prediction of reservoirs and seals through the analysis of the facies changes in time and space (Neal *et al.,* 1993).

This section will review the principles that govern sequence and seismic stratigraphy and their application to seismic interpretation. The concept of sequence stratigraphy has been around since the 1970's and was developed from seismic stratigraphy (Boggs, 2006, p. 434; Catuneanu, 2006, p. 3). Boggs (2006) defines seismic stratigraphy as a method of extracting stratigraphic information from the study of seismic data. Adapted from Mitchum *et al.* (1977), Table 3.1 and 3.2 illustrate common reflection patterns and seismic facies types that may be found in seismic sections.

Table 3.1:Seismic reflection patterns and their geological meaning. (Source: Mitchum *et al.*, 1977).

Reflection pattern	Name of the feature	Interpretations
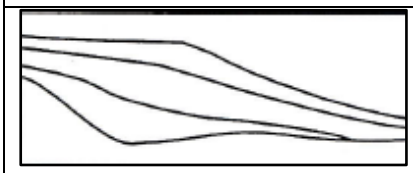	Sigmoid	Moderate to fast rate of progradation (e.g., during relative sea level fall)
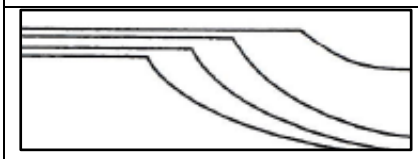	Oblique tangential	Accelerating rate of progradation offshore and slow rate of aggradation nearshore (e.g., during slow relative sea level rise after transgression)
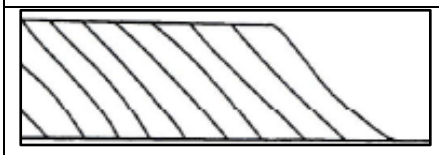	Oblique parallel	Fast rate of progradation (e.g., during relative sea level drop)
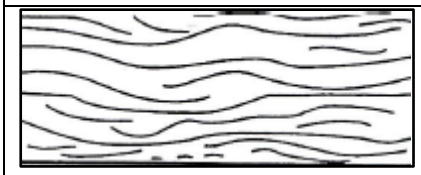	Hummoky	Aggradation in Shallow water (e.g., during slow relative sea level rise)

Table 3.2 Seismic reflection patterns observed in incised valley fills. (Source: Mitchum *et al.* 1977).

Reflection pattern	Type of fill	Interpretation
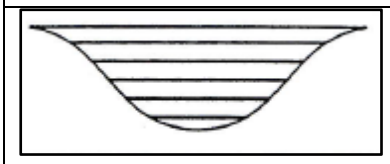	Onlap	Probably a low energy setting
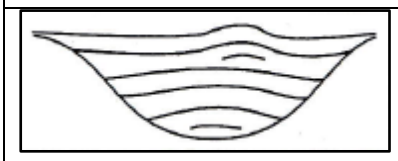	Mounded onlap	Probably a high energy setting with more than two infill stages
	Prograded	Lateral accretion of sediments in a meandering channel
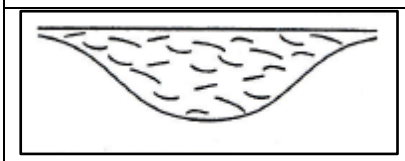	Chaotic	Post depositional soft sediment deformation (either physical or bioturbation) or

		very fast depositional rate
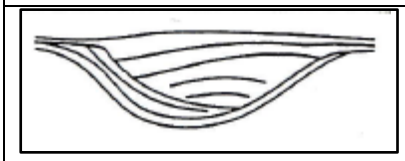	Complex	Change in sediment supply direction

Sequence stratigraphy is a relatively young subdiscipline of stratigraphy, and its definition and terminology have evolved through time (Catuneanu, 2006, p.3). Nowadays, it is defined as a chronostratigraphic method in which key geological surfaces are used to subdivide stratigraphic successions into sequences by integrating seismic data on the geometry of the strata (Figure 3.4) with borehole data on the sedimentology and palaeontology of the succession (Neal *et al.*, 1993; Boggs, 2006, p. 435; Catuneanu, 2006, p. 4). A sequence is defined as a relatively conformable succession of genetically related strata which are bound by key surfaces that signify specific events that happened during the depositional history of a basin, (Figure 3.4) (Catuneanu, 2006, p. 4). These key surfaces are unconformities (see detailed review in the next section) and their correlative, conformable surfaces (Figure 3.5) (Boggs, 2006, p. 435; Catuneanu, 2006, p. 3).

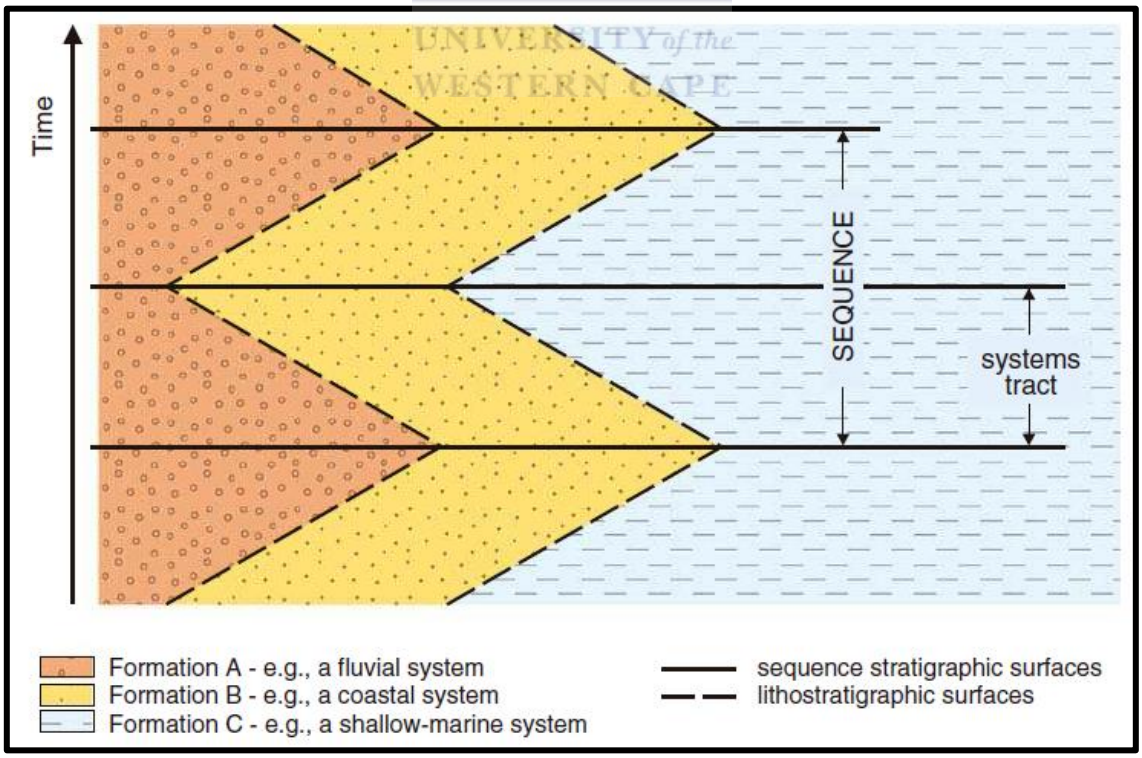

Figure 3.4: Sequence stratigraphic model showing the relationship between a sequence consisting of transgressive and regressive system tracts (upward-fining, retrogradational and upward-coarsening, progradational depositional trends, respectively) and various depositional systems (e.g., fluvial, costal and shallow marine) that make up the system tracts. (Source: Cataneanu, 2006, p. 3).

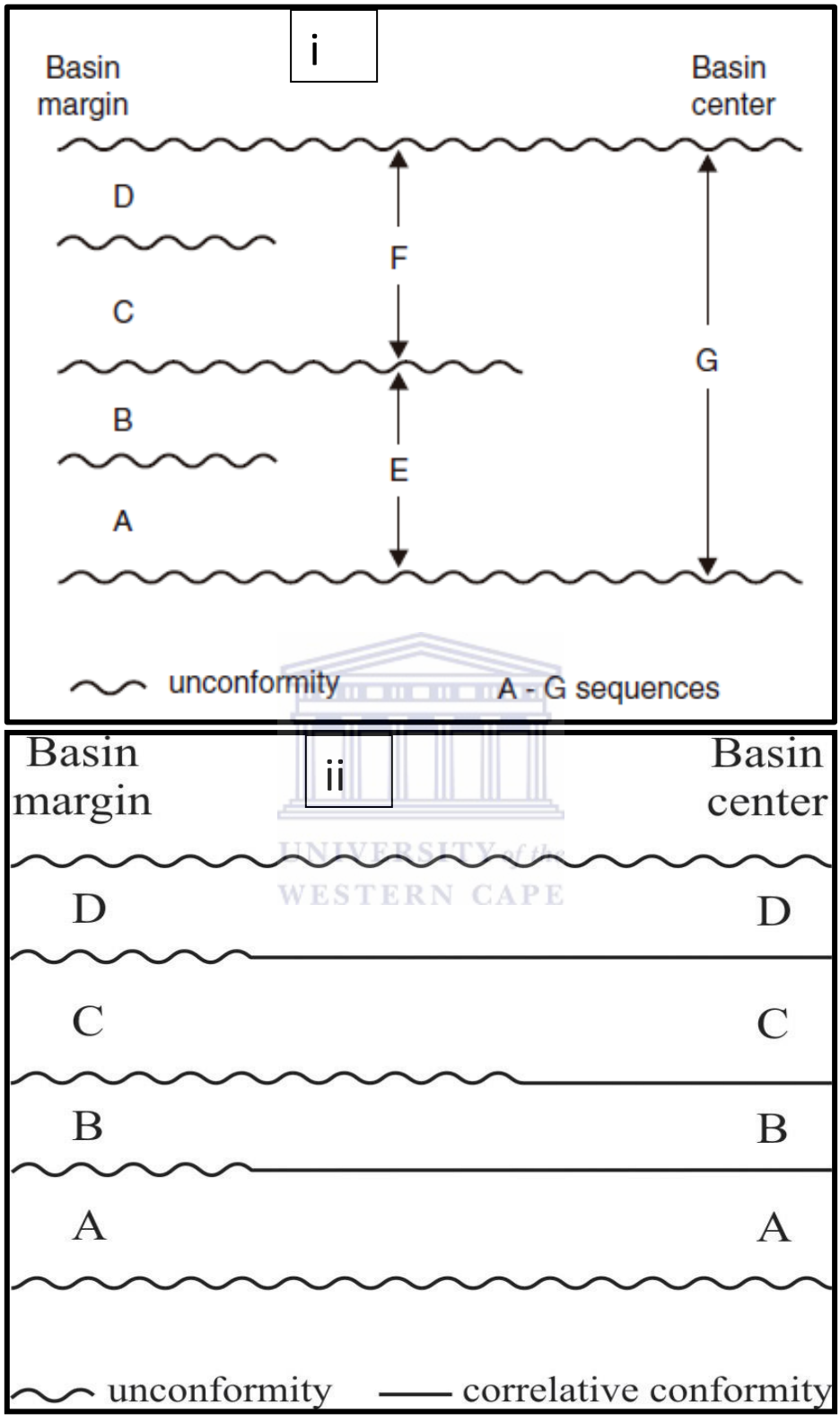

Figure 3.5: The number of unconformity-bounded sequences decreases from four (Ai to Di) at the basin margins to one (Gi) towards the basin centre (a), however the number of stratigraphic sequences is constant (four: Aii, Bii, Cii and Dii) across the basin, because unconformities at the basin margin transition into correlative conformable surfaces towards the basin centre (b) and thus allow tracing of sequences or system tracts across an entire basin. Source: (Catuneanu, 2006, p. 4,5).

Table 3.3: Key characteristics of systems tracts in seismic profiles and gamma-ray logs as well as their petroleum play significance (modified after Ca

Systems Tract	Key features	Fluvial	Coastal	Shallow-water	Deep-water
Falling-stage Systems Tract	**Depositional trends**	-	-	Progradation	Progradation
	Gamma-ray Signatures	-	-		
	Stratal termination	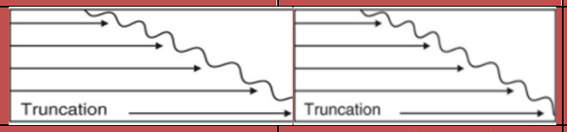		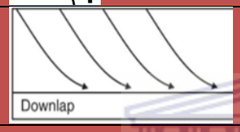	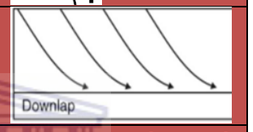
	Lower bounding Surfaces	Subaerial unconformity	Basal surface of forced regression	Regressive surface of marine erosion	- Basal surface of forced regression
	Sediment budget	Sediment bypass	Offlapping deltas, downstepping beaches	Sharp based shoreface and shelf facies	Debris flows deposits and turbidites
	Upper bounding surfaces	Subaerial unconformity	Correlative conformities	Correlative conformities	- Correlative conformities
	Reservoir significance	-	Good: Detached shoreline sands	Good: Shoreface sands	Good: Turbidites
	Source & seal significance	-	-	Fair: Shelf fines	Fair: Organic matter rich pelagics

Systems Tract	Key features	Fluvial	Coastal	Sha
Lowstand Systems Tract	**Depositional trends**	Aggradation	Progradation	Pro
	Gamma-ray Signatures	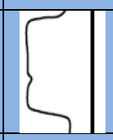		
	Stratal termination	-	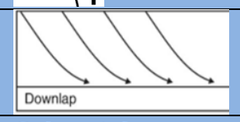	
	Lower bounding surfaces	Subaerial unconformity	Subaerial unconformity	Cor con
	Upper bounding surfaces	Maximum regressive surface	Maximum regressive surface	Ma reg
	Sediment budget	Amalgamated channel fills in incised valleys	Shelf/shelf-edge deltas, strandplains	Gra sho faci
	Reservoir significance	Good: Channel fills	Good: Shoreline and sands	Goo san
	Source & seal significance	-	-	Fai

Systems Tract	Key features	Fluvial	Coastal	Shallow-water	Deep-water
Transgressive Systems Tract	**Depositional trends**	Aggradation	Retrogradation	Retrogradation	-
	Gamma-ray signatures				-
	Stratal termination	-	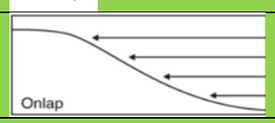	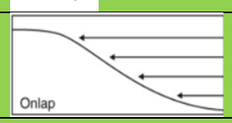	-
	Lower bounding surfaces	Maximum regressive surface	Maximum regressive surface	Maximum regressive surface	-
	Upper bounding	Maximum	Maximum flooding	Maximum	-

Systems Tract	Key features	Fluvial	Coastal	Sha
Highstand Systems Tract	**Depositional trends**	Aggradation	Progradation	Prog
	Gamma-ray signatures		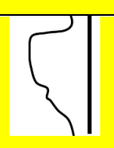	
	Stratal termination	-	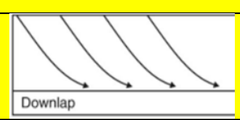	
	Lower bounding surfaces	Maximum flooding surface	Maximum flooding surface	Max surf
	Upper	Subaerial	Basal surface of	-Re

Since sequence stratigraphic events (i.e., transgressions and regressions) occur in cycles during the depositional history of a basin, theoretically every stratigraphic sequence that is contained in the basin fill can be subdivided into the following system tracts; Lowstand System Tract (LST), Transgressive System Tract (TST), Highstand System Tract (HST) and Falling Stage System Tract (FSST), (Figure 3.6) (Boggs, 2006, p. 453; Catuneanu, 2006, p. 165). The key features that identify the four system tracts in their various portions (fluvial, coastal, shallow-water, and deep-water) are listed in Table 3.3.

Falling Stage System Tract (FSST)

Falling stage system tract (FSST) occurs when the RSL falls from a highstand position irrespective of sedimentation rates, resulting in a forced regressing shoreline, (Figure 3.8) (Boggs, 2006; Catuneanu, 2006, p. 97). RSL can drop irrespective of sediment supply due to: (1) tectonic uplift and eustatic sea level fall; (2) when tectonic uplift is greater than eustatic sea level rise; (3) when there is no tectonic uplift movement and eustatic sea level falls; (4) when tectonic uplift occurs while the eustatic sea level is constant and (5) when the eustatic sea level fall is greater than subsidence rate of the basin (Figure 3.6) (Catuneanu, 2006, p. 85).

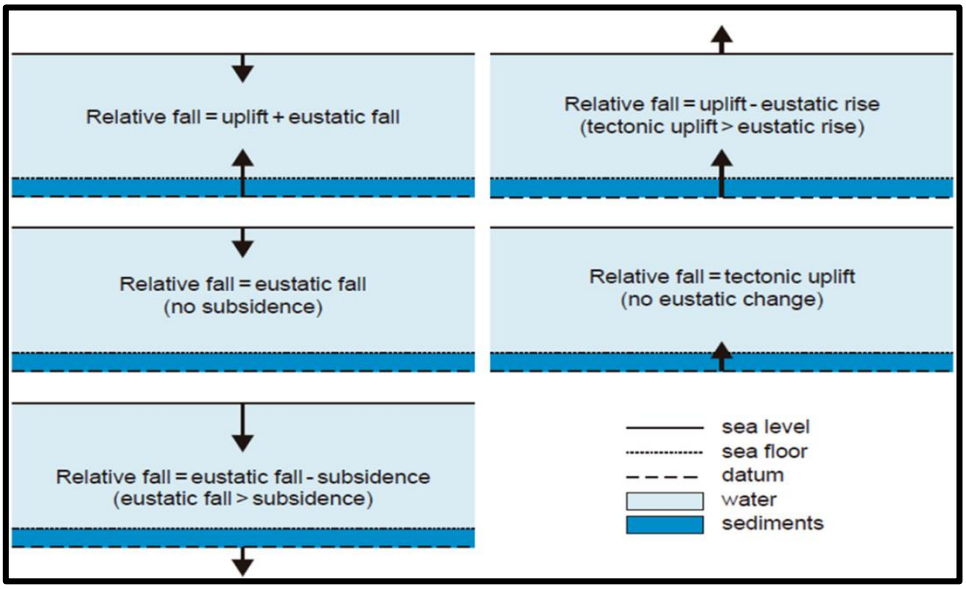

Figure 3.6: Fall in relative sea-level (RSL) can be achieved in a variety of ways. Relative sea level drop always results in the decrease in accommodation space. The length of the arrows is proportional to the rates of vertical tectonics and eustatic changes (Source: Cataneanu, 2006, p. 85).

In the marine settings, sediments that are deposited during FSST are bounded at the base by regressive surface of marine erosion (RSME), basal surface of forced regression (BSFR), with subaerial unconformity and correlative conformity bounding the top (Boggs, 2006; Catuneanu, 2006, p.97). FSST have an overall coarsening upwards gamma ray signatures in coastal and shallow marine succession (Neal *et al.*, 1993). Because accommodation space is reduced during FSST, subaerial unconformities form and sediment bypass occurs in the fluvial and coastal plain setting (Boggs, 2006, p. 453). Therefore, sediments are not preserved in the areas landward from the shoreline (Boggs, 2006, p. 453; Catuneanu, 2006, p.179). During FSST, subaerial erosion will generate truncational stratal termination over the top of the previously deposited nearshore deposits, whereas downlapping surfaces will form due to prograding clinoforms in shallow-water setting (Table 3.3, Figure 3.7 and 3.8) (Catuneanu, 2006, p.179). FSST is also characterized by significant slope fans, slumps and basin floor fans; these result from gravity flows that are generated due to instability of the shelf region (Catuneanu, 2006, p.179).

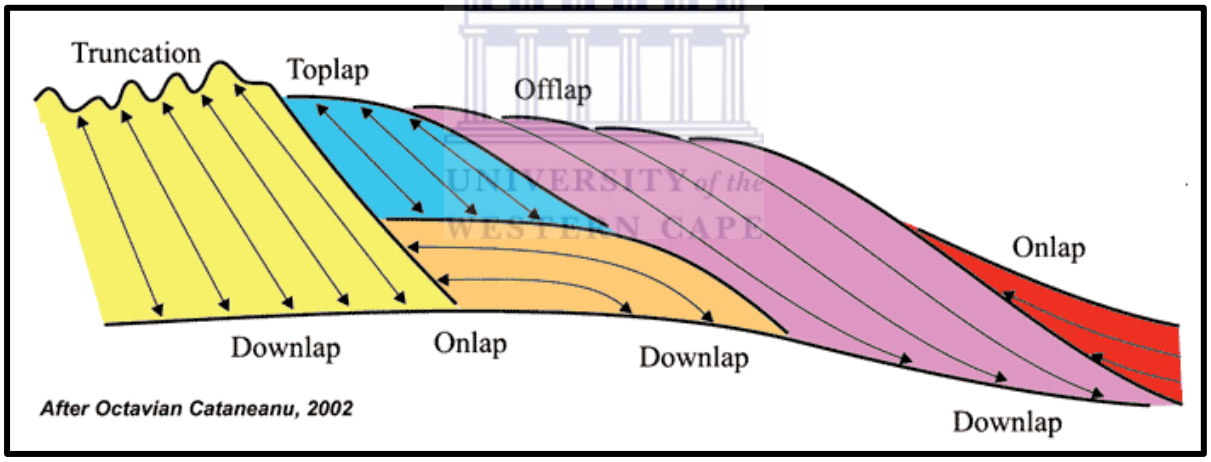

Figure 3.7: Simplified model of stratal terminations that occurs during different system tracts. These system tracts are associated with shoreline trajectories (retrogression and progradation), and each system tract result in a different stacking pattern and bounding surface (Source: Catuneanu, 2006, p. 106).

Lowstand System Tract (LST)

The lowstand system tract (LST) occurs when sea level is at its lowest, during the early (accelerating) stages of RSL rise, when the rate of RSL is outpaced by sedimentation rate (Boggs, 2006, p. 453; Catuneanu, 2006, p. 197). LST are bounded by subaerial unconformities and correlative conformities at the base, and by the Maximum Regressive Surface (MRS) at the top (Catuneanu, 2006, p. 197). During LST, sediments will fill

previously incised valleys first, and then sediments might 'spill' into the floodplain area, only then will sediments make their way to deeper marine sections (Boggs, 2006, p. 453; Catuneanu, 2006, p. 199). The influx of these sediments in deep marine setting can trigger turbidites and other gravity flows in deep marine settings (Boggs, 2006; Catuneanu, 2006, p. 199). LST is identified in gamma ray logs by coarsening-upward successions in the marine section and fining upward profiles in the nonmarine successions (Table 3.3) (Neal *et al.,* 1993). The prograding and aggrading strata that form during LST are made up of shallow marine, offshore marine, sub-marine fan and terrigenous (alluvial and coastal plain) sediments (Boggs, 2006, p. 454). As shown in Table 3.3, toplapping stratal terminations are common during LST in shallow-water environments (Catuneanu, 2006, p. 106).

Transgressive System Tract (TST)

The Transgressive System Tract (TST) occurs when the rate of RSL rise outpaces sedimentation rate along the shoreline, resulting in a landward shift of sediments (Figures 3.2; 3.4) (Boggs, 2006, p. 455; Catuneanu, 2006, p. 205). TST is bounded by maximum regressive surface at the base and maximum flooding surface (MFS) at the top (Catuneanu, 2006, p. 205). If the rate of sea level rise is fast, previously deposited unconsolidated LST sediments in floodplains can be removed by wave action in shallow waters, and this wave scour surface is called the transgressive surface or wave ravinement surface (Figure 3.8) (Boggs, 2006, p. 455; Catuneanu, 2006, p. 205). TST is identified by fining upwards gamma ray signatures trends in both marine and nonmarine successions (Table 3.3) (Neal *et al.,* 1993). A stratal termination during TST in shallow marine settings is onlap the geometry of which is observed when a semi-horizontal layer terminates against a steeper stratigraphic surface (e.g., healing phase deposits onlap onto the wave ravinement surface) (Figure 3.7) (Catuneanu, 2006, p. 210).

Highstand System Tract (HST)

The highstand system tract (HST) occurs when RSL rise is outpaced by sedimentation rate. This occurs during late stage (decelerating) relative seal level rise (Figure 3.7) (Boggs, 2006, p. 453; Catuneanu, 2006, p. 171). HST is bounded by the MFS at the base and by subaerial unconformity, regressive surface of marine erosion (RSME) and basal surface of marine

erosion (BSME) at the top (Boggs, 2006, p. 453; Catuneanu, 2006, p. 171). The overall gamma ray signature is a coarsening upwards profile in the marine successions and fining upward trends in the nonmarine successions (Neal *et al.*, 1993). HST is dominated by coastal-plain and deltaic sediments (Boggs, 2006). During HST normal regression of the shoreline occurs, allowing progradation and aggradation of sediments due to the abundant sediment supply (Neal *et al.,* 1993; Boggs, 2006, p. 453; Catuneanu, 2006, p. 171). At the bottom of prograding clinoforms formed during HST, downlapping stratal termination occur (Table 3.3), which is observed when strata terminate against a lower-angle surface (Figure 3.7 and 3.8) (Catuneanu, 2006, p. 171). Downlapping surface indicates either normal or forced regression and is usually observed at the base of prograding strata. Downlapping strata forms in shallow or deep marine setting and are uncommon in nonmarine settings with the exception of lacustrine environments (Catuneanu, 2006, p. 171).

As indicated in Table 3.3, potential reservoirs, source and sealing rocks are associated with different geological environments in the different system tracts. From a petroleum geological point-of-view, it is therefore crucial to recognise the sedimentary products (e.g., stacking patterns, stratal terminations) of each system tract in seismic sections and geophysical wireline logs. Only this knowledge would allow for the prediction of reservoir, seals and source rocks on a regional scale. During HST, reservoirs are prone to form in coastal shoreline facies and shoreface sands; whereas in TST, reservoirs form along the coast in estuaries, and beach sands. LST reservoirs tend to form in fluvial, coastal, shallow-water and deep water, because of the high sediment supply during LST. FSST reservoirs are found in deep-water turbidite deposits and a fair amount of reservoirs form in both coastal and shallow-water shoreline sands and shoreface sands respectively (Table 3.3 and Figure 3.8) (Neal *et al.,* 1993 and Catuneanu, 2006, p. 177). Source rock on the other hand, are mostly formed from pelagic and shelf fines in deep-water and shallow-water respectively during TST and HST. Source rock and seal deposition is not favoured during neither LST or FSST, (Table 3.3 and Figure 3.8) (Neal *et al.*, 1993 and Catuneanu, 2006, p. 177).

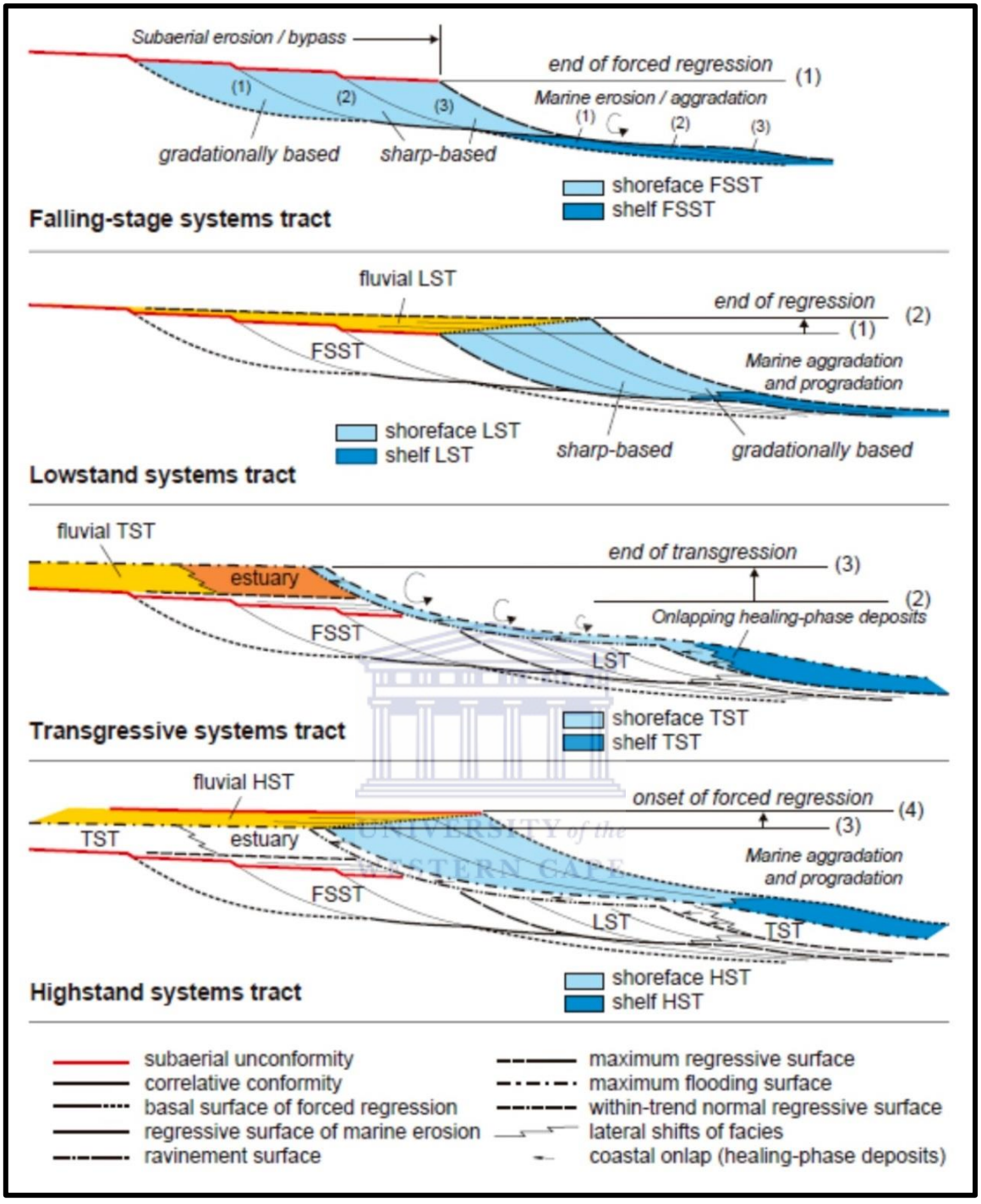

Figure 3.8: Depositional sequence as defined by its system tract. 1-4 shows the sedimentary dynamics each system tract form and the bounding surfaces of each system tract. The diagram further illustrates the relationship between sea level changes and system tracts (Source: Catuneanu, 2006 modified from Catuneanu, 2002, p. 172).

3.3 Unconformities

Several unconformities occur in the post-salt stratigraphy of the study area and the region, and these have been attributed to relative sea level fluctuations due to the splitting of South America from Africa during Early Cretaceous (Pletsch *et al.,* 2001; Oluboyo *et al.,* 2013), hence this brief review section on the topic of unconformities.

Unconformities are substantial breaks or gaps in the stratigraphic record that lasted millions or hundreds of millions of years, and represent a period of a) non-deposition or b) erosion (either subaerial or subaqueous) prior to the deposition of the younger beds. If the non-deposition and erosion only lasted for a short period, the resultant break in the rock succession is referred to as diastem (Shanmugan, 1988; Boggs, 2006, p. 404; Catuneanu, 2006, p. 15). In other words, unconformities are due to major changes in the dynamics of depositional environments, whereas diastems are due to a short change in sedimentation rate, which can occur at random, without changing the overall style of the depositional environment. Unconformities can also form sequence boundaries and may occur within system tracts, hence studying the nature of unconformities is important in the sequence stratigraphic interpretation of rock successions (Shanmugan, 1988). Unconformities can aid stratigraphic subdivision (e.g., in the correlation of different lithologies) and assist in determining the types of tectonic activities and global sea level changes that might have occurred in a basin (Shanmugan, 1988). Therefore, unconformities are fundamental in reconstructing the relative sea level changes in a given area.

3.3.1 Origin and types of unconformities

Unconformities originate from either allocyclic (e.g., tectonic, climatic, eustatic control) and/or autocyclic processes (intrabasinal, sedimentary control) in both subaerial and submarine depositional environments (Shanmugan, 1988). Figure 3.9 shows how allocyclic processes, especially tectonics play a role in creating regional unconformities, in settings where uplift is higher than the eustatic sea level rise or sea level is constant. Areas that were previously under water (e.g., a carbonate shelf) can be exposed and eroded, leading to the formation of an unconformity (Shanmugan, 1988).

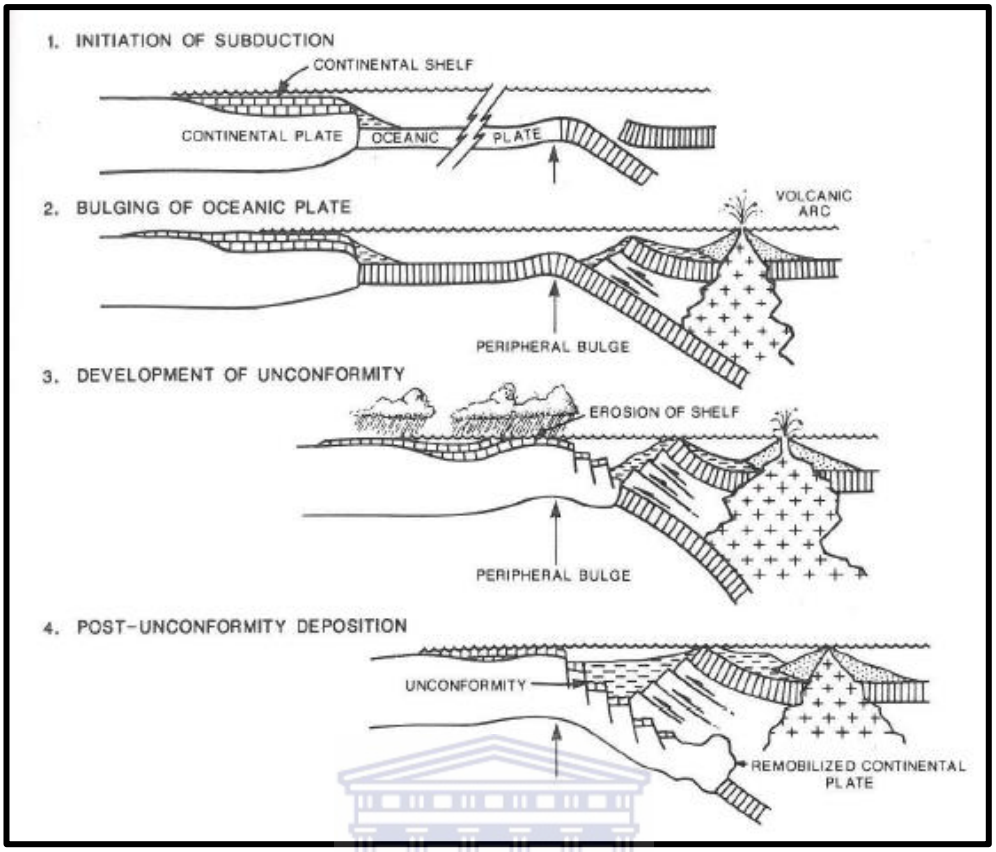

Figure 3.9: Development of tectonically driven unconformities, sea level rise is small or kept constant. Illustration in stage 3 shows the erosion of shelf carbonates during exposure to meteoric water along the tectonically uplifted peripheral bulge. Illustration in stage 4 shows that the carbonate sedimentation reassumes, because the tectonic uplift is less active (i.e., transgression occurs flooding the profile) (Source: Shanmugam, 1988).

Further examples of unconformity-generating allocyclic processes have been indirectly discussed in sections 3.1 and 3.2. Firstly, the processes that occur during the formation of falling stage systems tract is relevant here (see FSST in Ch. 3.2). Falling relative sea levels expose areas near the shoreline to erosion, and this results in the formation of subaerial unconformities (Shanmugam, 1988; Catuneanu, 2006, p. 85). During such times (Figure 3.10), large volumes of sediments, that are eroded from areas near the shoreline, will be transported firstly to the continental shelves. Moreover, because accommodation space over the shelves is also constantly being reduced during this time, the sediments are further removed and transferred from the exposed shelves into the deep sea where they can form excellent turbidite reservoirs (Shanmugam, 1988; Catuneanu, 2006, p. 85).

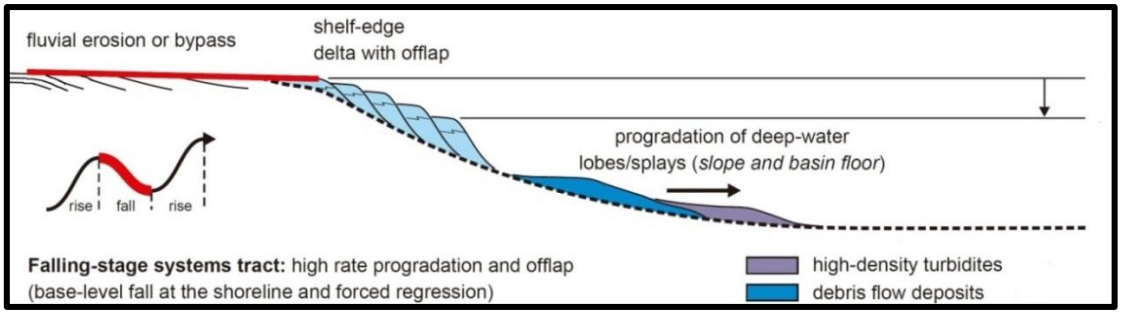

Figure 3.10: Subaerial unconformity (red line) is a key stratigraphic surface in the falling-stage systems tract. This major unconformity forms when the relative sea level falls (downward arrow on the right), destroying accommodation space in the area near the shoreline. The illustration also shows the regional architecture of depositional systems (e.g., the fast progradation in the self-edge delta) and the basal surface of forced regression (with dashed line) (Source: Catuneanu, 2006, p. 169).

Secondly, unconformities can also form in submarine environments when rapid relative sea level rise causes transgression (see TST in Ch. 3.2). As explained above, during this allocyclic process, the wave-scour generated submarine unconformity (also called "ravinement" or "transgressive surface") is covered by the "healing-phase" deposits that have characteristic onlapping stratal terminations (e.g., the transgressive lag onlaps on the ravinement surface) (Figure 3.11), (Shanmugam, 1988; Catuneanu, 2006, p. 93). According to Shanmugam (1988), submarine unconformities are sharp erosional surface that are generated or enhanced by autocyclic mass movements, density currents, carbonates dissolution and clastic influx in carbonates shelves.

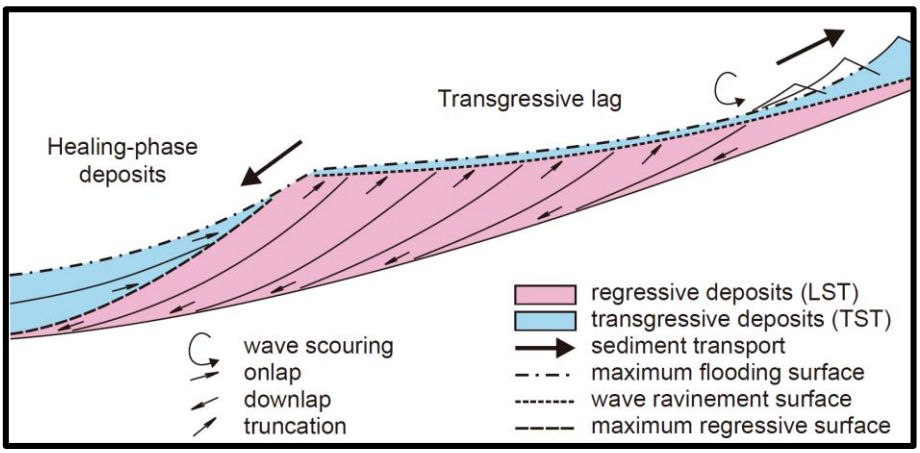

Figure 3.11: The wave-ravinement surface (close-spaced dashed line) is a key stratigraphic surface in the transgressive systems tract. This major submarine unconformity forms due to wave-scour when the rate of relative sea level rise outpaces the sedimentation rate in the shoreline area. The transgressive deposits are variable in grain size: a coarse-grained transgressive lag mantles the ravinement surface close to the shoreline, whereas a finer, healing-phase deposit onlaps onto this erosional transgressive surface in areas away from the shoreline. The illustration also shows the stratal terminations in the underlying LST and the other key stratigraphic surfaces. Abbreviations: TST - transgressive systems tract; LST - lowstand systems tract (Source: Catuneanu, 2006, p. 93).

The four types of unconformities are:

a) Disconformity (Figure 3.12a)

Disconformities occur when an uneven surface of erosion separates two strata with the same orientation, (Figure 3.12a) (Shangmugan, 1988; Boggs, 2006, p. 405; Catuneanu, 2006, p. 15). Disconformities might be difficult to see at a local scale and might sometimes only be recognised regionally (Boggs, 2006, p. 405).

b) Angular Unconformity (Figure 3.12b)

An angular unconformity result from angular discordance between two strata separated by an erosional surface, where one strata will lie at an angle at the contact of the two strata (Figure 3.12b) (Shanmugan, 1988; Catuneanu, 2006, p. 15). This unconformity types is characterised by younger, semi-reflectortal beds overlying tilted or folded older rocks (Figure 3.12b) (Boggs, 2006, p. 404).

c) Nonconformity (Figure 3.12c)

Nonconformities form between older, weathered, or eroded igneous/metamorphic rocks and a younger sedimentary succession (Figure 3.12c) (Boggs, 2006; Catuneanu, 2006, p. 15).

d) Paraconformity (Figure 3.12d)

This type of unconformity is marked by beds which lie parallel to one another with no evident surface of erosion (Figure 3.12d) (Boggs, 2006, p. 405; Catuneanu, 2006, p. 15). The absence of a visible surface of erosion makes this type of unconformity very hard to identify in an outcrop. They are usually conformed by laboratory age determination methods or detailed facies studies (Bordy *et al.* 2004a, b; Boggs, p. 405, 2006; Catuneanu, 2006, p. 15).

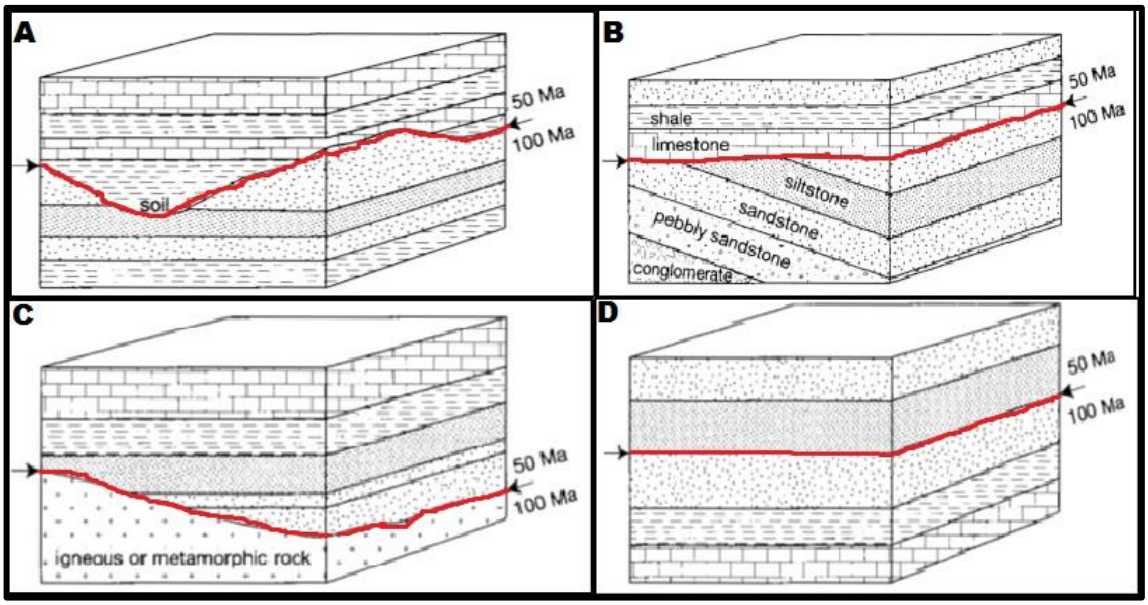

Figure 3.12: (a) Disconformity separating two units by an erosional surface, (b) angular unconformity showing an angular contact between two strata separated by an erosional surface, (c) nonconformity separating and older metamorphic or igneous rocks from younger sedimentary rocks (d) Paraconformity (Modified from Boggs, 2006, p. 404).

3.3.2 Economic importance of unconformities

Unconformities may be associated with major changes in permeability patterns of a succession or secondary mineral precipitations along the actual unconformity surface. This way unconformities can play a major role in hydrocarbon exploration allowing hydrocarbons to accumulate in a reservoir and restricting their further lateral or vertical migration (Shanmugam, 1988; Biddle and Wielchowsky, 1994; Boggs, 2006, p. 406). The different types of unconformities related to hydrocarbon traps are shown in Figure 3.13 (Biddle and Wielchowsky, 1994). According to Shanmugan (1988), reservoirs situated directly below an unconformity may have higher porosities because of the weathering and dissolution processes that occurred during the formation of the unconformity itself. In latter scenario, unconformities and the strata below may also act as a migration pathway of hydrocarbons (e.g., high permeability layer overlain by low permeability layer – see the case of the buried erosional relief/hill in Figure 3.13a) (Biddle and Wielchowsky, 1994).

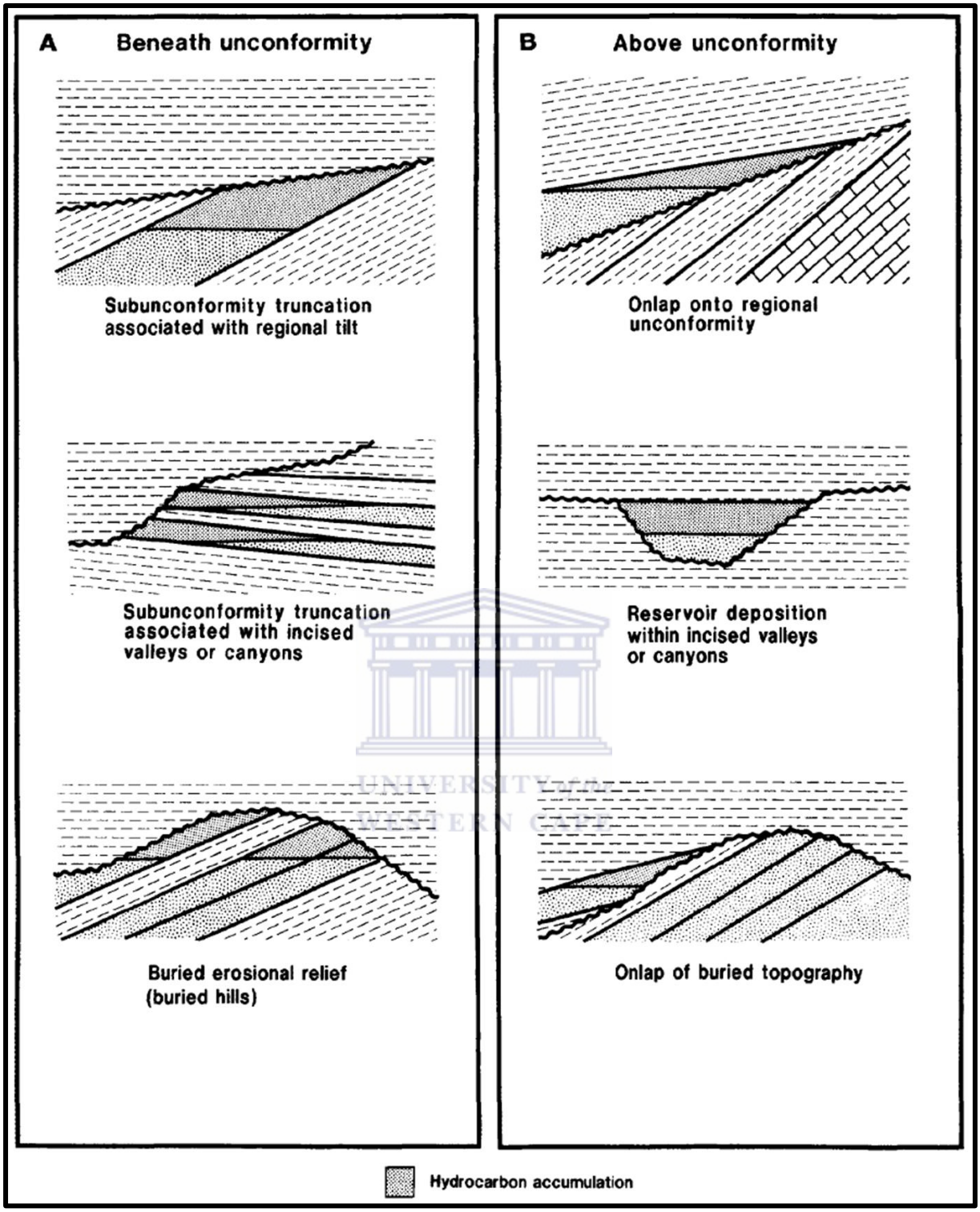

Figure 3.13: Different types of unconformity traps. (a) Traps beneath an unconformity (b) Traps above an unconformity. (Source: Biddle and Wielchowsky, 1994).

4 DATA AND METHODOLOGY

4.1 Data

SASOL Petroleum International (SPI) and VAALCO Energy supplied the data used, which are from the EPM as outlined in Figure 4. They include:

-Two 3D seismic volume profiles, which were processed using Pre-Stack Time Migration and Pre-Stack Depth Migration (PSTM and PDSM, respectively);

- An interpretation of the base of the salt (Gamba sandstone top) in depth and

-Twenty-six wells containing density, gamma ray and sonic logs (the three logs were not run in all wells, some wells do not have other logs).

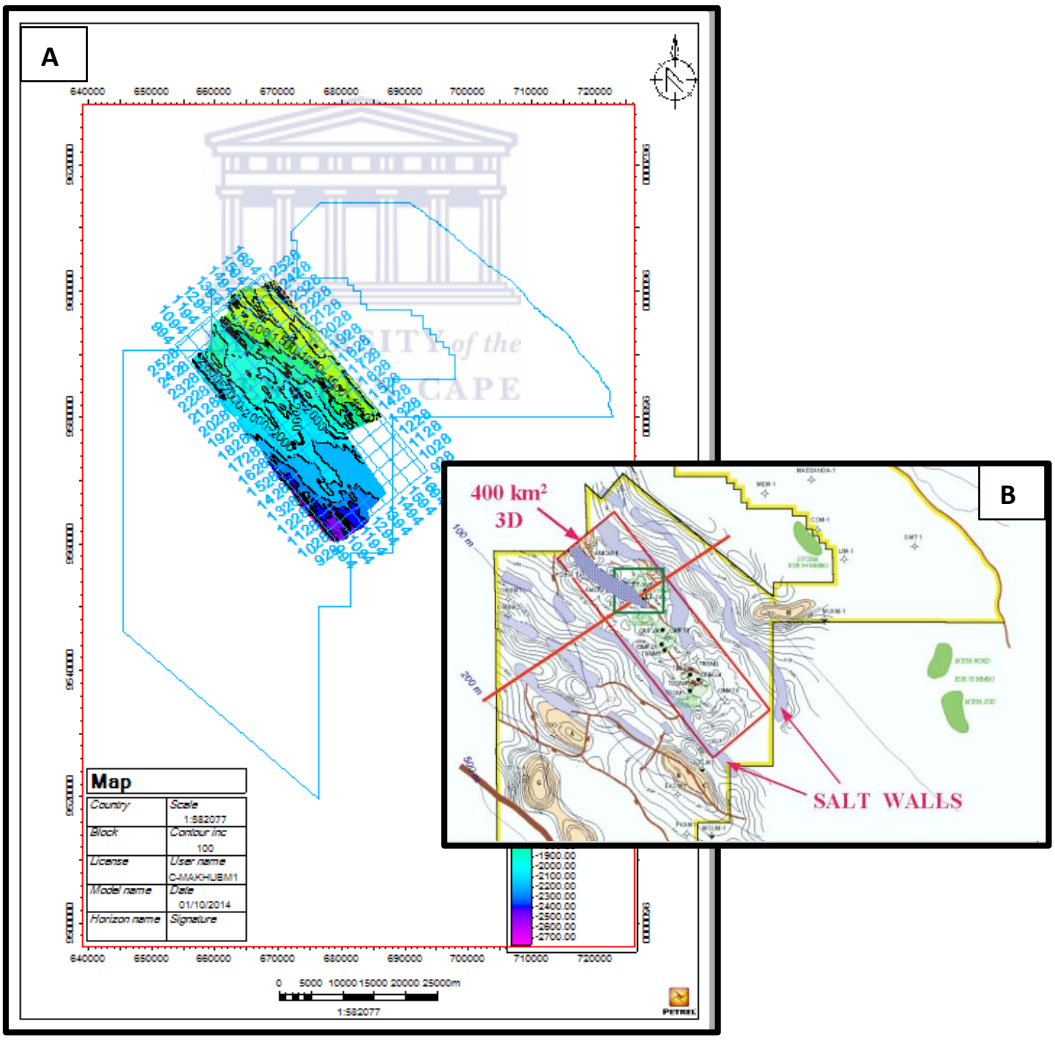

Figure 4.1: (a) Outline of EMP, with depth map outlying our study are within EMP. (b) Location of a study which was conducted by Gill and Cameron, (2002) covering the same area.

SEG-Y format seismic data were loaded and interpreted using Petrel® Interpretation software (Version 2012.1). Using welltop information, major reflectors were picked; this was followed by an interpretation of the position of major faults. The outputs created were of surfaces in two way time. Usually displayed in milliseconds (ms) in seismic profiles, two way time (TWT) is the time it takes a seismic wave to reach a subsurface layer from the source and return back to the receiver which is at surface (Sheriff, 1977). The surfaces were then depth converted by creating velocity models, which were then used to create thickness maps. This was followed by seismic stratigraphic interpretation, salt modelling, and basin restoration. Figure 4.2 shows the work flow that was followed during this study.

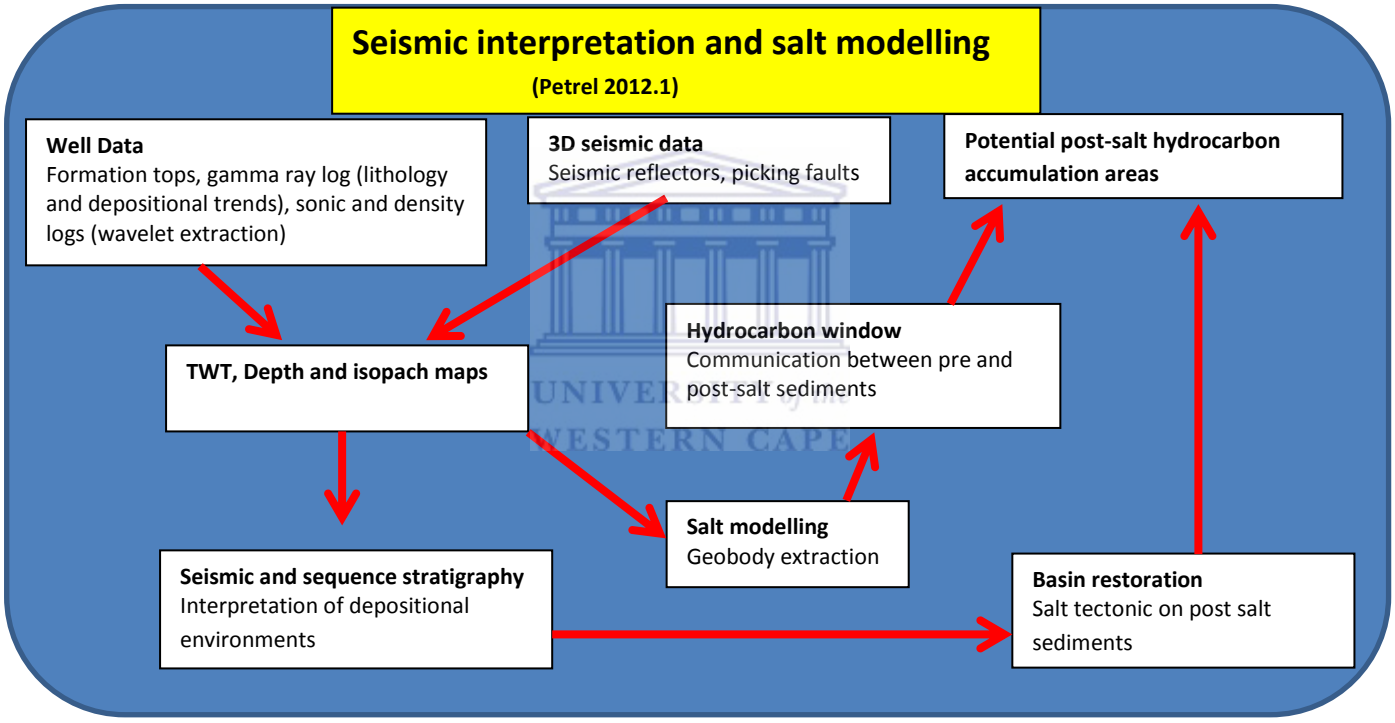

Figure 4.2: Flow chart showing the procedure followed in this study. Chart was modified after Boyd, 2010.

4.2 Well data

Well dataset was loaded as ASCII files in Petrel® and used for well-seismic tie and also helped in picking the seismic reflectors. Gamma ray logs, which measure the response of natural radioactivity of potassium (K40), thorium (Th232) and uranium (U238), were used for correlation and also interpreting depositional trends in the post-salt deposits (Merkel, 1979; Schlumberger, 1989). These elements tend to be higher in clays and shales, so if the gamma ray response is higher, the lithology is usually identified as shale or clay. In clean sandstones, evaporites and carbonates where radioactive elements are low, a low reading

gamma ray response will be observed (Merkel, 1979; Schlumberger, 1989). Gamma ray is measured in API (American Petroleum Institute) units ranging from 0-100, or 0-150 API. However in our case, where we have high gamma ray response and very low gamma ray response, our scale was set to 0-200 API, this was done so that lithologies can be fully defined. In order to define the limits of shale and sand in the gamma ray, equation 4.1 was used as defined in Merkel (1979); Schlumberger (1989), resulting in a shale line cut off set at 50 API units.

$$\text{Vshale}(\%) = \frac{(\text{GRlog} - \text{GRmin})}{(\text{GRmax} - \text{GRmin})} \quad \ldots\ldots\ldots\ldots\ldots\ldots\ldots\ldots\ldots\ldots\ldots\ldots 4.1$$

Where GRlog- average gamma ray response

GRmin- lowest gamma ray response in the lithology of interest

GRmax- highest gamma ray response in the lithology of interest

Sonic logs, which were used to extract velocities, measure the subsurface acoustic slowness, or the time that is taken by an acoustic pulse to travel through subsurface rocks (Merkel, 1979; Schlumberger, 1989). Δt (acoustic slowness), is inversely proportional to the P-wave velocity (1/velocity P-wave) (Schlumberger, 1989). The value of Δt increases with the degree of compaction of sediments, and also increases with depth, this is because deeper sediments are more compacted, hence in shallow, less compacted sediments, the value of Δt will be less (Schlumberger, 1989). Density log, which was also used, measures the attenuation of gamma ray (Merkel, 1979; Schlumberger, 1989). The combination of density and sonic log define the acoustic impedance. The acoustic impedance is then used in seismic-to-well tie, where synthetic wavelets can be extracted to tie the well information with the seismic data (Figure 4.3).

Table 4.1 summarises the well information, indicating hydrocarbon shows in the wells. This information will be used in a later section, where we will be investigating if hydrocarbons could have migrated through windows within the Ezanga salt, based on the proximity of the well and the window.

Table 4.1: Hydrocarbon shows information per well.

Oil wells	Dry wells with Oil shows	Dry well with Gas shows	Dry wells
EMP6	EMP22	EMP18	EMP1
EMP6.2	EMP21		EMP2
EMP6.3	EMP20		EMP6.4
EMP7			EMP6.5
EMP8			EMP11
EMP9			EMP12
EMP10			EMP15
EMP10.2			EMP16
EMP13.2			EMP21
EMP13			EMP23
			EMP25

4.3 Seismic Data

Seismic reflection occurs as a result of the product of the velocity and density of two subsurface layers, this is referred to as acoustic impedance (equation 4.2) (Sheriff, 1977). Acoustic impedance is then used to calculate the reflection coefficient, which is the fraction of amount of rays that are reflected back to the surface, as given in equation 4.3 (Sheriff, 1977). Using the sonic (Vp) and gamma ray (Gr) logs, velocity and density can be extracted from the two logs, respectively. Such information is used to create a synthetic seismic trace, which can be used to tie the well data with seismic data. Figure 4.3 is a simplified diagram indicating how synthetic seismic trace is created by convolving a pulse with reflection coefficient. Zero phase wavelet was extracted, which is symmetrical about the reflection coefficient, the arrival time of the peak is not frequency dependant, reflection coefficient is at the maximum displacement. However since there is motion before wave arrival, zero phase wavelet is not physical (Hampson and Galbraith, 1981). The advantage of zero phase wavelet is that it gives an optimum resolution and eases the process of seismic interpretation (Hampson and Galbraith, 1981). The extracted wavelet has a usable frequency of 9-24Hz, the phase spectrum shows valid data where there is amplitude from 9-24 Hz (we can ignore anything >24Hz). Using the extracted wavelet, synthetic seismogram was extracted by convolving the zero phase wavelet with the reflection coefficient (Figure 4.3) (as given by equation 4.3).

$Z=\rho V$……...4.2

$$R = \frac{\rho 2V2 - \rho 1V1}{\rho 2V2 + \rho 1V1} = \frac{Z2 - Z1}{Z2 + Z1}$$……...……..……4.3

Where: Z-acoustic impedance
R-reflection coefficient
ρ –density ($g.cm^{-3}$)
V-velocity ($m.s^{-1}$)

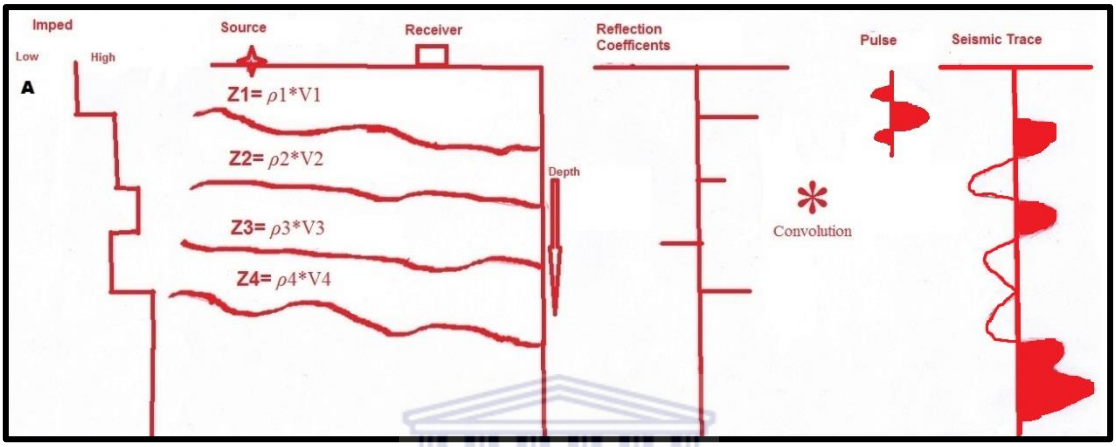

Figure 4.3: (a) Acoustic structure of the earth showing steps in creating a synthetic seismic trace by convolving a seismic pulse with reflection coefficient using the density and velocity of the subsurface lithology (modified after http://www.aapg.org/slide_resources/schroeder/6/index.cfm).

PSDM (pre-stack depth migration) 3D seismic volume was used to interpret the seismic section (i.e. picking reflectors, faults, etc.), this is because PSDM produces accurate images of the subsurface, where the resulting seismic image will have consistent geological features, with mapped faults and depth having an accuracy of close to real structures (Gray, 2000; Littau and Koremblit, 2011). To process seismic data using PSDM method, a velocity model is needed, which requires knowledge of the subsurface velocity (Littau and Koremblit, 2011). The disadvantage of using PSDM is that there is no unique answer, many models can be created based on who is processing the data, also because this method is expensive, companies do not run it on routine basis (Veeken, 2007, p. 21; Littau and Koremblit, 2011). Furthermore the highly variable velocities of the Madiela carbonates and Ezanga salts, makes it difficult to create a layered velocity model, and as such PDSM is more favourable (Mantovani and Dugoujard 2010; Dupre *et al.,* 2007). PSTM (pre-stack time migration) method uses consistent velocity, where a simple model can be created, (Littau and Koremblit, 2011). However the disadvantage of PSTM is that, when there is lateral velocity variation (such as within the Madiela carbonates and the salts), PSTM laterally places structures and amplitude in the wrong position (Littau and Koremblit, 2011). Figure 4.4 shows comparison

between PSDM and PSTM, showing that if the velocity model is more accurate, depth migration will result in better resolution, hence PSDM will be favoured for interpretations (Veeken, 2007, p. 32).

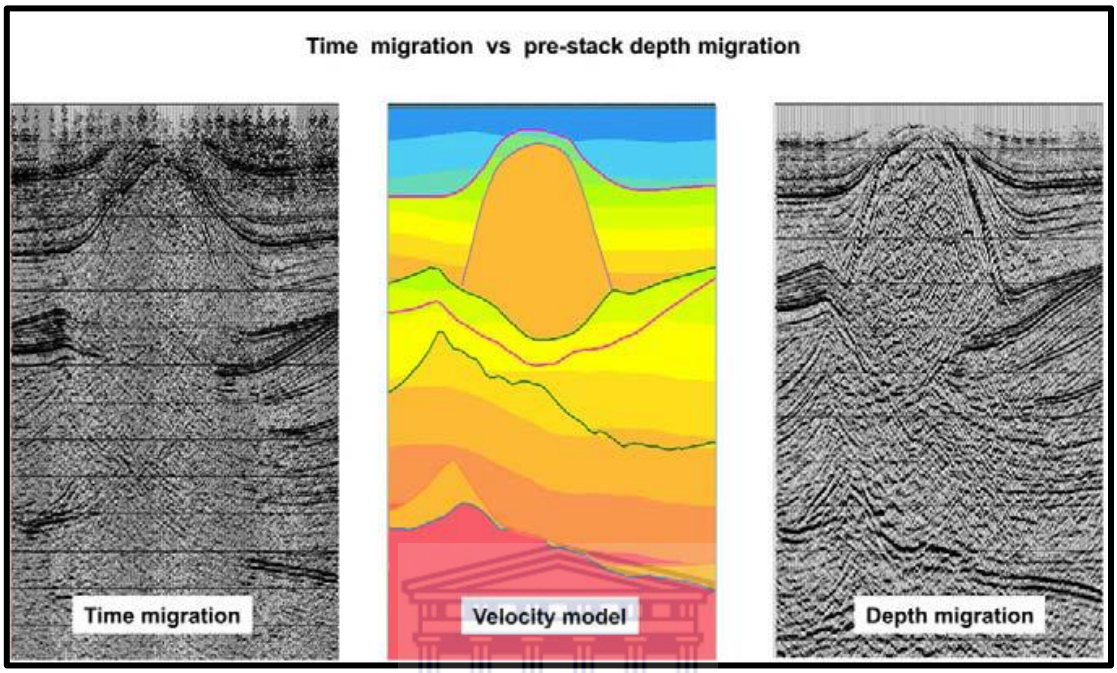

Figure 4.4: Comparison between PSDM and PSTM. Because the velocity model created is more accurate, PSDM will show a high resolution than PSTM (Source: Veeken, 2007, p. 32).

After extracting the wavelet and tying in the seismic and the well data, sonic log derived average velocities and extracted instantaneous frequency were used to calculate vertical and horizontal resolution to see if welltops can be resolved on a seismic section. This required a good understanding of the subsurface velocity and frequency. According to Brown (1999), typical velocities range from 2000 m/s in shallow, less consolidated sediments to 5000 m/s in igneous and deeper rocks, which have been metamorphosed, with carbonates and evaporites having velocities of 3500 m/s to 5000 m/s. Therefore, in general, due to compaction with increasing depth, velocity increases with depth (Figure 4.5). Two other major parameters in seismic interpretations, which are used to define the resolution of the seismic data are frequency and wavelength (Brown, 1999). Frequency decreases with depth, this is because the deeper you go, higher frequencies are attenuated and only low frequencies can reach greater depth. Higher frequencies are attenuated with depth because seismic signal is rapidly attenuated with depth and typically ranges from 50 to 20 Hz (Brown, 1999; Eilertsen, 2010). Wavelength increase with depth and as a result, resolution decreases with depth, and is typically 20 to 50 m (Brown, 1999; Eilertsen, 2010). However, the large velocity variation in

the Madiela carbonates and evaporites increase the uncertainty in calculating the resolution of those sequences. Figure 4.5 shows the relationship between, velocity, depth, frequency and wavelength.

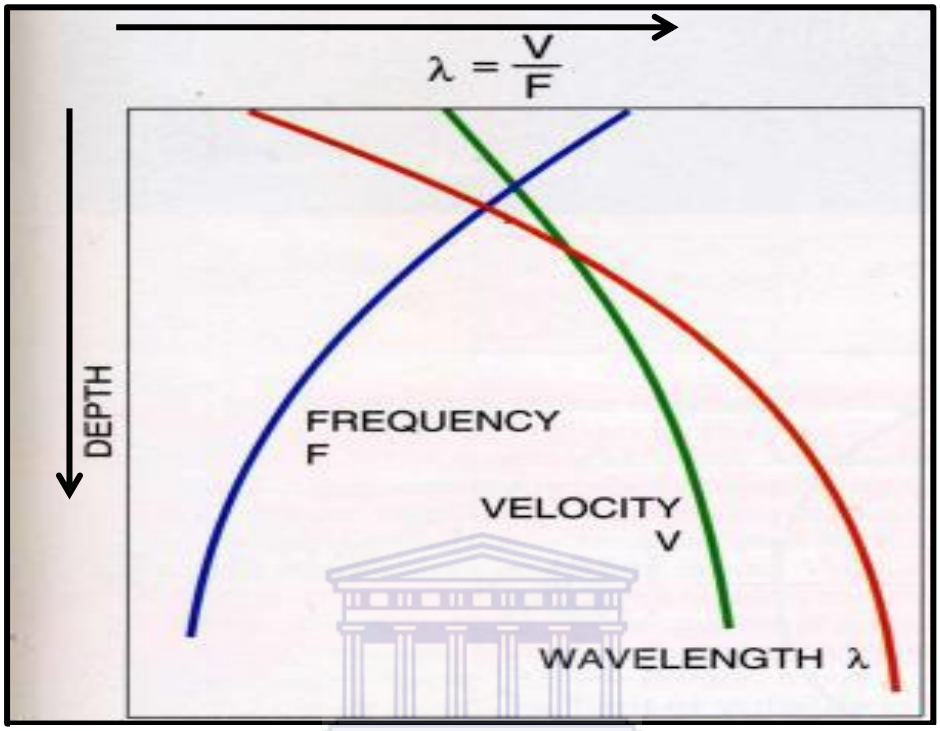

Figure 4.5: The relationship between, depth, velocity, wavelength and frequency, with velocity and wavelength both increasing with depth and frequency decreasing with time (Source: Brown, 1999).

Knowledge of seismic resolutions allows us to interpret seismic volume efficiently. Sheriff (1977) and Cartwrite and Huuse (2005) define resolution as the ability to be able to distinguish two features form each other on a seismic volume. Seismic resolution can be separated into vertical and lateral (Fresnel zone) resolution. The distance between two interfaces that is needed in order to give rise to one reflection for that reflection to be observed on a seismic section is called vertical resolution (Chopra *et al.*, 2006). According to Sheriff (1977) as well as Emery and Myers (1996), vertical resolution is determined by the frequency of the signal, the bandwidth of the seismic data, the internal velocity of strata of interest and the acoustic impedance between two layers. Geological features/structures that will be less than the calculated vertical resolution as given by equation 4.5 will not be resolved in a seismic volume. Although equation 4.5 gives the best resolution estimate, it is a theoretical estimate because; the vertical resolution is reduced by noise (Long, 2003).

Vertical resolution

The wavelength is calculated by:
$\lambda = V/F$……..….4.4

The vertical seismic resolution is calculated by:
$\lambda/4$……....4.5

λ = Wavelength (m)
F = Seismic frequency (Hz)
V = Seismic velocity (m/s)

Horizontal resolution means when two lateral geological features can be recognised and distinguished as two different adjacent events (Chopra *et al.*, 2006). The subsurface sampling and trace spacing are the most important factors that control horizontal resolution of seismic data (Veeken, 2007, p. 39). Horizontal resolution is given by the Fresnel zone, where geological features which are smaller than the Fresnel zone will not be distinguishable in a seismic section (Hubral *et al.*, 1993). According to Veeken (2007, p. 39) and Hubral *et al.* (1993) the Fresnel zone increases with depth, velocity and a decreasing frequency. As indicated in Figure 4.6, $\lambda/4$ can be used to estimate the Horizontal resolution on a 3D seismic volume (Hubral *et al.*, 1993; Brown, 1999).Table 4.2 shows calculated values of both vertical and horizontal resolution.

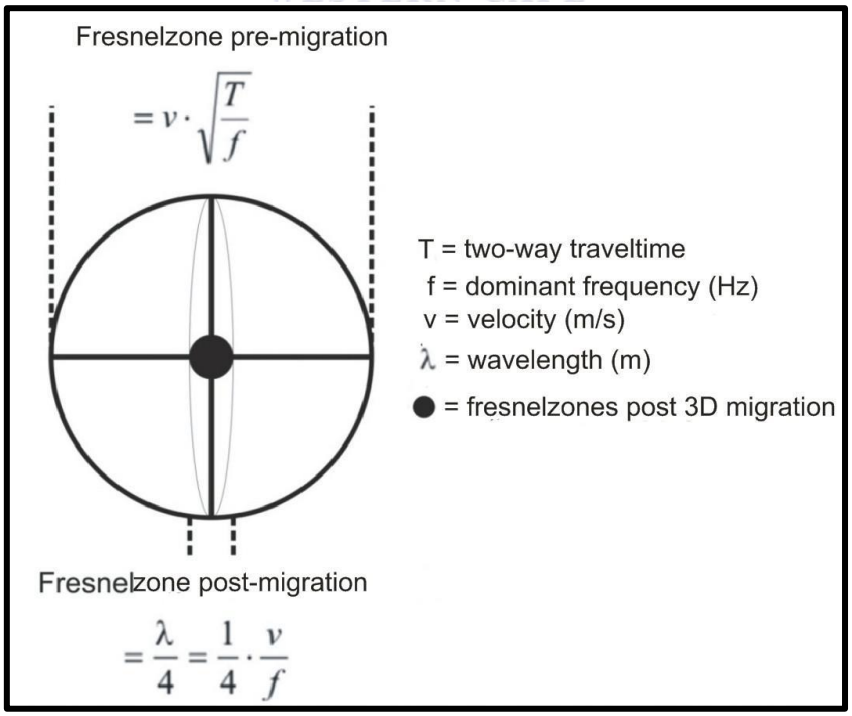

Figure 4.6: Fresnel zone showing the radius at which geological features can be picked up on a seismic section (Source: Brown, 1999)

Table 4.2: Estimated velocities and frequencies that were used to calculate the resolution of the seismic cube, calculations were done using well EMP18.

Formation	Average Velocity (m/s)	Frequency (Hz)	Wavelength (m)	Vertical resolution (m)	Horizontal resolution Post-migration (m)
Akasso	1800	50	36	9	9
M'Bega	2030	43	47	12	12
Animba	2345	40	59	15	15
Ewongue	2770	35	79	20	20
Azile	2990	30	100	25	25
Madiela	5540	14	396	99	99
Ezanga	4690	16	293	73	73
Gamba	3900	22	178	44	44

After picking major reflectors, surface maps in TWT were created, which were then depth converted in order to calculate sedimentation rates. Since seismic sections are in two way time, in order to estimate the depth to reflectors, equation 4.6 was used to make the time to depth conversions.

$$z = \frac{VT}{2} \qquad \ldots 4.6$$

Where z-depth (m)

V-velocity ($m.s^{-1}$)

T-travel time (s)

(We divide by 2 because this is two way time (TWT))

Converting TWT time surface maps into depth maps in Petrel® also takes into account the rate of velocity change (k) between the reflectors; this is because there is velocity gradient change with depth in our study area. Taking into account the rate of velocity change, the following equations as also defined by Dupre *et al.* (2007) was used:

$V(z) = Vo + kz$ ……...4.7

z depth (m)

V(z)-interval velocity ($m.s^{-1}$)

Vo-initial velocity ($m.s^{-1}$)

k-rate of change in velocity with increasing depth (s^{-1})

$V(t) = Vo \,.\, e^{kt}$ ……..4.8

t-one way travel time (s)

$z = Vo\,(e^{kt}-1)/k$……..4.9

Below are Petrel® -derived values of k, derived from well EMP18 by cross plotting the depth vs. interval velocity, where the gradient of the curve is the dimensionless k value (Figure 4.9 and 4.8). Figure 4.7 shows different trends within the depth (z) vs. interval velocity plot represent different lithology as interpreted in chapter 5. Figure 4.8 was then derived using the cross plots in Figure 4.7 in order to calculate the gradient k. The values of k derived from Petrel® were compared with the values that were obtained by Dupre *et al.* (2007) (see chapter 5). Table 4.3 gives the values of k that were obtained for each reflection package, with the Gamba sandstone used as an example to show how the k value was calculated (Figure 4.8). Welltop information provided in well EMP18 was used to QC the trends identified, to check if the depth corresponded with the interpreted lithology.

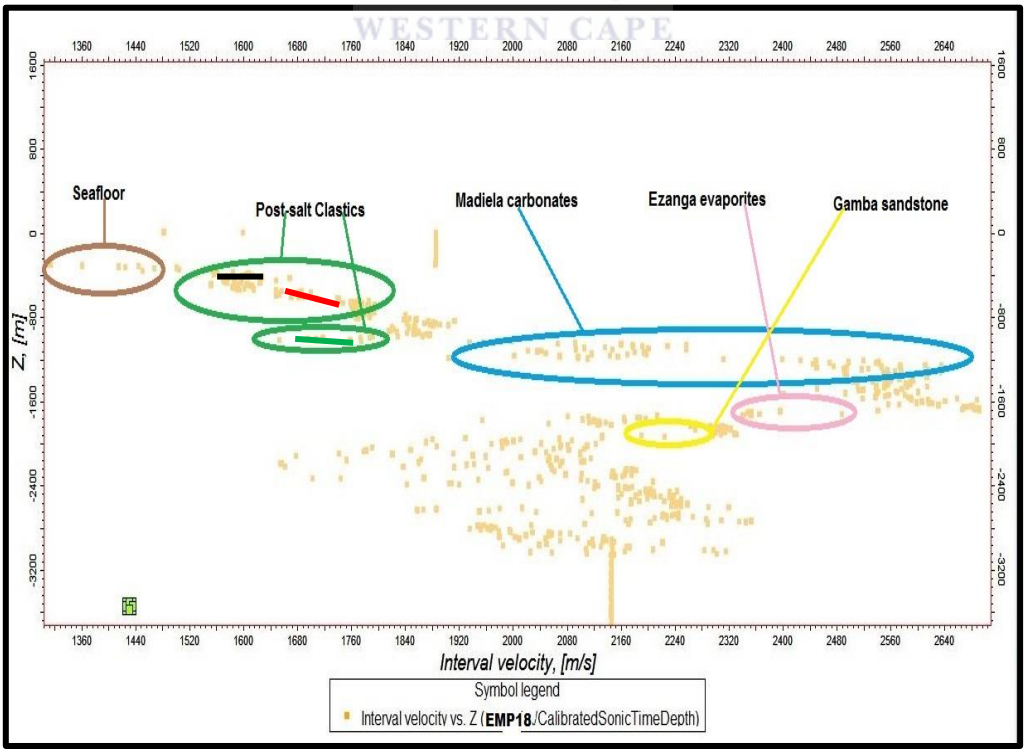

Figure 4.7: Depth vs interval velocity plot derived from Petrel® , indicating trends which were used to estimate the value of k, which was used to create velocity models, based on EMP18 well.

Table 4.3: Calculated k-values based on the interval velocity gradient.

Reflector	k-value
A3	0.07
M2	0.3
A2	0.1
E2	0.2
A1	-1.3
M1	0.43
E1	0.08
G	-0.8

Gamba sandstone

$$k = \frac{\Delta z}{\Delta Vint}$$

$$= \frac{1868-1948}{2280-2180}$$

$$= -0.8$$

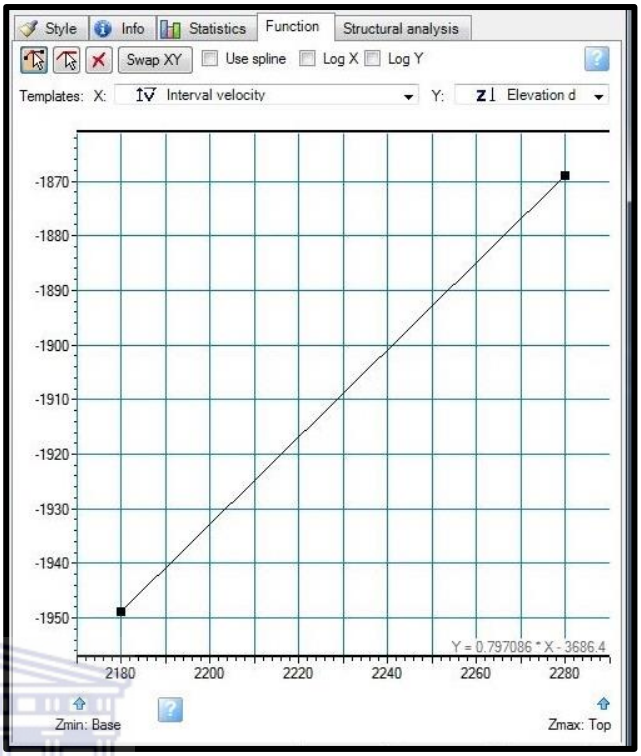

Figure 4.8: Gamba Depth vs. interval velocity cross plot.

Using depth maps, thickness maps were created by subtracting the value of the depth of top of the reflector of interest to the top of the undelaying reflector. From thickness maps, sediment transport direction and the depocenter were determined. Using gamma ray logs, depositional trends were interpreted and correlated across the study area, this was followed seismic stratigraphic interpretations. The combination of both gamma ray and seismic stratigraphic study allowed us to create depositional models for the Lower Congo Basin, and hence identify potential hydrocarbon reservoirs, traps and also create model to see if there are windows in the Ezanga salt.

5 RESULTS AND INTERPRETATIONS

5.1 Seismic interpretation

Eight stratigraphic units were identified in the study area using seismic, sequence stratigraphic and welltop information (e.g., seismic facies changes, stratal terminations) and regional geological consensus (e.g., Gill and Cameron, 2002; Jackson *et al.,* 2008; etc.). When welltop information was unavailable, the units were picked based on seismic and sequence stratigraphic principles only. These stratigraphic units represent the Late Cretaceous to recent transitional and drift-sag tectonic phases of basin evolution (Figure 1.3).

Due to the limited resolution of the current seismic profiles, units G and E1 (Gamba and Vembo Formations and Ezanga evaporates (Ezanga salt and anhydrite), respectively) cannot be identified as individual reflectors, due to their limited vertical resolution of 40 m and 70 m respectively (see calculations in Chapter 4). A1, E2, A2, M2 and A3 reflectors were picked based on the stratal terminations, which were seen on the seismic section and also by inferences from literature. Figure 5.1a, 5.1b and 5.2a, 5.2b show the interpreted inline 1075 and crossline 1889 respectively, with (a) showing interpretations to the top of the sequence and (b) showing stratigraphic unit. Unless or otherwise stated, all inlines derived from the data have a NW-SE strike, with crosslines striking SW-NE and both (crossline and inlines) were interpreted at 10 increments spacing on Petrel®. The vertical distance of the seismic data is in two way time (TWT) expressed in milliseconds and the horizontal distance is showed by a scale bar in metres, unless otherwise stated.

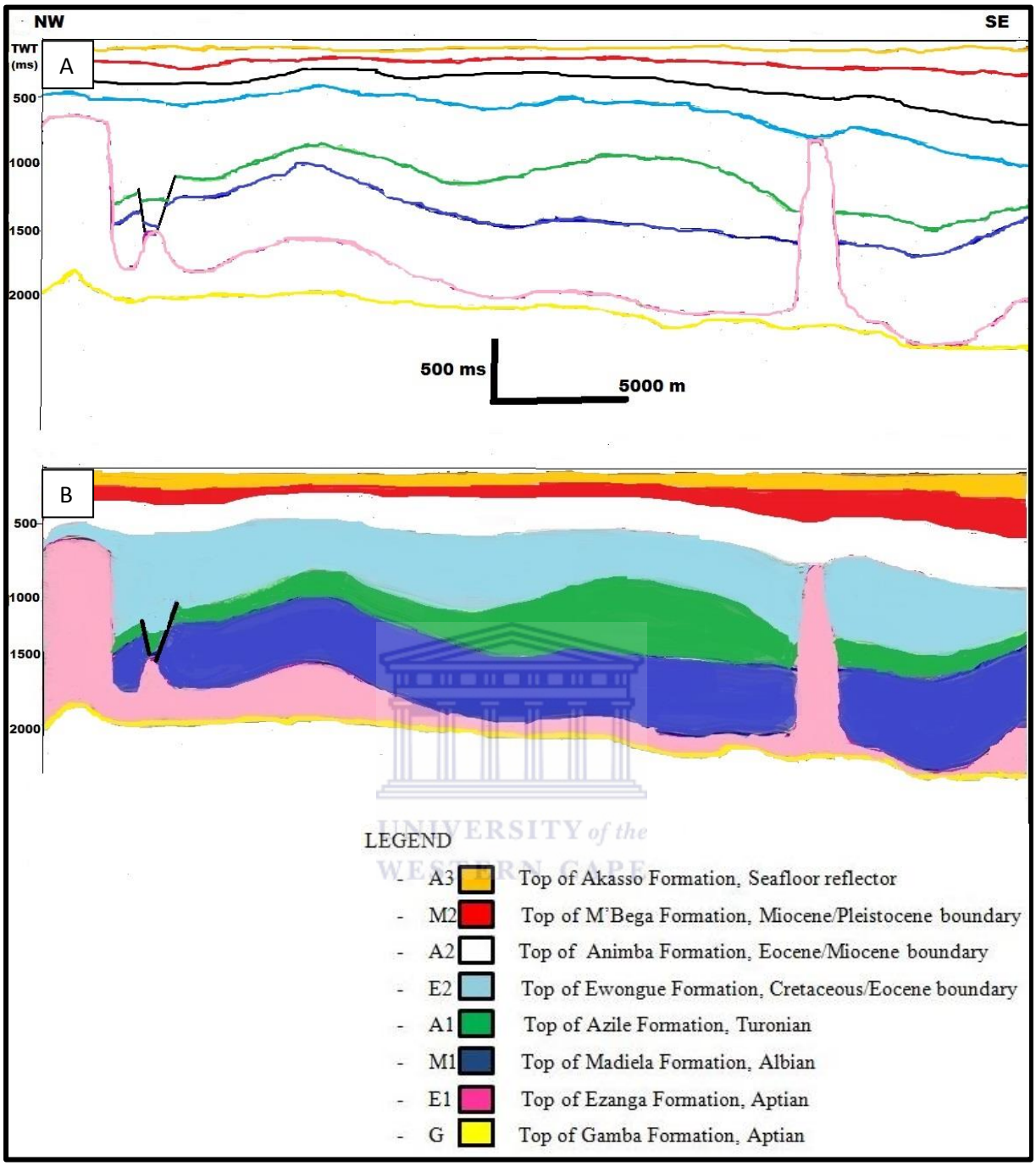

Figure 5.1: Inline 1075, representing major stratigraphic boundaries deposited during transitional and rift-drift phase. (a) Interpretation to the top of a stratigraphic boundary and (b) represents the stratigraphic unit.

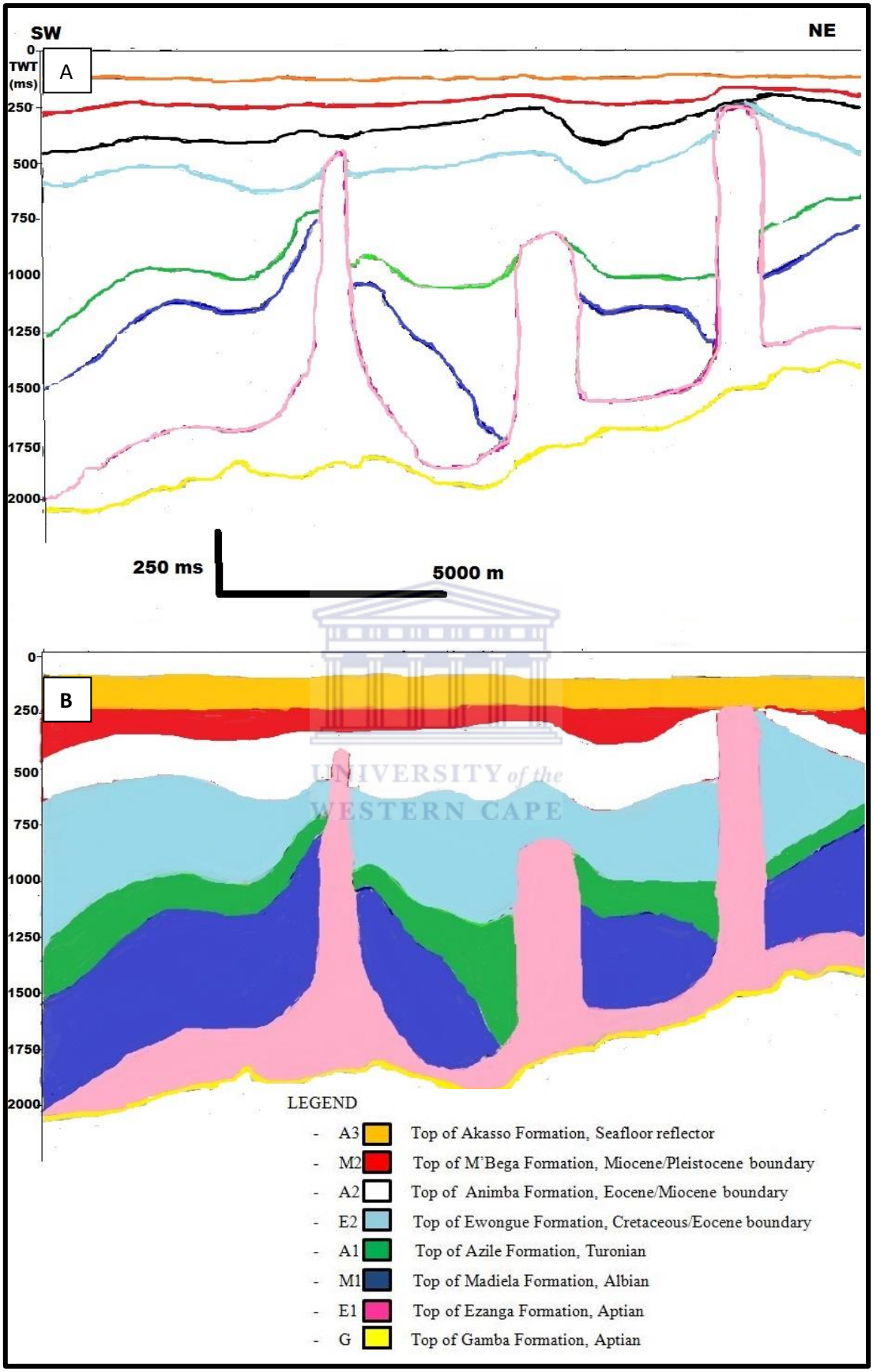

Figure 5.2: Interpretation of crossline 1889, representing major stratigraphic boundaries deposited during transitional and rift-drift phase. (a) Interpretation to the top of a stratigraphic boundary and (b) represents the stratigraphic unit.

5.2 Surface and thickness map

Using Petrel® software, thickness maps were created by first picking reflectors and generating TWT surfaces maps, which were then depth converted using the velocity modelling option. Dupre *et al.* (2007) and Mantovani and Dugoujard (2010) state that the varying lateral and horizontal velocities of carbonates and salt limits the generation of a layered cake velocity model, so in order to quality check (QC) the depth of each reflector, depth conversions were done one reflector at a time. Welltops were used to QC isopach (true stratigraphic thickness) maps created and asses if they reflect the actual stratigraphic thickness and show the correct position of the depocenters. According to Dupre *et al.* (2007) these types of depth conversions can have an uncertainty of 100 to 200 m. Due to the interplay between RSL changes, rate of sediment supply and the available accommodation space, the isopach maps of the various stratigraphic units differ significantly from each other (Boyd, 2010). Studying thickness change of each stratigraphic unit from the isopach maps created (e.g., the different location of the depocenters in the successive maps) insights into the evolution of the basin in the study area through geological time can be achieved. Well EMP16 was used to QC the maps created and also calculate the rate of velocity change (k-value), which were then compared with those published in Dupre *et al.* (2007) (Table 5.1 and 5.2). Interval velocities were derived from sonic logs.

Table 5.1: Depth estimation to top of interpreted reflectors using sonic derived velocities and two way time from well EMP16.

Reflector	Average interval velocity (m/s)	TWT (s)	Petrel® formation tops (depth in m)	Formation tops (depth in m)	Literature k value (1/s)	Calculated k value (1/s)
A3	1800	0.13	97.5	-	0.00	0.07
M2	2030	0.16	121.6	-	-	0.3
A2	2345	0.17	193.69	-	-	0.1
E2	2770	0.25	258.66	-	-	0.2
A1	2990	0.46	428.66	-	-	-1.3
M1	5540	0.51	601.26	600.28	0.45	0.43
E1	4690	1.20	1185.54	1193.4	0.00	0.08
G	3900	2.20	2203.70	2214	0.85	0.8

Reflector G is interpreted to represent the top of the Gamba sandstone. The depth to the top of Gamba sandstone (reflector G) varies from 1700 to 2200 m and dips towards the south (Figure 5.3). This reflector is also considered to be the replica of the contact between pre-salt

Gamba sands and post-salt sediments within the study area. It is particularly important in areas where the salt diapirs create possible migration pathway for pre-salt sourced hydrocarbons by detaching from the main salt layer and then penetrating into the Gamba sandstone and younger sedimentary layers (see section 5.5).

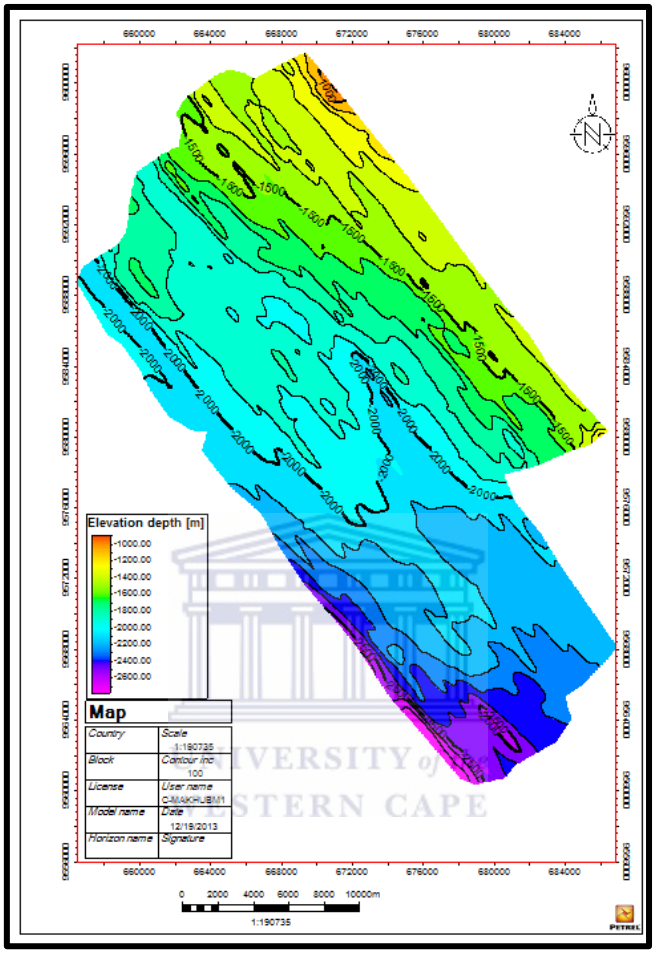

Figure 5.3: Depth map to top of the south dipping Gamba sandstone, which is the main reservoir in EMP.

Reflector E1 marks top of the south dipping Aptian Ezanga evaporites, which, due to diapirism has varying depths of 250 to 2000 m (Figures 5.4a and 5.4b). Thickness of evaporate could range from 0 to 2000 m, although the vertical resolution in the dataset is 77m, therefore the lower end of this range is uncertain (Figure 5.4a and 5.4b). The diapirs have a NW-SE strike, appear to be connected, subvertical, parallel to each other and the main fault plane (which is parallel to the shoreline as discussed in section 1.3.1) (Dupre *et al.*, 2007) . Although there are no exact salt thicknesses published in the literature for the study area, the pre-diapirism evaporite thicknesses of ~1000 m in Angola and ~600 m in the south Gabon region,were reported by Dupre *et al.* (2007) and Jackson *et al.* (2008). Without the exact depositional thickness of the evaporites, determining sedimentation and subsidence rates of the Aptian period is difficult (Dupre *et al.*, 2007).

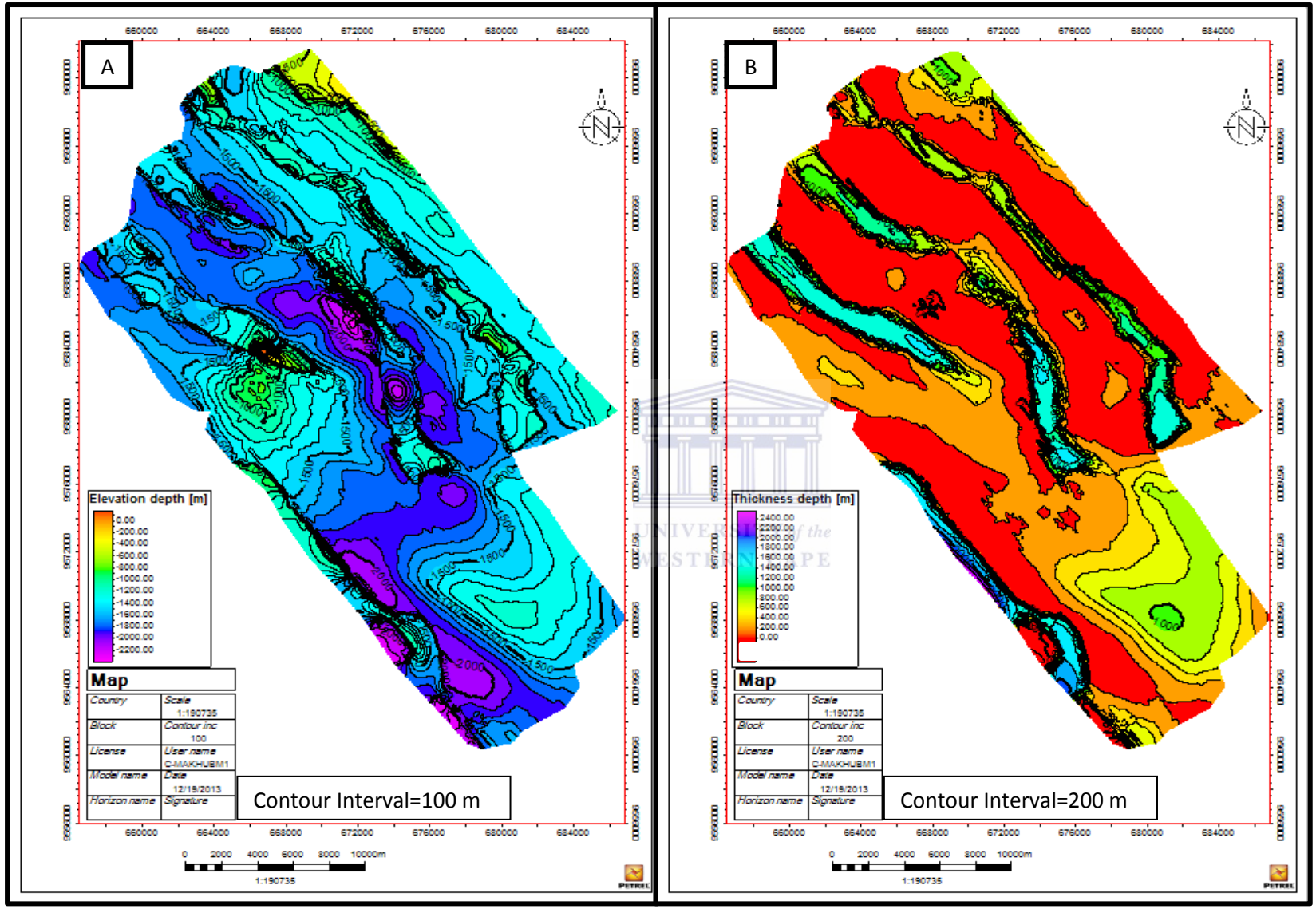

Figure 5.4: (a) Depth map to the top of the evaporites, with very shallow depth representing top of the diapirs, (b) stratigraphic thickness of the Aptian salt, with thicker sections indicating diapirs.

Marking the top of Madiela carbonates is the south dipping reflector M1, at depths ranging from 450 to 1500 m, with the average thickness of the carbonates being 500 m (Figures 5.5a and 5.5b). Isolated thicknesses of 0 to 200 m in Figure 5.5b are caused by diapirs penetrating from below but have not yet pierced through the Madiela Formation, areas which have been pierced through by diapirs are not seen as holes on the maps because Petrel® software extrapolate over the holes. Hudec and Jackson (2004) and Dupre *at al.* (2007) indicate that during the Albian times, sedimentation rates were very high, reaching 100 m/Ma, where an average of ~800 m of shallow marine carbonates accumulated in ~13 Ma on the ~100 km wide NE-SW trending carbonate platform. Thickness of the carbonates in the EMP also indicates a high sedimentation rate, averaging at 39 m/Ma (Table 5.2). These carbonates, which were initially deposited as limestones are predominately made up of dolomite (secondary diagenetic product of the original limestones) (Pletsch *et al.*, 2001), using the carbonate Dunham carbonates classification model and also as defined by Richard (1989), Madiela carbonates were formed in shallow marine conditions (Seranne and Anka, 2005 and Dupre *et al.*, 2007).

Reflector A1 is at depth of 450 to 1000 m, marking the top of south dipping, 100 to 400 m thick Azile clastics (Turonian) (Figures 5.6a and 5.6b). The depocenter is towards the NW of the the EMP, thinning out toward the south (Figure 5.6b). The thickest portions (~600 m deep), are interpreted as channel fills. The shape and orientation of the feature may also indicate that transport direction was possibly from the NW (Figure 5.6b). An alternative interpretation could be that the geometry of the Azile clastics are due to salt withdrawal; a higher resolution seismic facies could have been used to determine if these geometries are associated with erosional channels vs. passive infill. According to Dupre *et al.* (2007), average sedimentation rates were 50 m/Ma in the Cenomanian-Turonian, indicating a decrease in sedimentation in comparison to the Albian time. Considering that the Cenomanian-Turonian represent ~10 Ma, sedimentation rates of the Azile package can be assumed to have been about 10 to 40 m/Ma in the study area (average 23 m/Ma).

Reflector E2 marks the south dipping, 100 to 500 m (average of 300 m) thick Ewongue Formation (Senonian), intersected at depths of 250 to 600 m (Figures 5.7a and 5.7b). The Senonian is a European Epoch from 89.3 Ma to 65.5 Ma, containing the following stages of the International Commission on Stratigraphy (ICS): Coniacian (89.3 - 85.8 Ma), Santonian (85.8 - 83.5 Ma), Campanian (83.5 - 70.6 Ma) and Maastrichtian (70.6 - 65.5 Ma). The depocenter was also towards the NW (Figure 5.7b), with sedimentation direction also from NW to SE, as evident by the channel fill features occurring within this package. Senonian sediments were deposited for ~15 Ma (from the Turonian to the Campanian major uplift 75 Ma) (Seranne and Anka, 2005), which suggests sedimentation rates of 7 to 33 m/Ma, averaging (average 20 m/Ma).

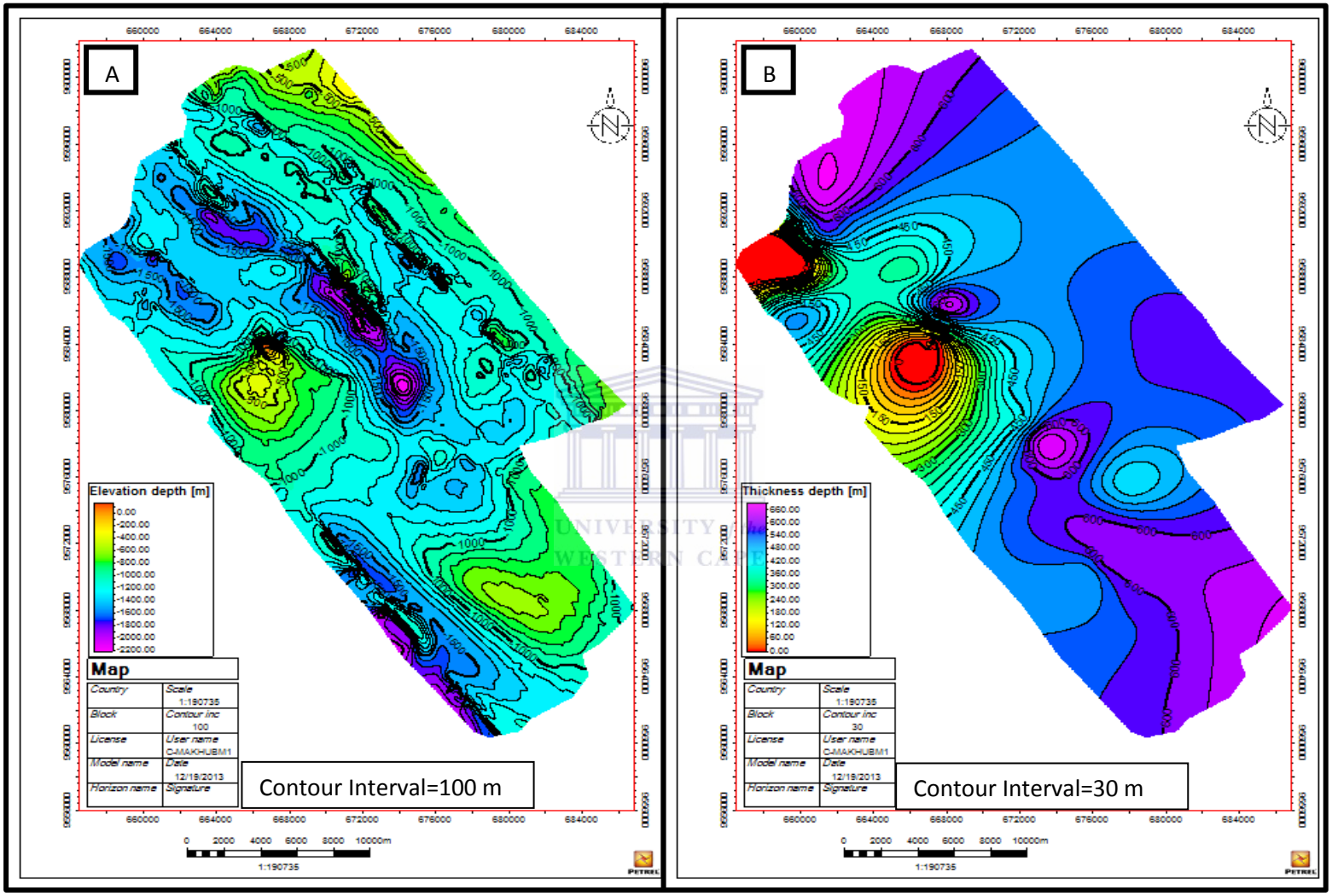

Figure 5.5: (a) Depth map to the top of Madiela carbonates, shallow parts are diapirs that have pierced through the carbonates, (b) stratigraphic thickness of Madiela carbonates, areas where the thickness is close to zero are areas where there is a diapir is rising below carbonates, but have not yet pierced through the entire formation.

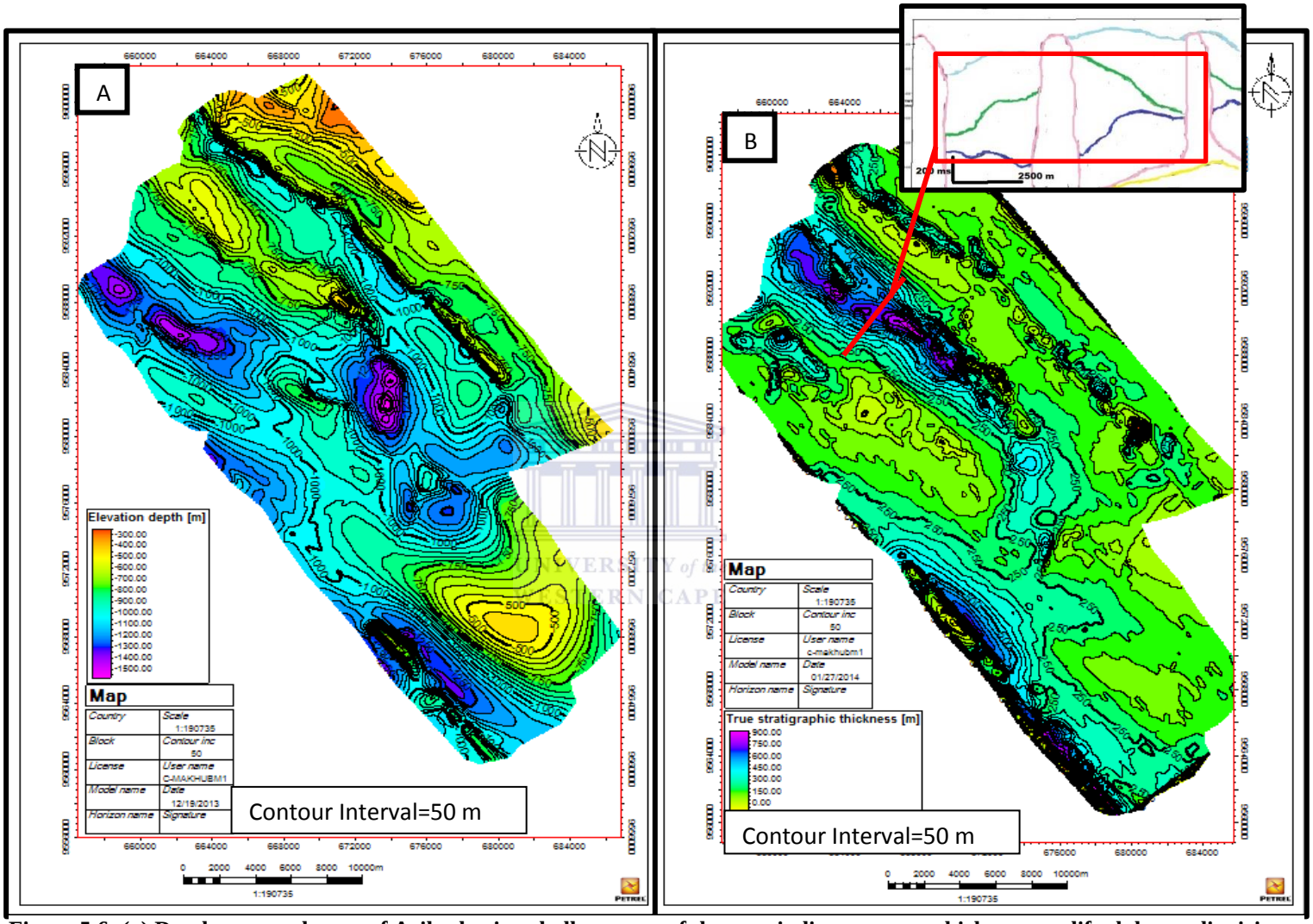

Figure 5.6: (a) Depth map to the top of Azile clastics, shallow parts of the map indicates areas which were uplifted due to diapirism (b) stratigraphic thickness of the Azile Formation, with the thickest part of the map indicating a channel feature which was used to infer the NW to SE sediments transport direction.

After the Campanian uplift and erosion (Seranne and Anka, 2005; Jackson *et al.,* 2008), Palaeocene sediments were deposited basinwards and not preserved at the shelf. therefore at depths varying from 150 to 450 m is reflector A2, which marks the top of the south dipping, 80 to 350 m thick (averaging at 215 m) Animba Formation (Eocene) (Figures 5.8a and 5.8b). According to Sarenne and Anka (2005); Dupre *et al.* (2007), the Eocene was a period of little sedimentation on the shelf, and since the Animba Formation took ~23 Ma to accumulate (from the ~75 Ma ago to the end of the Eocene), this means that sedimentation rates were 3.5 to 15.2 m/Ma (average at 9.3 m/Ma).

Reflector M2, which is at a depth of 150 to 450 m, marks the top of M'Bega Formation (Miocene), with thickness of 40 to 300 m (average 170 m) (Figures 5.9a and 5.9b). Sedimentation transport direction changed from NW to SE in the Cretaceous and the Eocene to more from NE/E to SW/W in the Miocene (Figure 5.9b). This was after a major climate change in the Oligocene coupled with the uplift of the African continent, hence these changes might have influenced alteration of sedimentation transport direction (Hudec and Jackson, 2004; Seranne and Anka, 2005; Dupre *et al.*, 2007; Jackson e*t al.,* 2008). Since the Miocene sediments were deposited in ~18 Ma, sedimentation rates ranged from 2.2 to 16.6 m/Ma (average 9.4 m/Ma). According to Rasmussen (1996), the shelf area offshore Gabon was uplifted in the Miocene, hence the low sedimentation rates in the shelf EMP section and larger expected depositional rates in basinwards direction.

Reflector A3 (or the seafloor reflector) marks top the youngest 10-200 m (average 100 m) thick Akasso Formation (Pleistocene), dipping slightly towards the south west, and is intersected at depths of 100 to 135 m (Figures 5.10a and 5.10b). The depocenter is towards the east. These sediments have been accumulating for the past 2.5 Ma, resulting in 38 m/Ma average Pleistocene sedimentation rates.

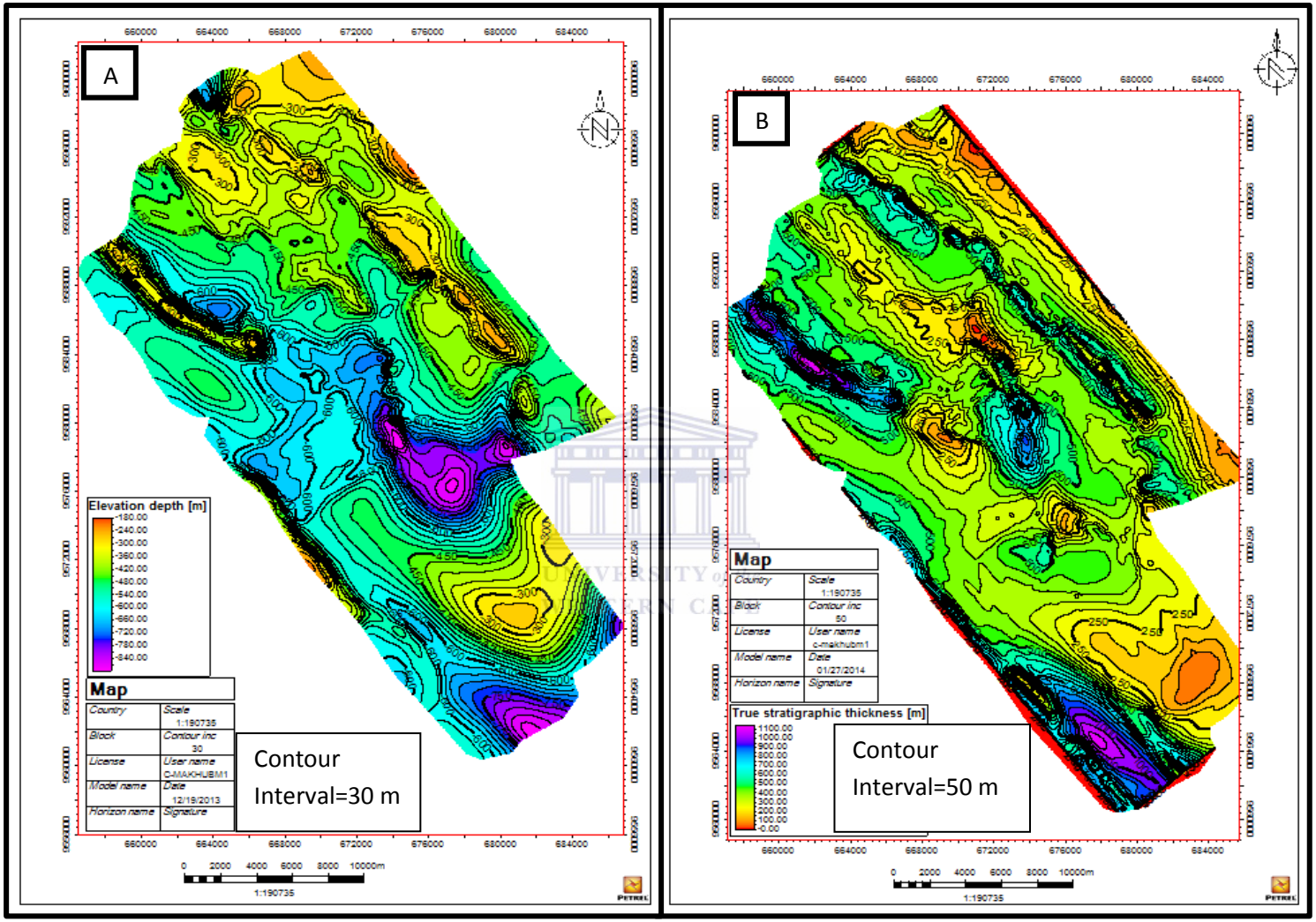

Figure 5.7: (a) Depth map to top of the Ewongue Formation, with very shallow part of the map indicating areas being pushed up by diapirs, (b) stratigraphic thickness of Ewongue Formation, also showing channel features such as in the Azile formation.

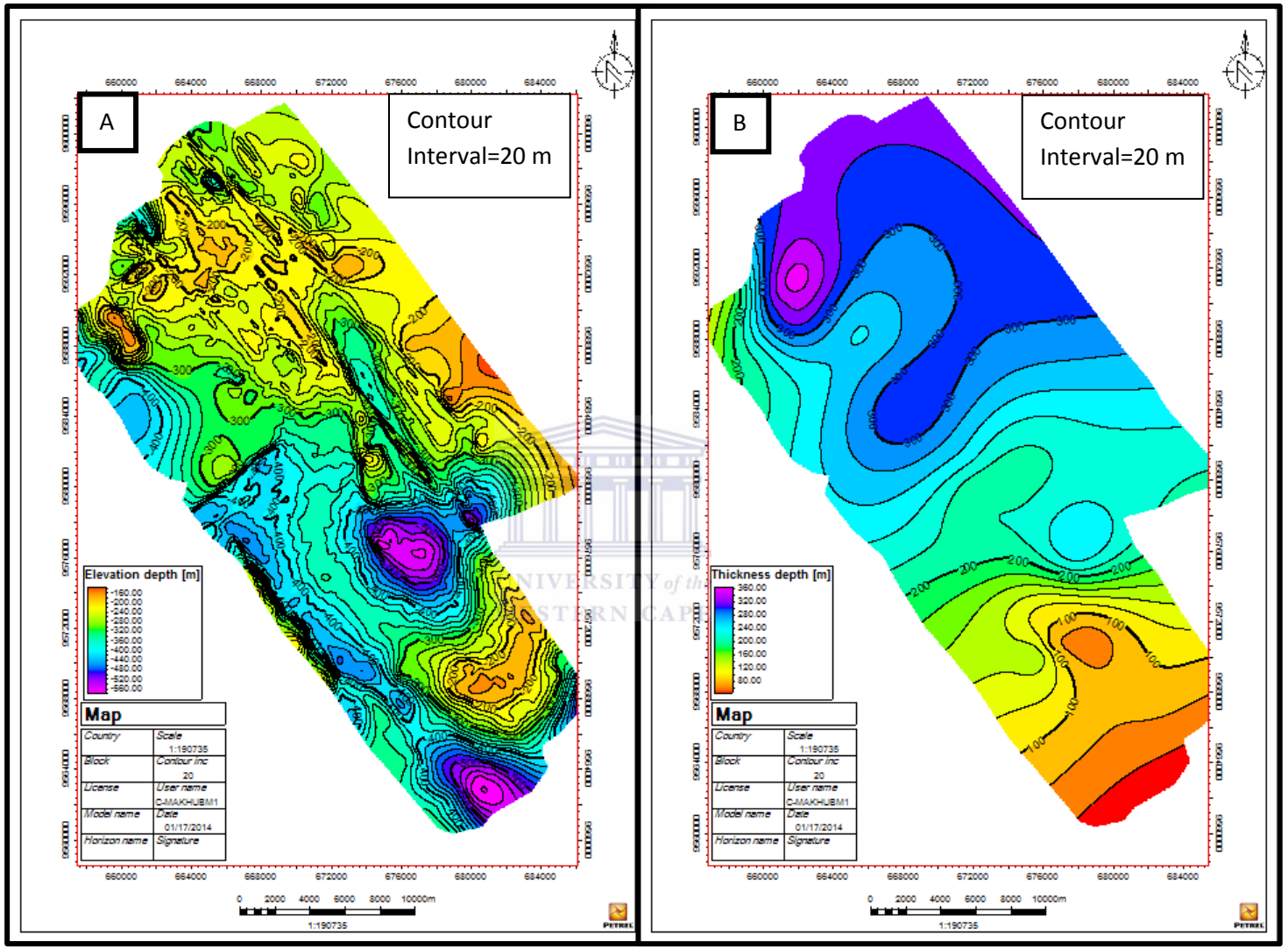

Figure 5.8: (a) Depth map to top of Animba Formation, very shallow parts of the map also due to diapirism (b) the stratigraphic thickness of the Animba Formation.

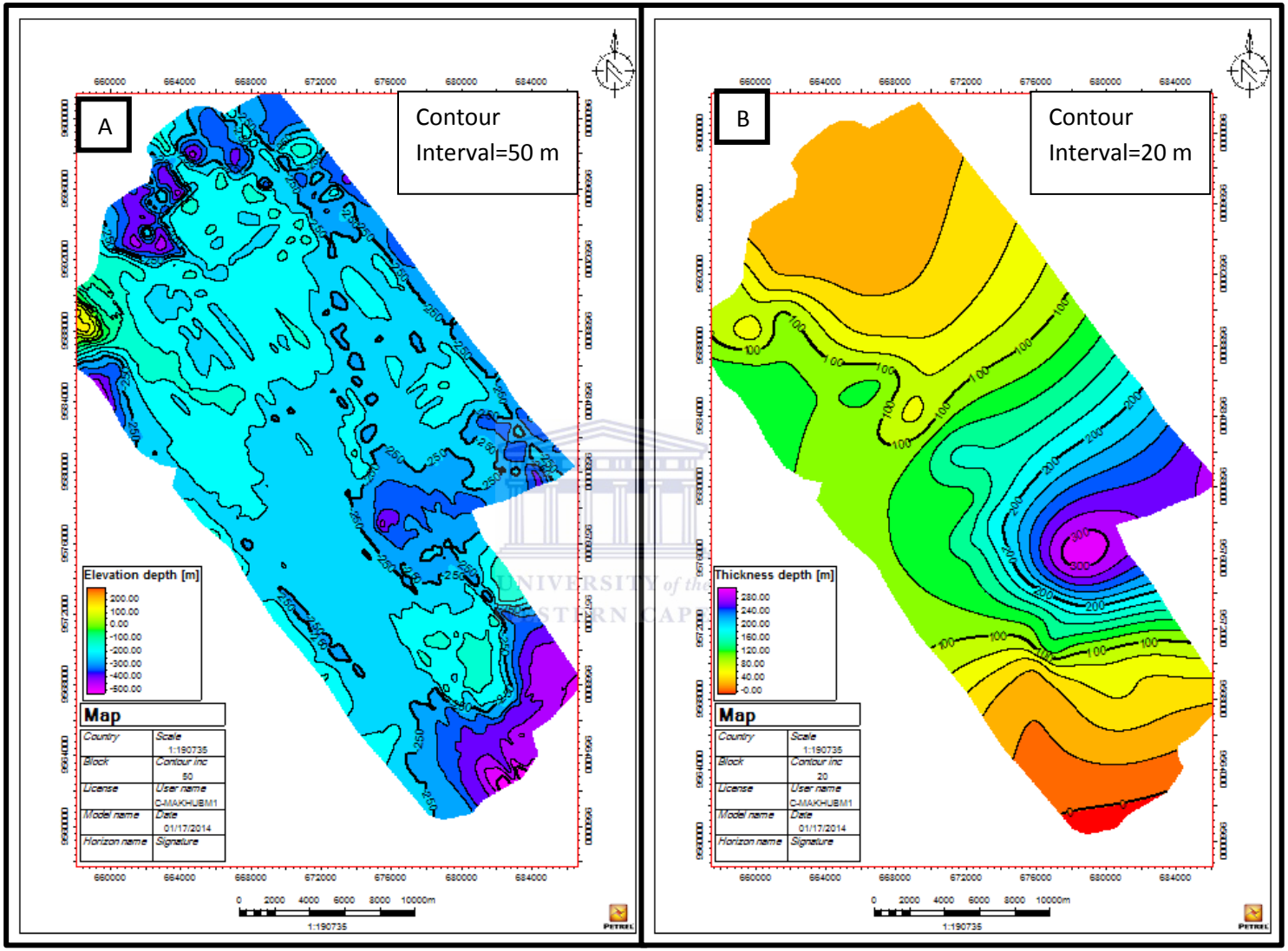

Figure 5.9: (a) Depth map to the top of M'Bega Formation, which is less deformed by diapirism (b) the stratigraphic thickness of M'Bega Formation, showing a change in the depocenter, which could be due to the change in climate or uplift that occurred during the Oligocene.

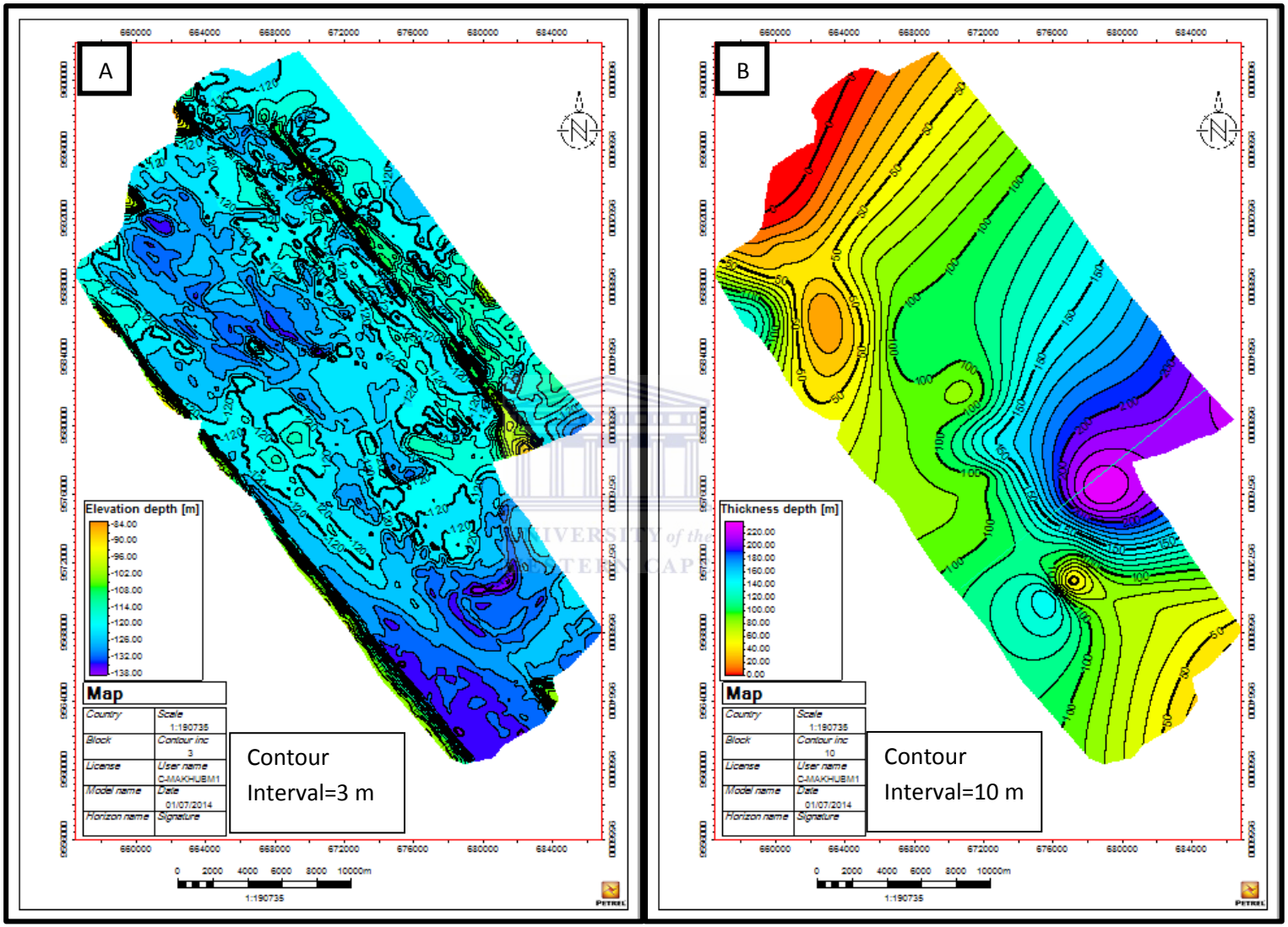

Figure 5.10: (a) Depth map to the top of the Akasso Formation, also representing the depth to the seafloor, (b) the stratigraphic thickness of Akasso Formation, showing that the depocenter is more towards the east, indicating the influence of western margin river system that feed sediments to the basin.

As shown in Table 5.2, sedimentation rates have changed through time in the post-salt sediments of the EMP. Although the actual values might be different to these calculated figures, the results are in good agreement with the calculated values and trends reported by Rasmussen (1996); Hudec and Jackson (2004); Seranne and Anka (2005); Dupre *et al.* (2007); Jackson *et al.* (2008); Oluboyo *et al.* (2013). In summary, in the West African region, the general sedimentation rates were high in the Albian, increasingly lower until the Eocene. Following this, there was slight increase in sedimentation throughout the Miocene and then a sudden increase occurred in the Pleistocene. Compared to the current study area, the above authors report higher sedimentation rates in the Miocene for their respective study areas, which were mostly deeper than the uplifted shelf region of the Etame area (Rasmussen, 1996).

Table 5.2: Sedimentation rates for post-salt sediments in the EMP from the Albian to present times.

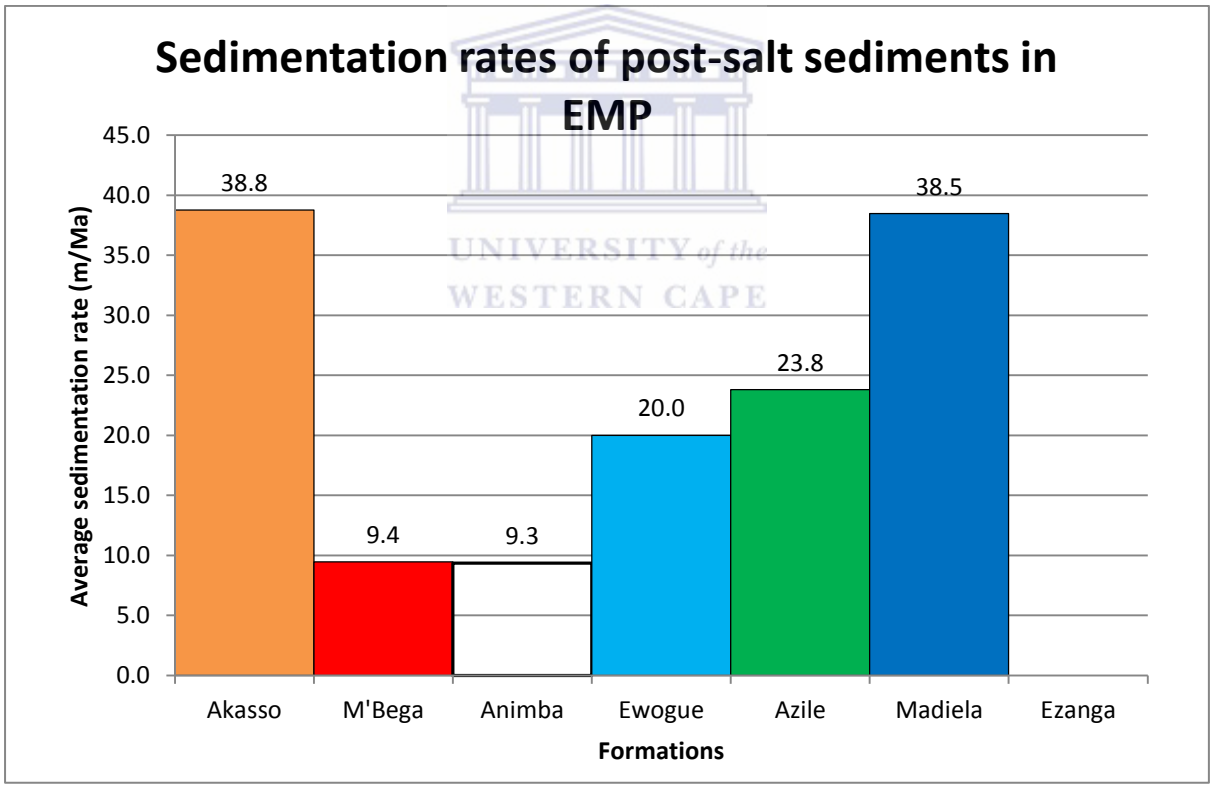

5.3 Seismic and Sequence stratigraphy

Gamma ray data of the following wells were used for correlation and stratigraphic interpretations: EMP8, EMP6.2, EMP15, EMP16, EMP17, EMP18, EMP19, EMP22, EMP23, EMP24, EMP25 and EMP26 (see-Figure 5.11 for location of these wells,). This section discusses the depositional trend of the post salt sediments (Figure 5.12) and their reservoir and seal potential. This was achieved by applying seismic and sequence stratigraphic techniques as well as assessing the gamma ray log signatures and seismic reflection patterns.

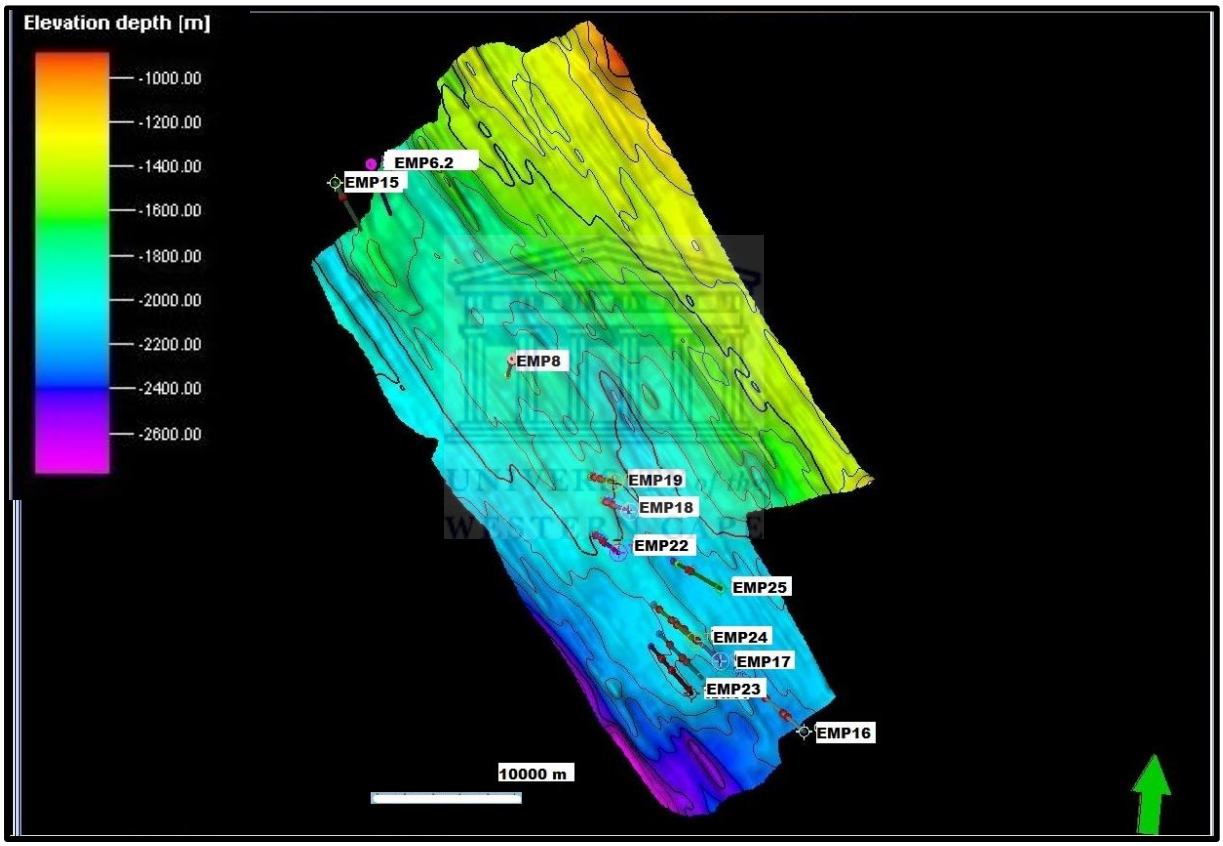

Figure 5.11: Location of the wells in the EMP used for depositional trend and correlation purposes. It should be noted that the well database is in a strike section to the main Gabon Basin and current day shelf edge. Thus, due to the very limited dip section data, the 3D geometry of the basin fill is not well constrains.

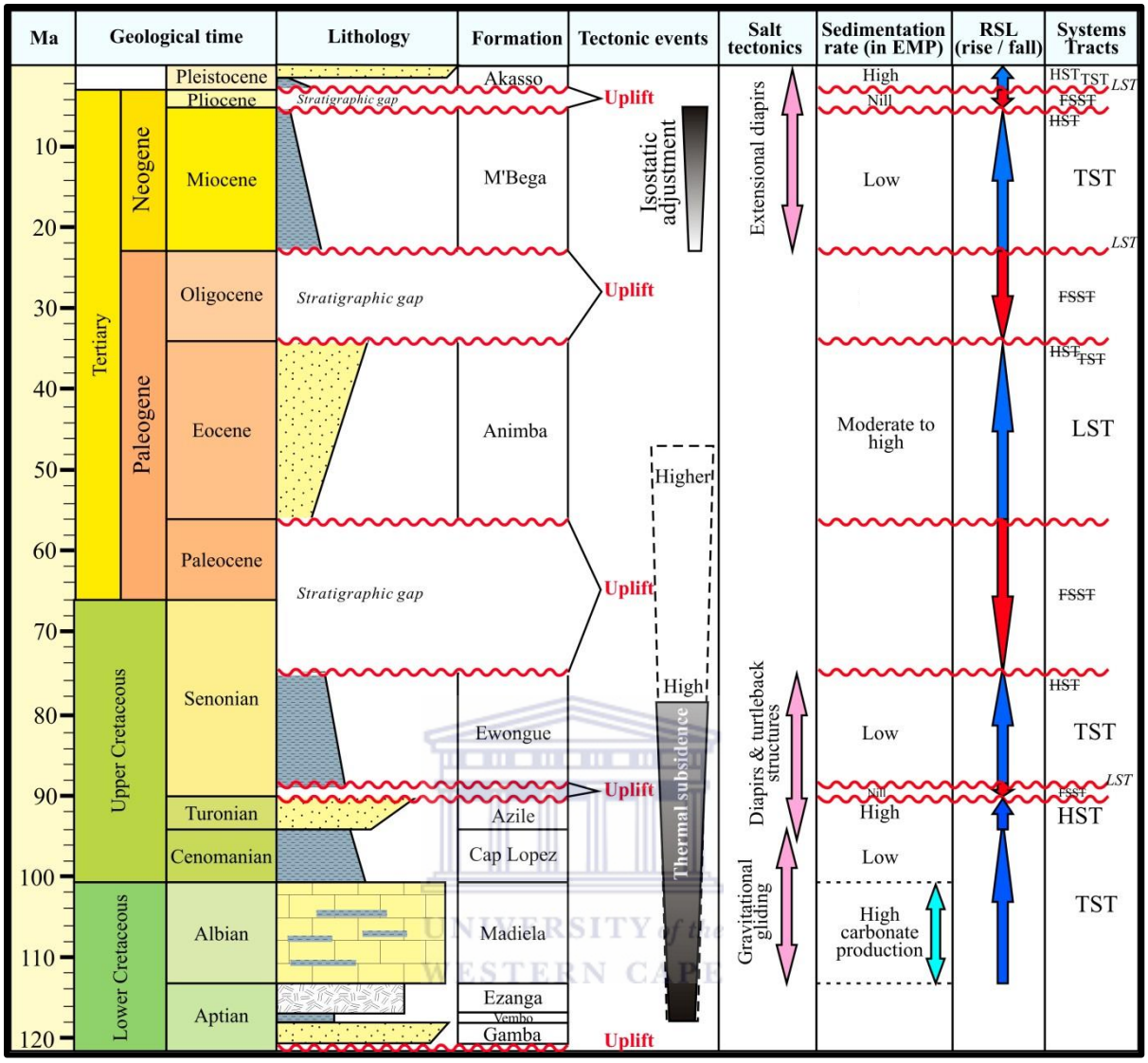

Figure 5.12: Stratigraphic chart indicating system tracts in the EMP and how they were affected by the interplay between sedimentations rates, RSL and tectonics, the system tracts that has been strikethrough represent system tracts that were deposited by was removed by ersosion (Chart modified after Gill and Cameron, 2002).

Salt typically shows low gamma ray signatures (Schlumberger, 1989), and accordingly, the Ezanga salt shows gamma ray signatures that range from 10 to 25 API. Some intraformational high gamma ray signatures (~90 API) could be the result of the radioactive potassium or the shallow marine shales (5.13). As discussed in Chapter 2, evaporite deposition commonly ends with the precipitation of a highly saline thin layer of anhydrite, and this distinct anhydrite layer is identifiable in the gamma ray logs of the EMP (Figure 5.13).

When evaporites move upwards they form diapirs due to overburden pressure, the Ezanga evaporites form various diapir morphologies or salt structures, such as shown in Figure 5.14

(Reading, 1996). Top of the salt is easily identified in seismic sections, because the high acoustic impedance contrast between the salt and the surrounding sedimentary rocks generates very strong reflections (Dupre *et al.,* 2007). As calculated in Chapter 4, the high velocity of the salt results in poor seismic resolution within the salt layers and bodies. Because of this high velocity; the salt usually causes a velocity pull up effect when surrounded by low velocity layers. However the Ezanga salt appears to be causing a velocity push down effect (Figure 5.14), probably because it is overlain by the carbonates, which have higher velocity than the salt.

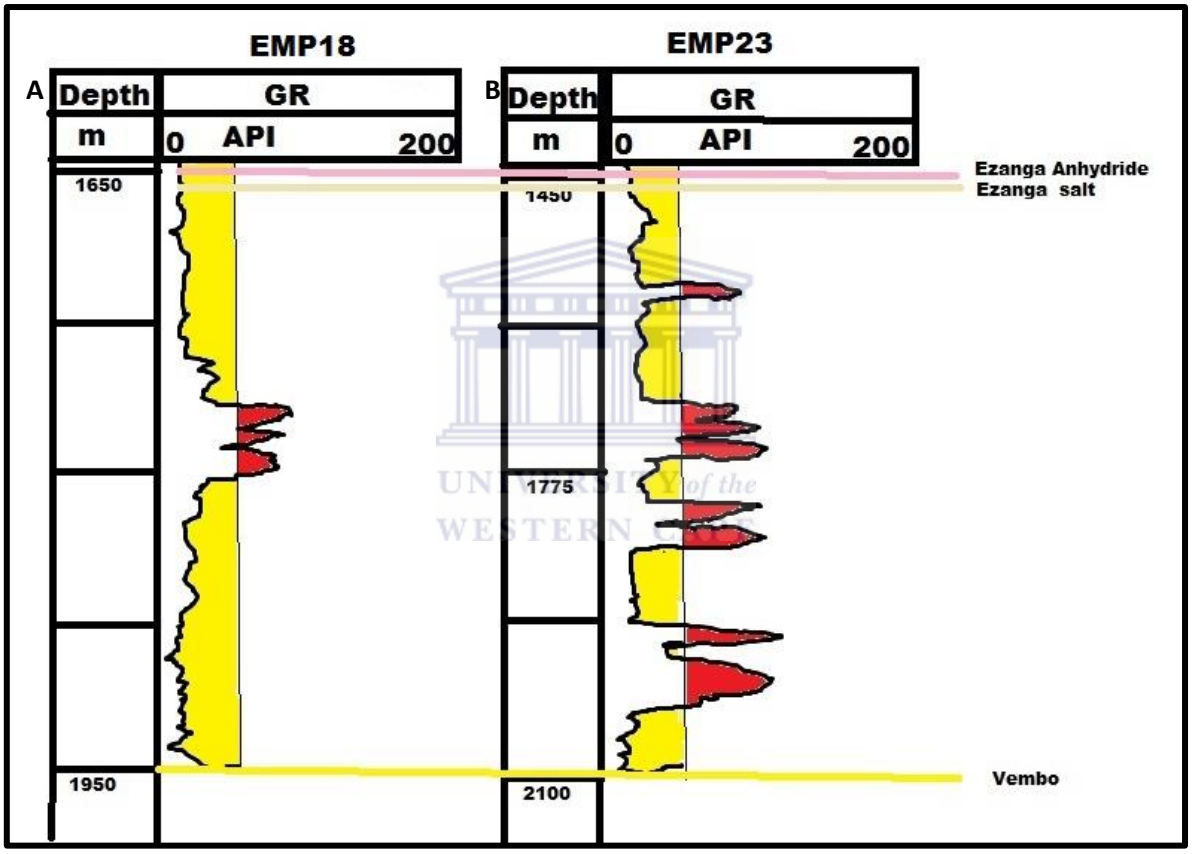

Figure 5.13: Gamma ray signatures of well (a) EMP18; (b) EMP23 all indicating the low gamma ray signature of the salt with higher gamma ray interbeds, which could represent potassium content of the Ezanga evaporites.

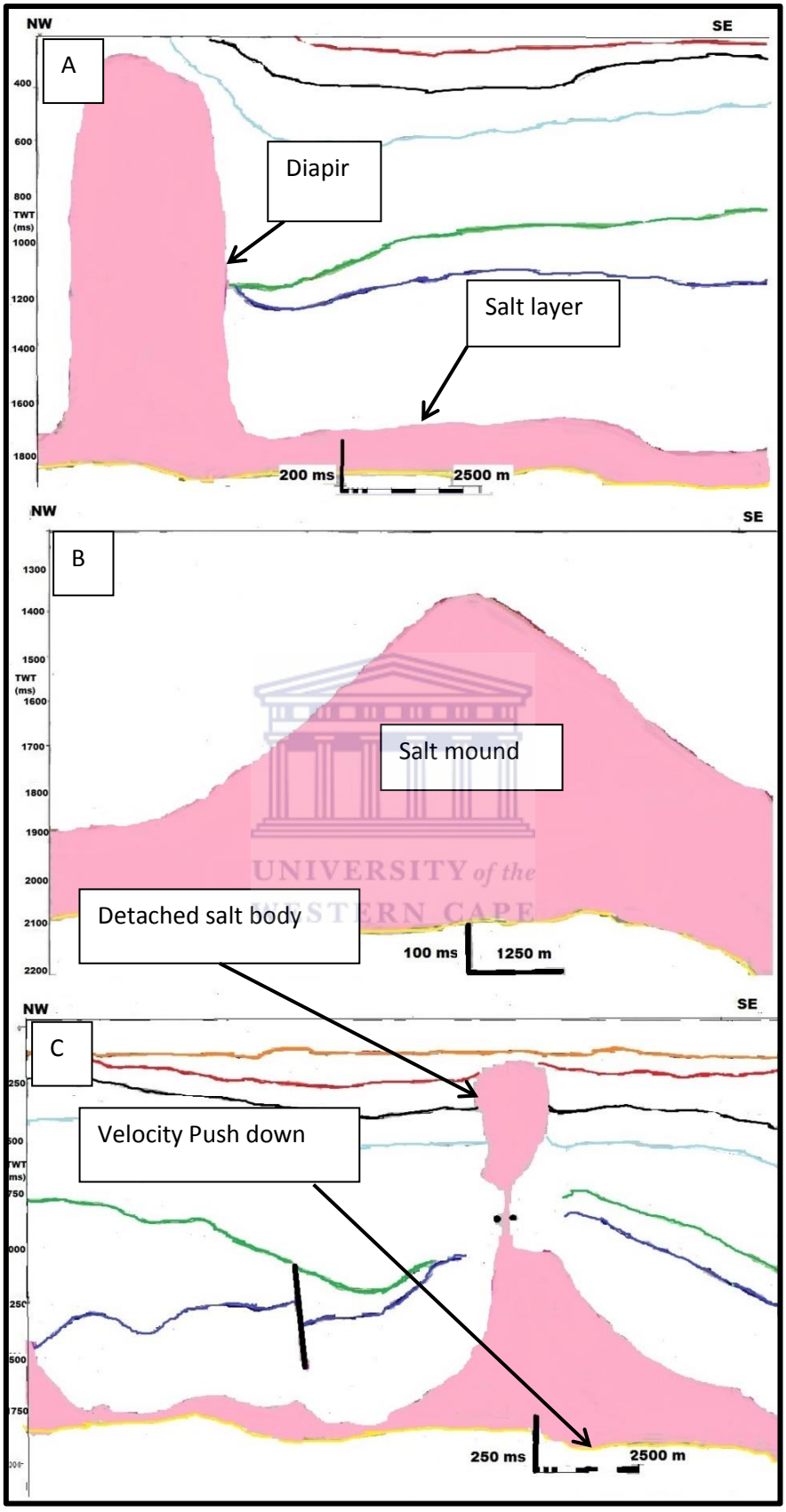

Figure 5.14: Seismic response of the salt and the different salt structure, (a) shows the salt diapirs and salt wall (inline 1165); (b) salt mound (inline 1165) and (c) shows detached salt structures and the velocity push down effect of the salt (inline 1265).

Carbonates typically show a low to moderate deflection, and an aggrading gamma ray signature (Figure 5.15) (Schlumberger, 1989), and Madiela carbonates are no exception, having gamma ray signatures of 15-55 API units (e.g., well EMP18 and EMP 25). In addition, some wells (EMP19) show carbonates with alternating high (90 API) and low gamma ray signatures (Figure 5.15). Since the Madiela carbonates comprise dolomite, oolitic limestone and clastic interbeds, the high gamma ray signatures could be indicative of shale interbeds, which explains the highly variable lateral velocities of these carbonates (Figures 5.12 and 5.15) (Pletsch *et al.*, 2001; Beglinger *et al.*, 2012).

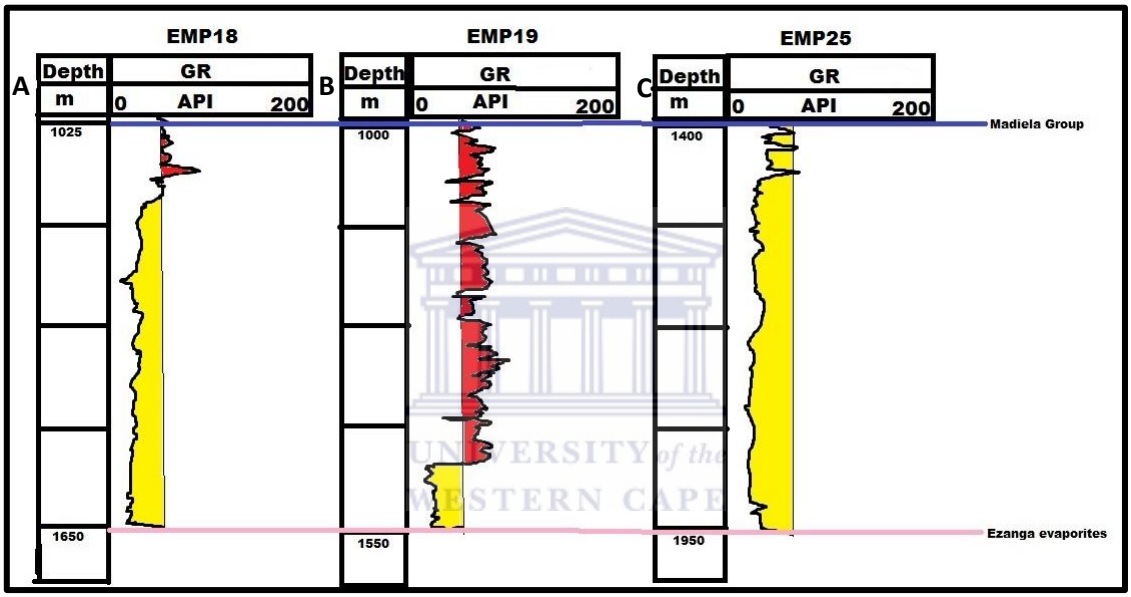

Figure 5.15: Madiela carbonates gamma ray signatures. Carbonates typically show low gamma ray reading. The aggrading low gamma ray signature can be correlated across the study area, with some areas showing high gamma rays. From well; (a) EMP18; (b) EMP19 and (c) EMP25.

Madiela carbonates are readily identified on the seismic sections because of the strong acoustic impedance contrast with the surrounding lithologies. These carbonates show low amplitude, and appear to be laterally continuous in areas where they are not affected by salt diapirism (Figure 5.16). Except in areas affected by salt tectonics, the Madiela carbonates show aggrading reflections, indicating carbonates production was keeping up with the increasing accommodation space.

The presence of turtleback structure and onlaps, indicates that during the Albian, salt tectonics were active (Hudec and Jackson, 2004; Dupre *et al.*, 2007). One peculiar feature of the carbonates is the presence of syn-depositional normal faults, which according to Hudec

and Jackson (2004); Dupre *et al.* (2007); Jackson *et al.* (2008) formed as a result of the thermally subsiding basin (Figure 5.16c) (Albian tectonics is covered in detail in section 5.5).

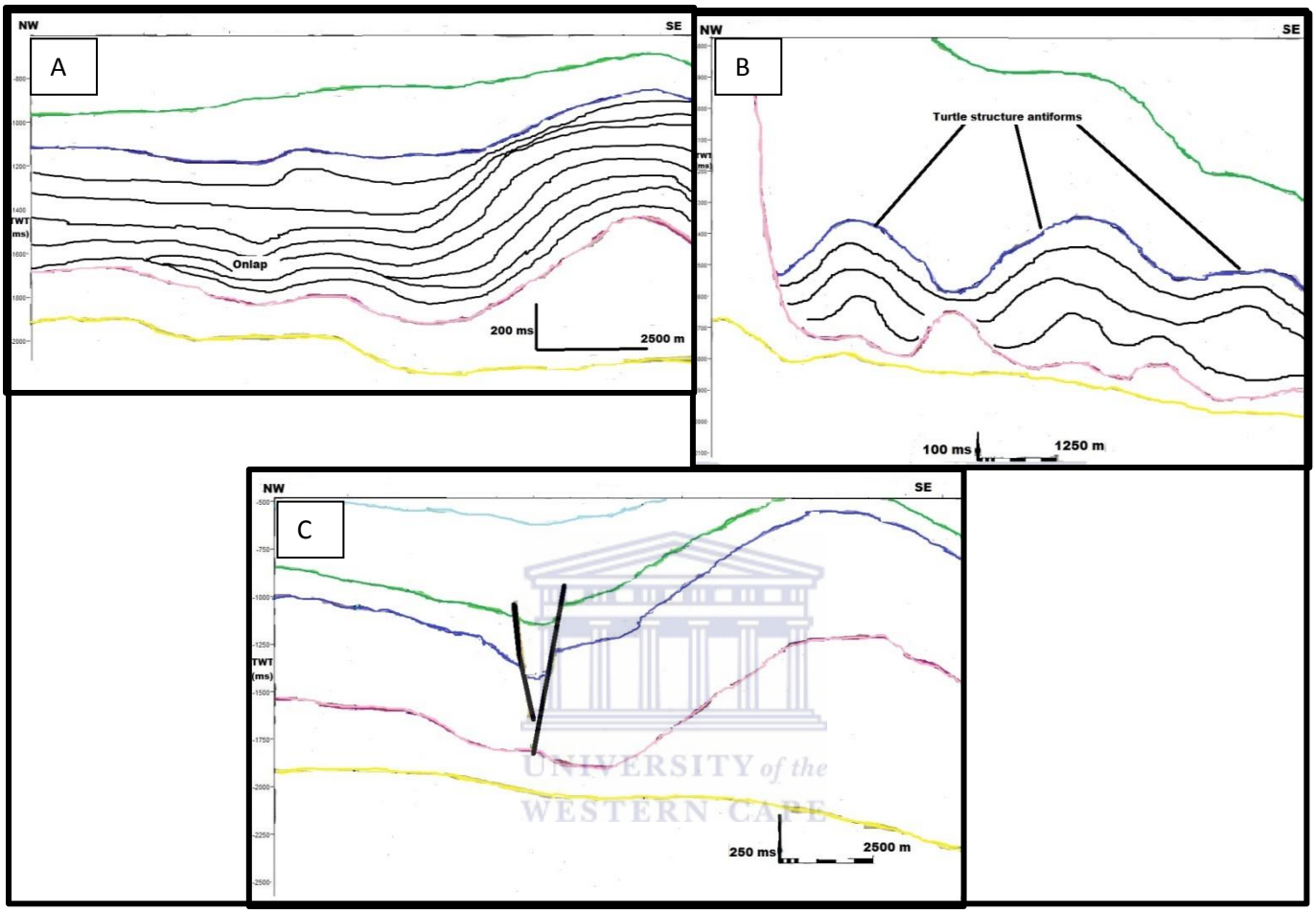

Figure 5.16: Carbonates reflectors, with strong acoustic impedance at the top and the base of the carbonates. (a) shows the low amplitude and laterally continuous carbonates reflectors (inline 1155), (b) turtleback structure anticline (inline 1375). (a) onlapping stratal terminations indicating that salt tectonics was active in the Albian. (c) Albian syn-depositional normal faults interpreted on inline 1225.

Carbonates are generally considered good reservoirs, especially in the case of porous reef limestones and grainstones (Reading, 1996, p. 325). The Pinda Formation in Angola, which is the facies equivalent of the Madiela carbonates is a hydrocarbon exploration target. However according to Ala and Selley (1997), there has been little success in exploring the Madiela carbonates for hydrocarbons offshore Gabon.

The Madiela/Cap Lopez boundary shows a sharp transition, where low gamma ray signatures suddenly increase to > 20 API (Figures 5.12 and 5.17). The high gamma ray signatures represent the Cenomanian Cap Lopez Formation (80 API) at the base, conformably overlain by the Turonian Azile sands (20 API) at the top (Figure 5.17). Using wells EMP19; EMP16

and EMP24 as examples, the general vertical grain size trend coarsens upwards from Cenomanian to Turonian (Figures 5.12 and 5.17).

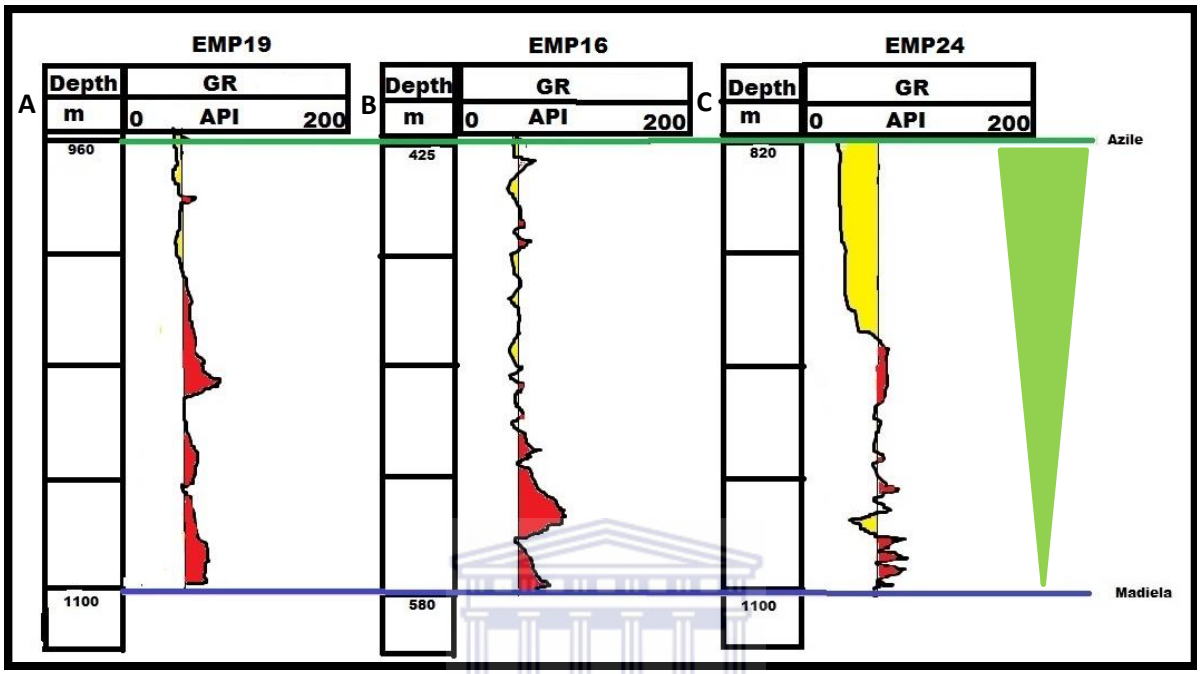

Figure 5.17: Progradational staking pattern of the Azile package, which can be correlated across wells in the study area.

The Cap Lopez and Azile clastics (Cenomanian and Turonian sediments, respectively) conformably overlay the carbonates, which were deposited, and clastic sedimentation dominated, when the Madiela carbonates could no longer keep up with the relative sea level change (Gill and Cameron, 2002; Hudec and Jackson, 2004; Seranne and Anka, 2005; Dupre *et al.*, 2007; Beglinger, *et al.*, 2012). Welltop information of post-Madiela stratigraphy was not provided with the data; as a result, interpretations of stratigraphic boundaries were inferred from the literature (Figure 5.18), and by applying sequence stratigraphy principles.

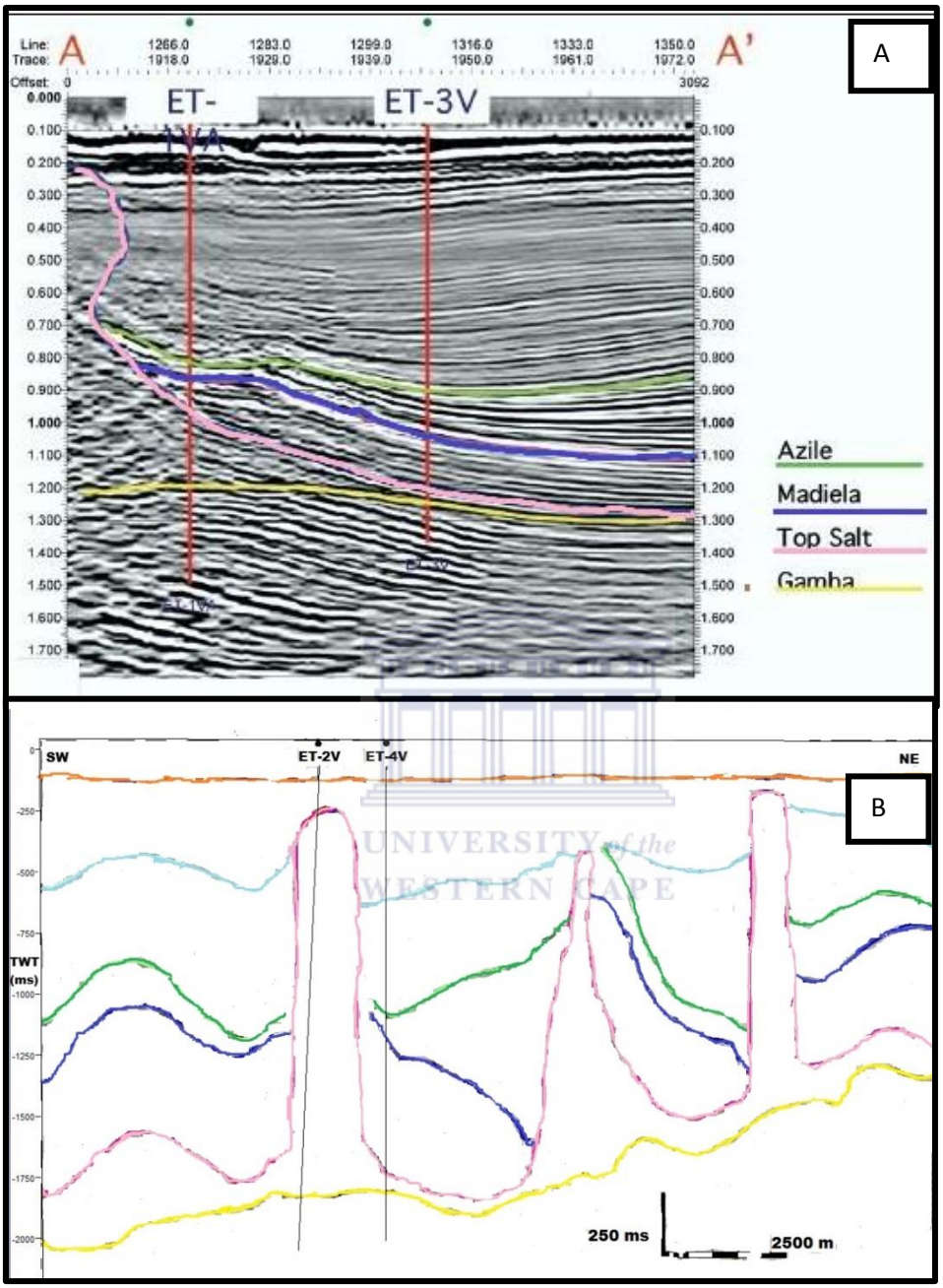

Figure 5.18: (a) Gill and Cameron (2002) interpretation of the first of post-Madiela stratigraphy as the Cenomanian Cap Lopez Formation overlain by Turonian Azile clastics (in green) (b) our interpretations on crossline 1889 of the Azile clastic matching up with Gill and Cameron (2002) interpretations.

The contrasting acoustic impedance between the underlying Madiela carbonates and the clastics of the Cap Lopez Formation can easily identify the base of Cenomanian/Turonian sediments. Although Cap Lopez and Azile formations have been deformed by salt tectonics, they form continuous, strong reflection patterns. In addition to considering interpretations

suggested by Gill and Cameron (2002), the top of the Azile sediments was also identified based on stratal terminations, where reflectors on the crosslines is truncated, which could represent uplift during the Turonian (Figures 5.12 and 5.19). As described in Pletsch *et al.* (2001), this uplift could be due to the relaxation of the African continental margin after the breakup of South America and Africa.

This Cap Lopez and Azile clastic unit can thus be interpreted as an upward-coarsening succession of shaly sands (fine sands) at the base to coarser-grained sands at the top, indicating a regressive shoreline. According to Hudec and Jackson (2004); Seranne and Anka (2005); Dupre *et al.* (2007) and Jackson *et al.* (2008) the first package of sediments above the carbonates was deposited on the continental shelf as shallow marine sands as well as siltstones and shales in the more distal regions. The truncation at the top of this succession could represent a local uplift during the Turonian, which eroded the top of this package.

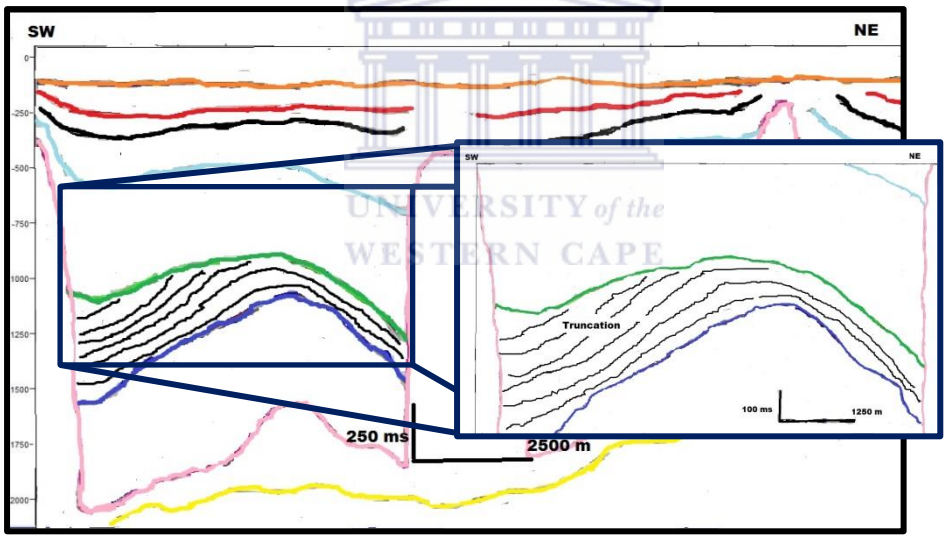

Figure 5.19: The Azile Formation unit with strong and continuous reflectors, also showing truncation stratal termination at the Late Cretaceous boundary, interpreted from crossline 1668.

The Azile clastics were also affected by salt tectonics during deposition as suggested by the turtleback strutures (Figure 5.20). This sedimention occurred while differential subsidence was active as suggested by syn-depositional normal faults (Figure 5.16c). Onlapping stratal terminations illustrated Figure 5.20 are unlikely due to rapidly increasing realtive sea level, but rather due to the laterally migrating and bulgeing salt below, which resulted in a local elevation and surrounding depression in which the accumulation of the Azile clastics

occurred (for the dynamics of salt tectonics, see Chapter 5.4). The chaotic, poorly reflected amplitudes at the base of the Azile clastics resembles a gravitational flow, probably slumpled beds which could have been caused by the active salt tectonics during the deposition of the Azile clastics. Chaotic patterns such as in Figure 5.20 indicate post depositional soft sediment deformation either due to bioturbation or physical disturbance (upward escaping pore waters) under very fast depositional rates (Miall, 2009).

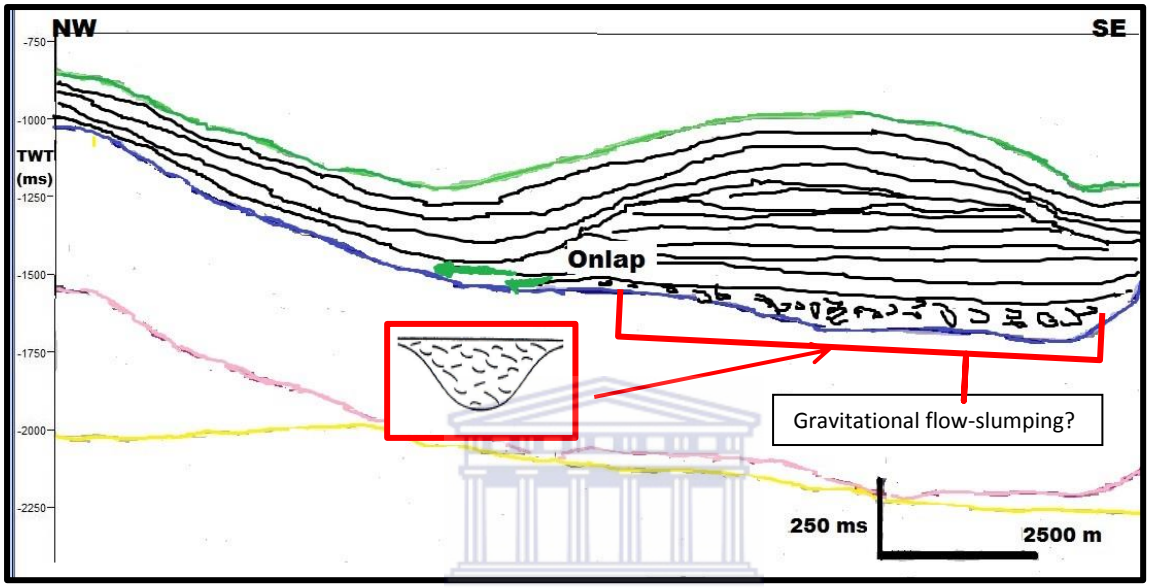

Figure 5.20: Interpreted inline 1045, indicating the onlapping stratal termination at the base of Azile Formation and also showing a chaotic infill, which would be a result of slumping.

Lithology changes from the shaly sands and sands of the Azile clastics to silty sands and fine silt in the overlying sediments, forming an overall upward-fining succession in the Senonian Ewongue Formation (Figures 5.12 and 5.21). Towards the south eastern part of the study area, in wells EMP16 and EMP23, the gamma ray signatures suggest fine sands giving way to shaly deposits, and thus denoting a fining upwards sequence (60-100 API). While the fining-upward trend is common in most wells (Figure 5.21), in the far NW part (well EMP6.2) of the study area, the Ewongue Formation shows a coarsening upwards trend (75 to 30 API).

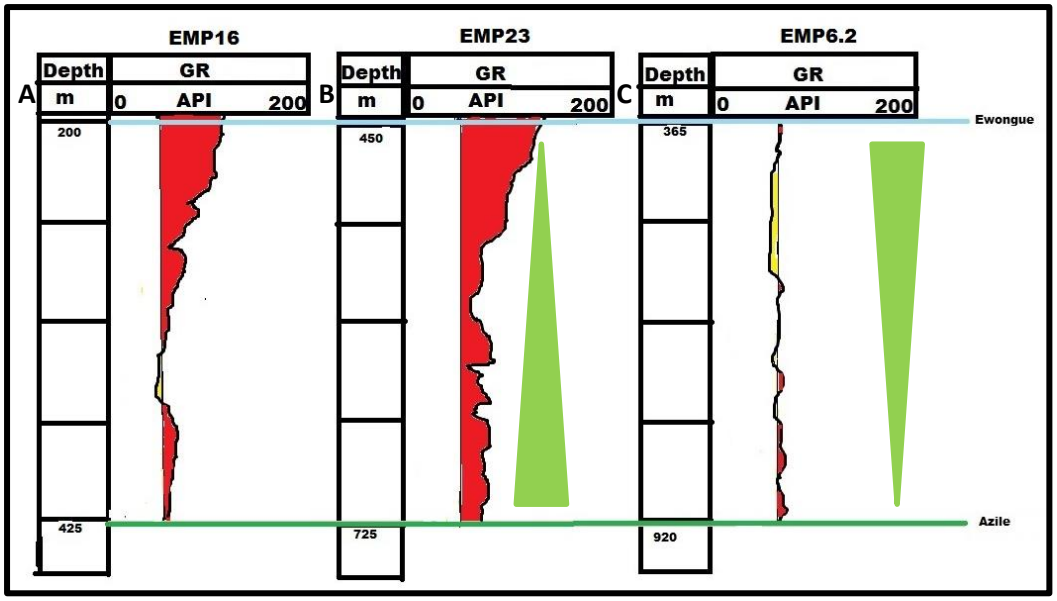

Figure 5.21: Gamma ray depositional trends for the Senonian Ewongue package, (a) well EMP16, (b) well EMP23 and (c) well EMP6.2.

The Ewongue Formation shows lower amplitude reflectors compared to the overlying and the underlying sediments. The top of the Ewongue Formation was picked based on what appears to be an erosional surface/unconformity on the crossline (Figures 5.12 and 5.22). The truncated boundary shows an angular unconformity, where the older strata are truncated against the overlying sediments (Figure 5.22).

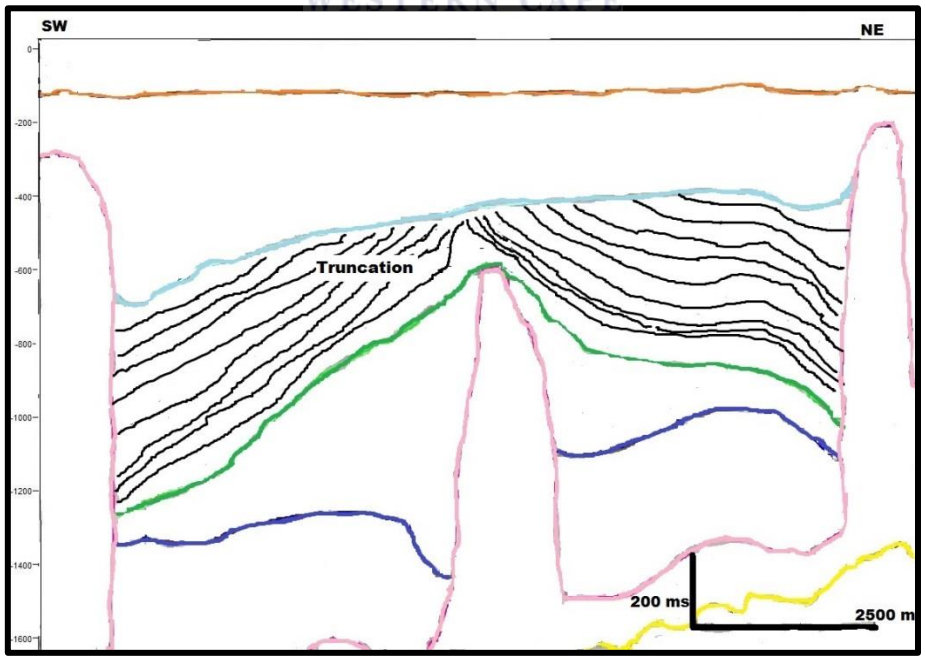

Figure 5.22: Reflection patterns of the Ewongue Formation truncated at the top. Interpretations done on crossline 2149.

The presence of Albian normal faults, which appear to be syn-depositional at the base of the Ewongue Formation suggest that the basin was still subsiding in Late Cretaceous (Figure 5.16c). Figure 5.23 is an inline interpreted showing prograding clinoforms; the clinoforms were also interpreted in the crossline (Figure 5.23). These prograding sediments were due to salt tectonic, which were likely active during the Senonian and also indicating the direction of sedimentation in the basin.

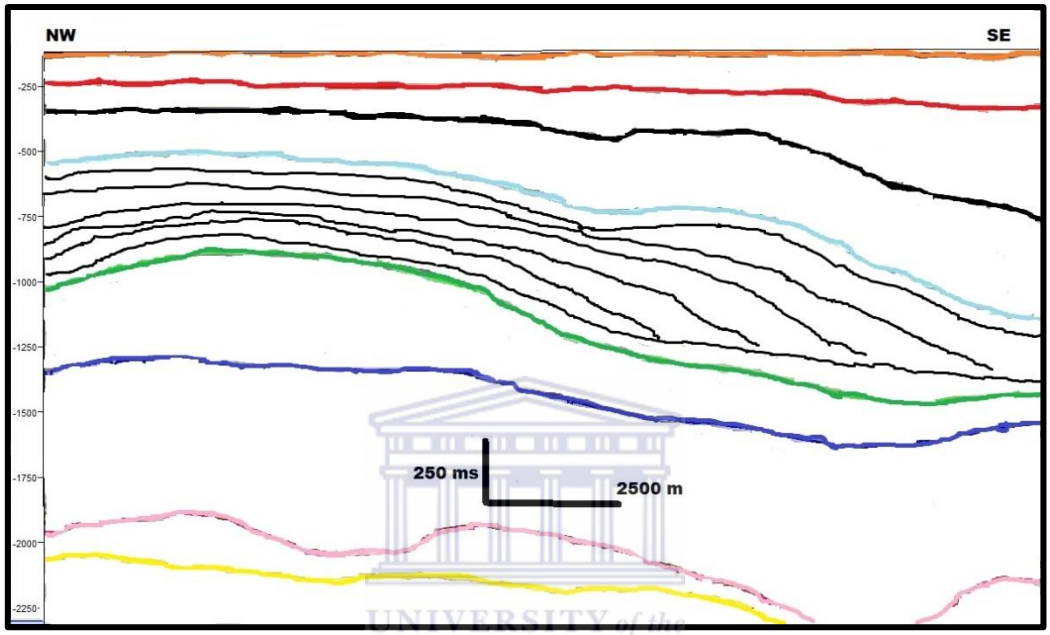

Figure 5.23: Salt tectonics related prograding clinoforms, interpreted from inline 1095, indicating sediment transport direction of NW-SE.

Gamma ray values changes from being predominantly 85 API at the top of Cretaceous to being less than 70 API at base of the Animba (Eocene) Formation (Figures 5.12 and 5.24). Eocene unit shows a coarsening sequence (70 to 50 API) (Figure 5.24). This trend can be correlated across the entire study area, representing a period where shoreline was regressing.

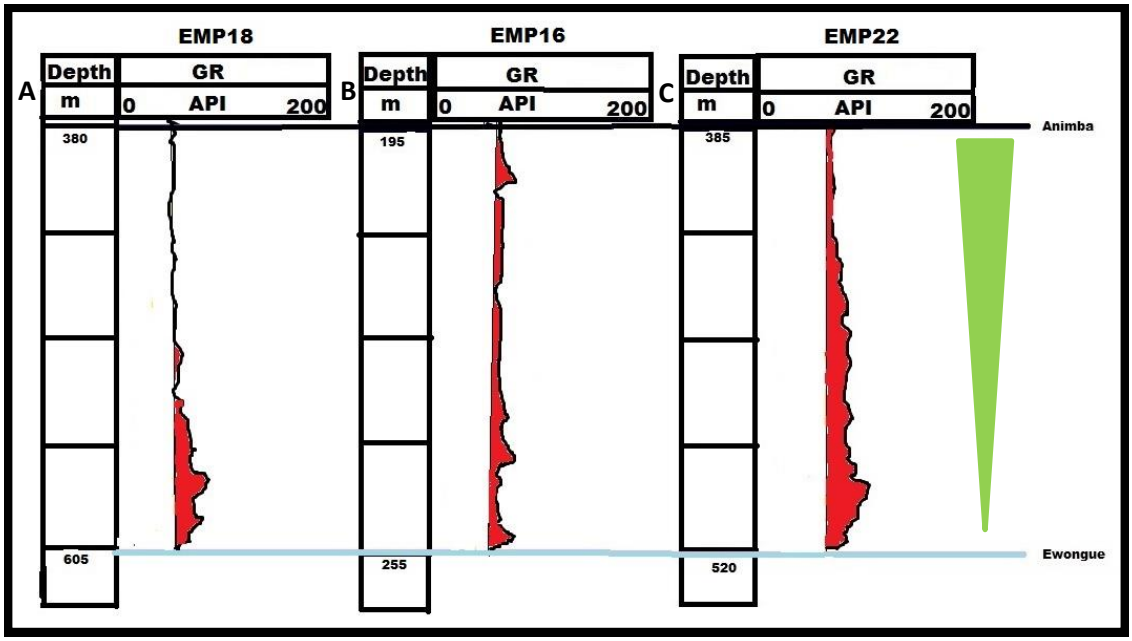

Figure 5.24: Depositional trends of the Eocene Animba Formation. (a) well EMP18, (b) well EMP16 and (c) well EMP22, all three wells shows a coarsening upwards sequence during the Eocene.

The Animba Formation is easily identified on the seismic section by the underlying truncated Senonian stratal termination. Although there is evidence of folding in certain areas, the Animba Formation has moderate amplitude reflectors, which are continuous and sub-horizontal in the inline, and very discontinuous in the crossline (Figure 5.25). According to Seranne and Anka (2005); Dupre *et al.* (2007); Jackson *et al.* (2008) and Oluboyo *et al.* (2013), there was a major uplift during the Late Eocene, which lasted for 10-20 Ma, and eroded up to 3000 m of sediments in certain areas. This major uplift event could be the reason why Oligocene sediments are not preserved in the EMP (Figure 5.12). Furthermore, the erosional boundary that resulted from this major uplift event can be correlated on a regional scale all the way to the southern part of Africa in the Orange Basin (Seranne and Anka, 2005). Truncations seen at the top of the Eocene sequence probably represent this period of erosion (Figure 5.25).

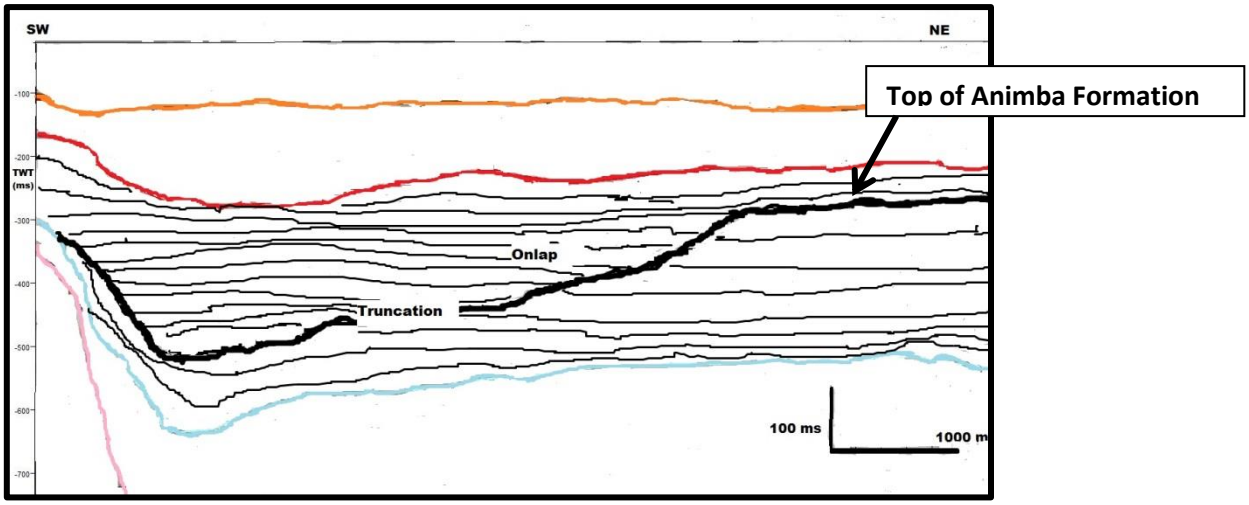

Figure 5.25: Eocene/Miocene boundary marked by truncating stratal terminations.

Across the entire study area, there is a sharp contact between the Miocene and the Eocene sediments, with gamma ray increasing from the ~50 API in the Eocene to clay dominated upward-fining sequence (60 to 180 API) in the Miocene M'Bega Formation (Figures 5.12 and 5.26).

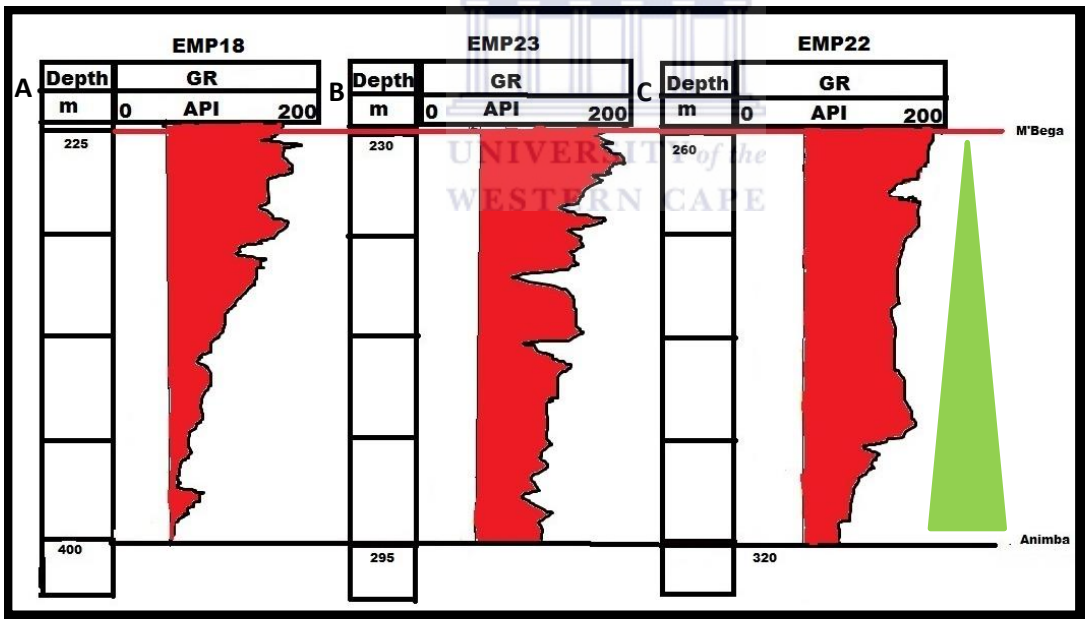

Figure 5.26: Fining upwards sequence of M'Bega Formation, correlated across the study area, using (a) well EMP18, (b) EMP23 an d (c) EMP22 as examples.

Miocene sediments also show moderate amplitude reflections, which are continuous and sub-horizontal in the inline, and very discontinuous in the crossline. The Onlapping stratal termination (Figure 5.25) indicates a TST that occurred during the Miocene as the M'Bega Formation was being deposited. The top of the Miocene reflector is marked by truncating

stratal terminations (Figure 5.27) which could be due to the uplift during the Late Miocene (Rasmussen, 1996).

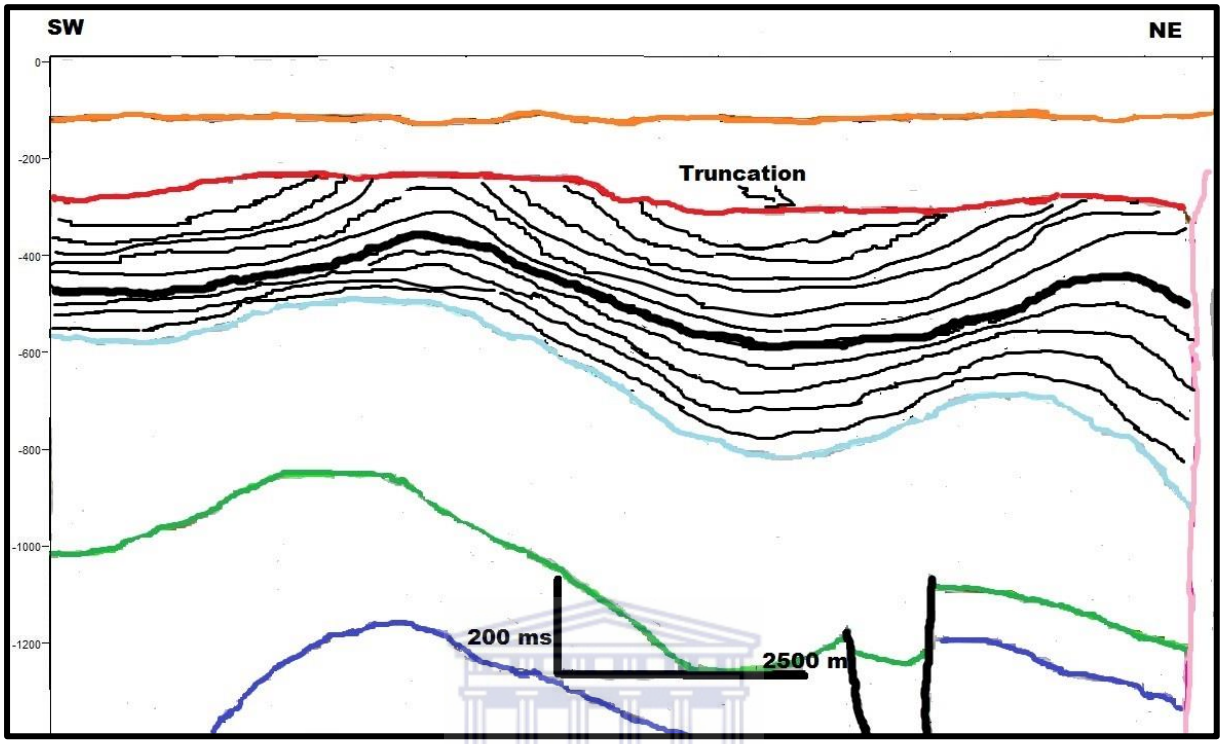

Figure 5.27: Seismic reflection pattern of M'Bega Formation showing truncation, which could be a result of the uplifted shelf during the Miocene, interpreted from crossline 1489.

Gamma ray signatures change from being clay dominated to sand dominated, marking the start of deposition of the Pleistocene Akasso Formation. At the base of the Pleistocene sequence gamma ray signatures are predominantly around 70 API (shaly sands), which suddenly decreases to 20 API (coarser sands) (Figures 5.12 and 5.28). The coarsening-upwards trend is present in wells across the entire study area, indicating a regressive shoreline.

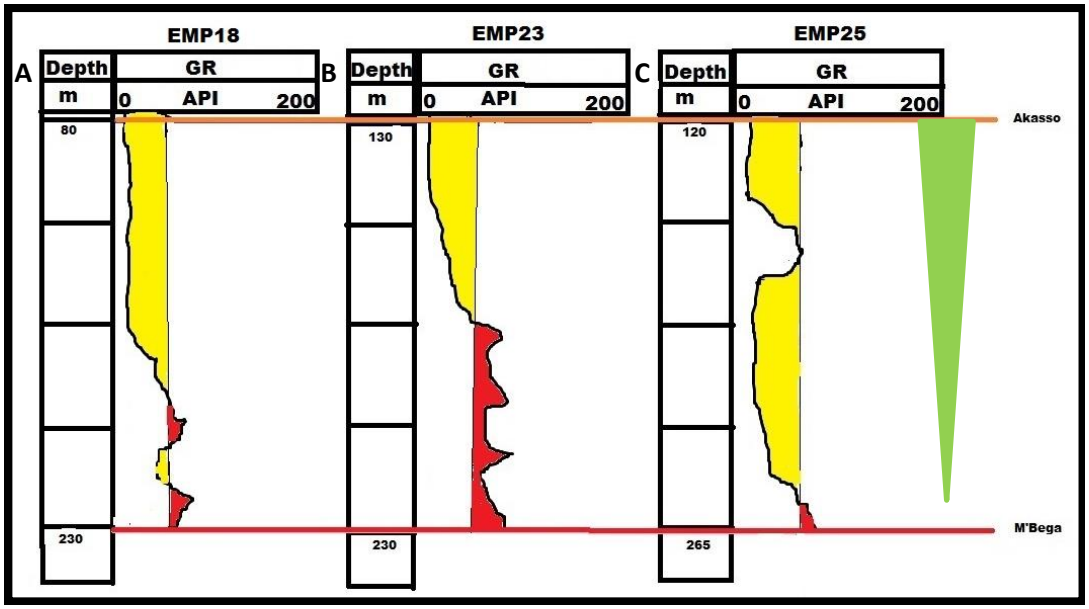

Figure 5.28: Well EMP18, EMP23 and EMP25 used to show the Pleistocene coarsening upwards trend.

The Pleistocene sediments show very weak amplitudes, which are very discontinuous and subparallel. The base of the Pleistocene is marked by the underlying truncational surface, which formed after the Late Miocene shelf uplift (Figures 5.12 and 5.29). These sediments are pierced through by diapirs, which also pierce through the seafloor reflector, suggesting that salt tectonics is active to date.

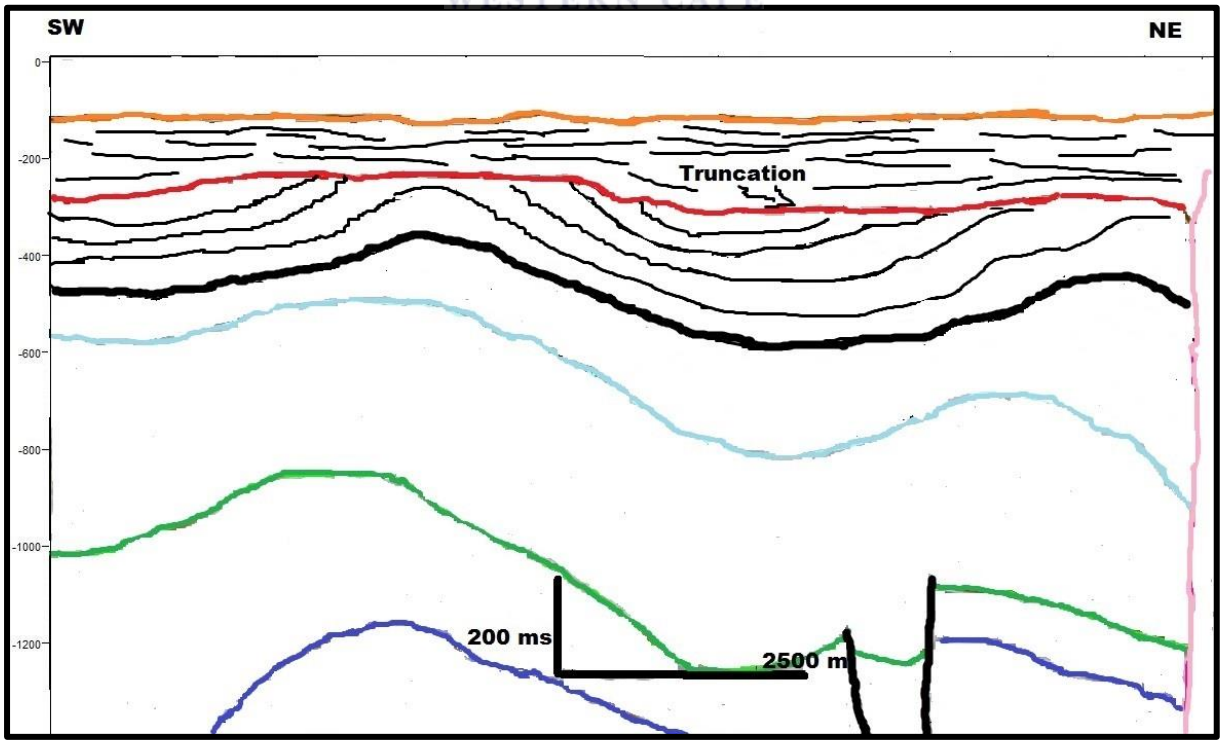

Figure 5.29: Seismic reflection pattern of the upper reflector, Miocene package, interpreted from inline 1205.

5.4 Tectonics and salt tectonics

Dupre *et al.* (2007) argues that although it is difficult to model past subsidence rates during salt accumulation phases, the thickness of the salt suggests that the basin was probably subsiding at high rates during the Aptian. After the deposition of the evaporites, thermally driven high, but steady subsidence rates created the accommodation space for the platform carbonates (Huduc and Jackson, 2004; Dupre *et al.,* 2007; Jackson *et al.,* 2008). The thick carbonates triggered salt tectonics, moving the salt basinwards (Dupre *et al.,* 2007). Furthermore, resulting in gravitational gliding over the salt decollment surface caused extension landwards and compression basinwards (Huduc and Jackson, 2004; Dupre *et al.,* 2007; Jackson *et al.,* 2008). Figures 5.30a and 5.30d show the decollment nature of the salt, where the NW-SE trending normal faults start in the Madiela carbonates stretching into the Turonian Azile Formation and in certain areas into the base of Senonian Ewongue Formation (Figure 5.31). The NW-SE trending faults are associated with the subsidence, whereas the randomly trending faults, usually found at the tip of the diapir are mostly due to extensional diapir intrusions (Figure 5.31). Faults are tilted towards the southwest and according to Dupre *et al.* (2007) and Jackson *et al.* (2008) have tilted the basin seawards, resulting in the subsequent seaward deposition of the post-Madiela sediments (Figure 5.31). The consequence of this gliding in the shelf, is that, carbonates will tend to form 'pre-rafts', which are, fault blocks that have undergone less extension and still in contact with each other (Figure 5.230a) (Duval *et al.,* 1992). However more distal carbonates (in the Kwanza Basin) form raft fault blocks, which are, fault blocks that are no longer in contact with each other (Duval *et al.,* 1992).

Furthermore, according to Dupre *at al.* (2007) although salt tectonics could partly be responsible for subsidence during the Albian, at the time of carbonates formation, salt tectonics was not as active in offshore south Gabon and the main driving force of a subsiding basin was a thermal anomaly. Folding in the Azile sediments suggests that turtleback structure in the Madiela carbonates formed after the deposition of the Turonian clastics (Figure 5.30). Turtleback structures are mini-basins (elongated antiforms) that form as the salt withdraw and move outwards, creating a local depression within sediments, the two main driving forces behind turtleback structures are; (1) sedimentary differential loading, and (2) regional extension (Vendeville and Jackson, 1992). Asymmetric turtleback structures are another type of structures that might form during salt tectonics, which according to Vendeville and Jackson (1992), form between two diapirs that have been rising for a long

time and sagging due to extension (Figure 5.33). Evidence of Albian salt tectonics is onlapping stratal terminations of the carbonates on the salt, showing that salt was moving upwards during carbonate deposition (Figure 5.30c).

After the Albian, thermal subsidence rates decreased, but still influenced sedimentation architecture of Cenomanian/Turonian sediments, as shown by the syn-depositional normal faults cutting through these sediments (Figure 5.30). However, in addition to thermal subsidence the presence of the turtleback structures in the Azile Formation is evidence that salt tectonics also strongly influenced the deposition of these sediments (Figures 5.32c and 5.32d). Diapirism in the shelf was mainly initiated by sedimentary loading as a result of clastic influx (Séranne and Anka, 2005). Figure 5.32c and 5.32d shows the wedge shaped geometry (due to uneven thickness) of the Cap Lopez and Azile formations; which usually forms due to a localised subsidence, a depression, which is rapidly filled by sediments. Cramez and Jackson (2000) and Dupre *et al.* (2007) also point out that during the Cenomanian-Turonian, gravitational gliding changed the salt diapirs from being extensional to being compressional. However this is more evident in the slope to deep sea setting (Kwanza Basin); in the shelf region the diapirs are still extensional. According to Pletsch *et al.* (2001), there was local uplift of the shelf during the Turonian, which could be what we observe as preserved as truncations at the top of reflector A1.

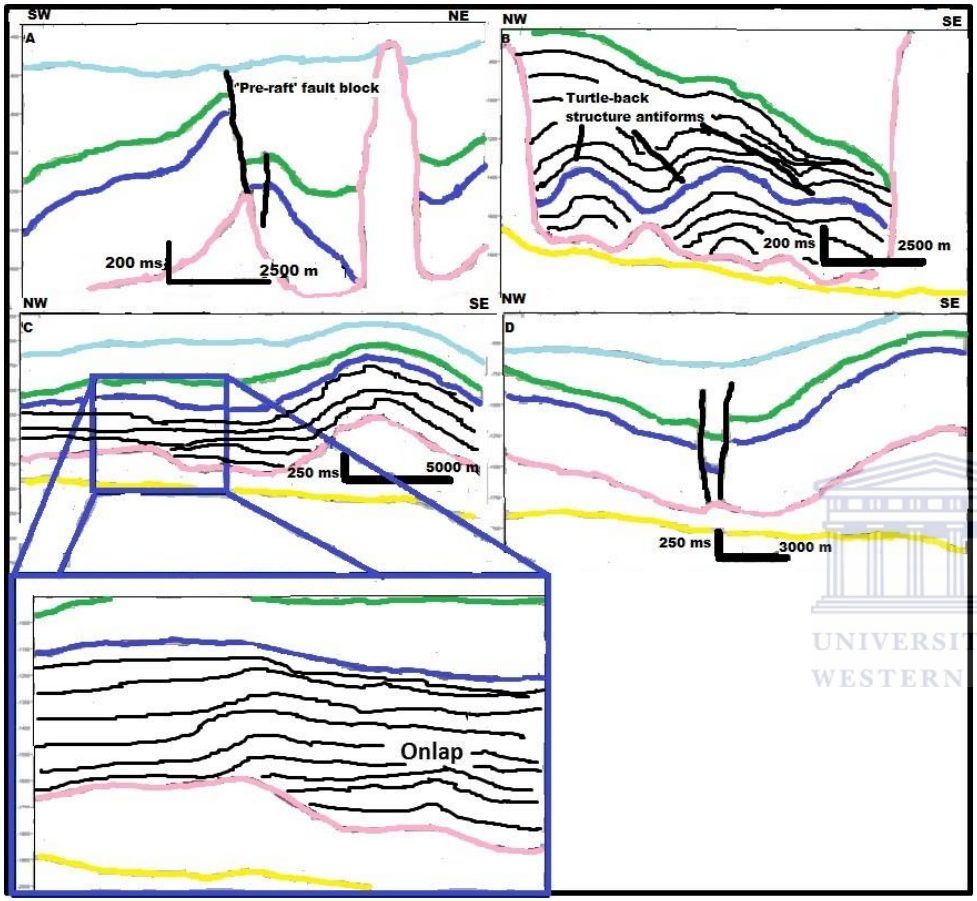

Figure 5.31: Interplay between sedimentation, thermal subsidence and salt tectonics, indicating how each had an effect on the sedimentary architecture of the Madiela Carbonates. (a) pre-raft fault blocks, (b) turtleback structures as descibed by , Vendeville and Jackson (1992). (c) Onlapping stratal temination that formed due to salt tectonics, (d) syn-depositional normal faults.

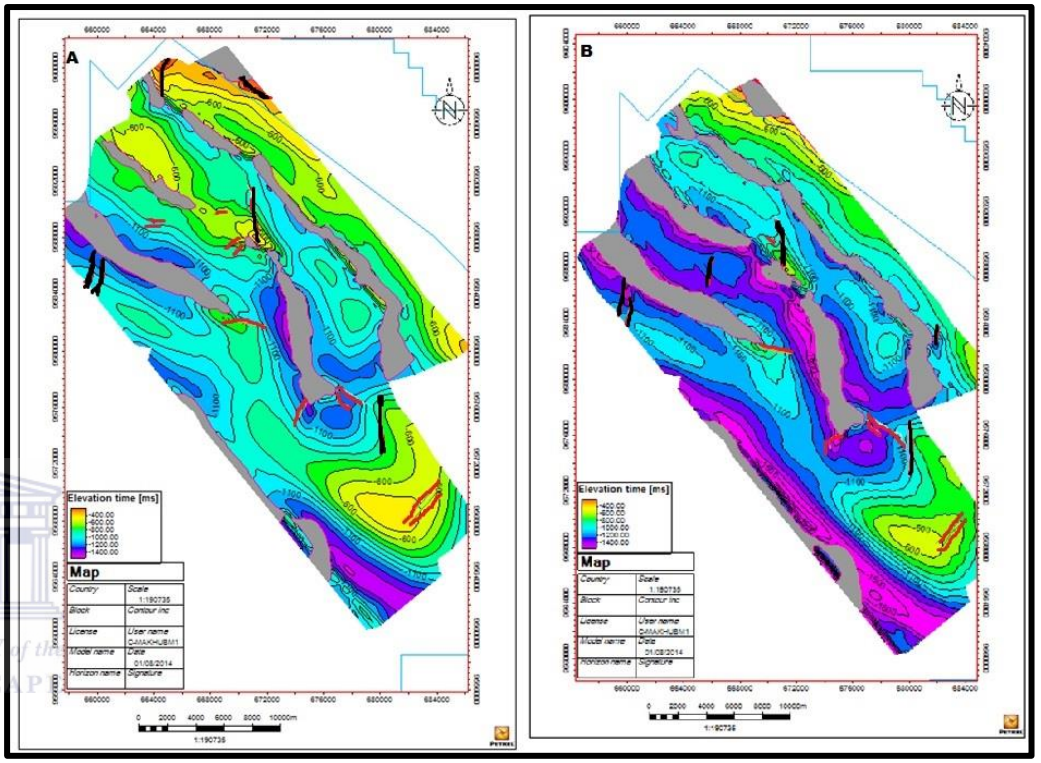

Figure 5.30: Strike pattern of faults in the EMP. Indicated in black are the NW-SE striking faults which dip seawards. The red fault lines (randomly orientated) indicate faults that resulted from extensional diapirs. Figure A marks the top of the Albian and Figure B marks top of the Cretaceous.

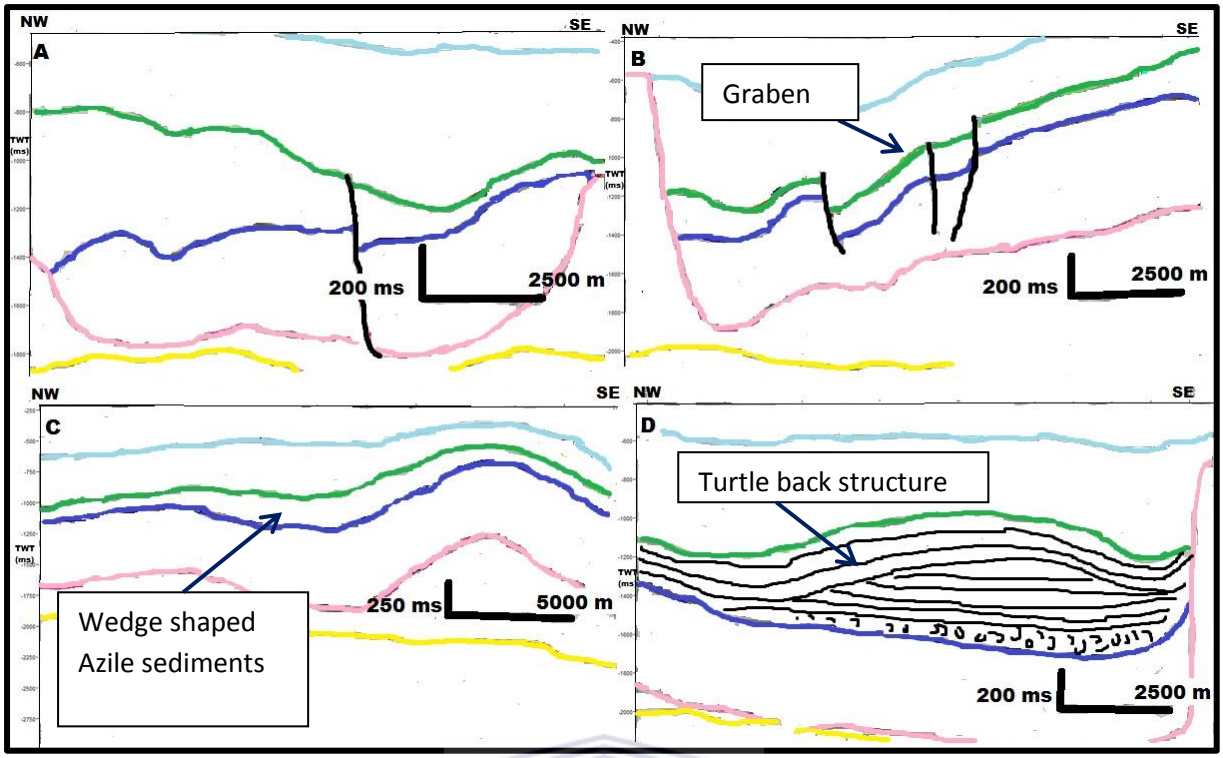

Figure 5.32: The effect of thermal subsidence and salt tectonics on the sedimentary architecture of the Cretaceous sediments. (a) syn-depositional growth fault, (b) grabens formed as a result of thermal subsidence and (c) wedge shaped structure, (d) turtleback structures.

Overlaying reflector A1 is the Senonian Ewongue Formation, which was deposited during a period of decreased thermal subsidence rates in the basin (Dupre *et al.*, 2007). However, syn-depositional normal faults (Figures 5.30a and 5.33a,b) that cut the base of the Ewongue Formation indicate that, although subsidence rates were decreasing, thermal subsidence still had an influence of the sedimentation architecture of Senonian sediments. Salt tectonics was very active during the Senonian as shown by the asymmetric turtleback structure (Figure 5.33), such as described by Vendeville and Jackson (1992). The prograding salt tectonics driven clinoforms in Figure 5.33c confirm that during the Senonian sedimentation was still from the NW. Towards the Late Cretaceous (75 Ma) there was a major uplift of the African continent, which, according to Hudec and Jackson (2004); Seranne and Anka (2005); Jackson *et al.* (2008); Oluboyo *et al.* (2013) was caused by an inversion of tectonics when North Atlantic changed its tectonic movements as it continued to open during the Late Cretaceous.

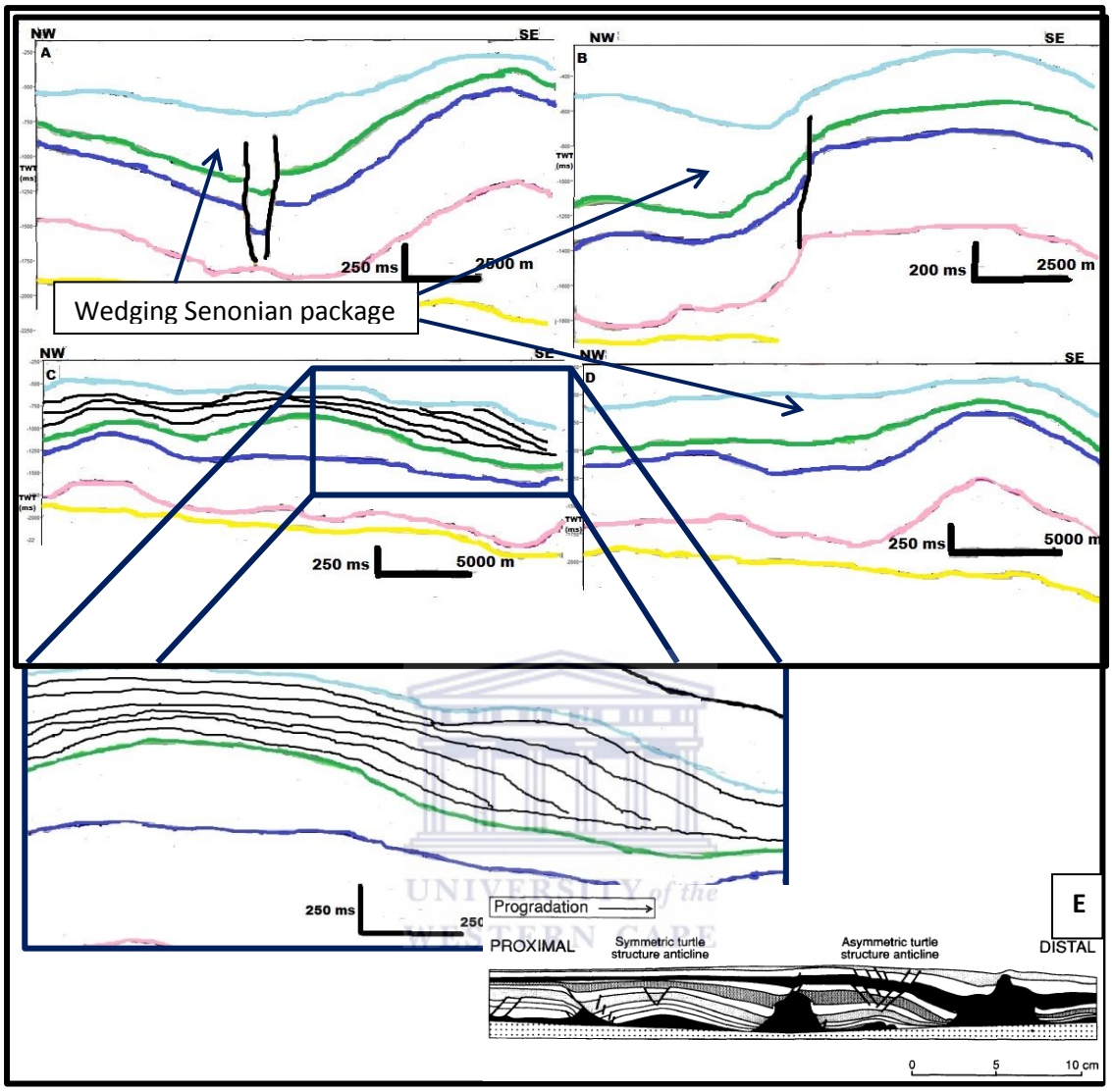

Figure 5.33: Effect of salt tectonics and thermal subsidence on the sedimentary architecture of the Senonian sediments. (a), (b) and (d) wedging Senonian sediments which is due to both thermal subsidence in the Senonian and salt tectonics in the Late Senonian; (c) and (e) assymmetric turtleback structures (provided for comparision) from Vendeville and Jackson (1992).

After the Late Cretaceous uplift, deposition of the Eocene Animba Formation contributed further salt tectonic and thermal subsidence probably ceased sometime during mid-Senonian, shown by the lack of fault cutting older Senonian sediments (Dupre *et al.*, 2007). The top of the Animba Formation is marked by an erosional boundary between the Eocene and Miocene sediments, which according to Oluboyo *et al.* (2013) is an unconformity that lasted for 10-20 Ma, and hence the Oligocene is not persevered in the shelf, but rather, basinwards. Although the origin of the unconformity is debatable, its genesis was linked to climate change, sea level fall and regional uplift of Central African during the Oligocene (Seranne and Anka, 2005;

Dupre *et al.*, 2007; Anka *et al.*, 2009). The evidence for active salt tectonics during the Eocene (Figure 5.34a) is an extensional diapir with normal faults cutting through the Eocene to recent sediments.

The succeeding Miocene M'Bega Formation was deposited during a period of high subsidence rate triggered by a rapidly cooling lithosphere basinwards (Rasmussen, 1996). However, during the Late Miocene, the shelf started to be uplifted as a result isostatic adjustments due to flexure of the oceanic crustal profile that resulted from the supracrustal loading of basinwards deposition of Eocene and Oligocene sediments (Rasmussen, 1996). In addition, the Miocene was a period of reactivation of salt tectonics, as extensional diapirs appear to have extended upward and reached the recent seafloor (Figure 5.34a). Onlapping Miocene sediments on the diapirs indicate that diapirism was active as the sediments were being deposited (Figure 5.34b).

The youngest Akasso Formation has been accumulating since the Pleistocene and underlain by a regional unconformity (Oluboyo *et al.*, 2013). Akasso Formation is also intruded by the currently active salt diapirs that reach the modern seafloor (Figure 5.34b).

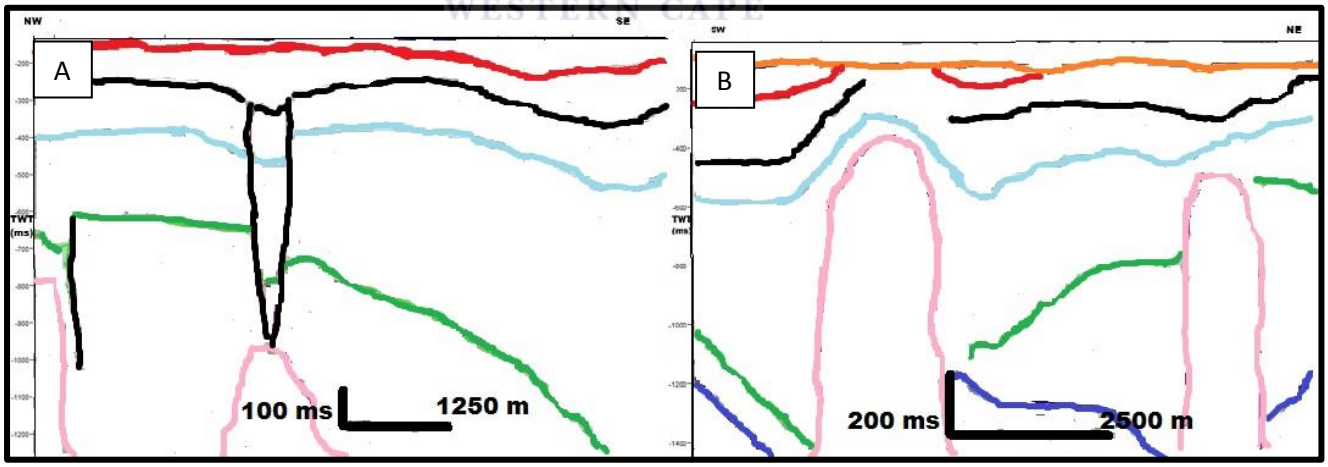

Figure 5.34: (a) Reactivation diapir, indicative of Miocene salt tectonics. (b) diapir intruding into the seafloor and offsetting Miocene sediments indicative of modern salt tectonics.

5.5 Post-salt hydrocarbon prospectivity

Although to date, the only economic plays in the EMP are confirmed in the pre-salt succession, this thesis aims to refine the identification of two potential petroleum plays and their petroleum system components in the post-salt sediments. (Table 5.3; Figure 5.35):

Table 5.3: System components of the potential petroleum plays in the post-salt sediments.

	PLAY 1	PLAY 2
Reservoirs	Madiela carbonates	Turonian shelf sands
Traps	Fault dependent 3 way structures and also the Albian, Cenomanian shales and also four way dip structures.	Four way dip structures, Senonian shales and Late Cretaceous unconformity boundary
Maturation & Hydrocarbon generation	During the Cretaceous for the Melania shales; possibly during Miocene in case of the Late Cretaceous shales (Martin *et al.*, 2009; Beglinger *et al.*, 2012)	During the Cretaceous for the Melania shales; possibly during Miocene in case of the Late Cretaceous shales (Martin *et al.*, 2009; Beglinger *et al.*, 2012)
Migration pathway	Windows within the Aptian Ezanga evaporites for the pre-salt sourced hydrocarbons	Windows within the Aptian Ezanga evaporites for the pre-salt sourced hydrocarbons

Both plays are charged by (a) an already proven lacustrine syn-rift Melania shale source rock, (b) potentially by the Albian shale stringers as well as (c) the Cenomanian shales (Figure 5.35) (Gill and Cameron, 2002; Martin *et al.*, 2009; Beglinger *et al.*, 2012). Since detailed modeling of the migration pathway of hydrocarbons is beyond the scope of this project, for practical reasons, this project assumes a simple migration pathway that follows the gradient of the steepest slope vertically.

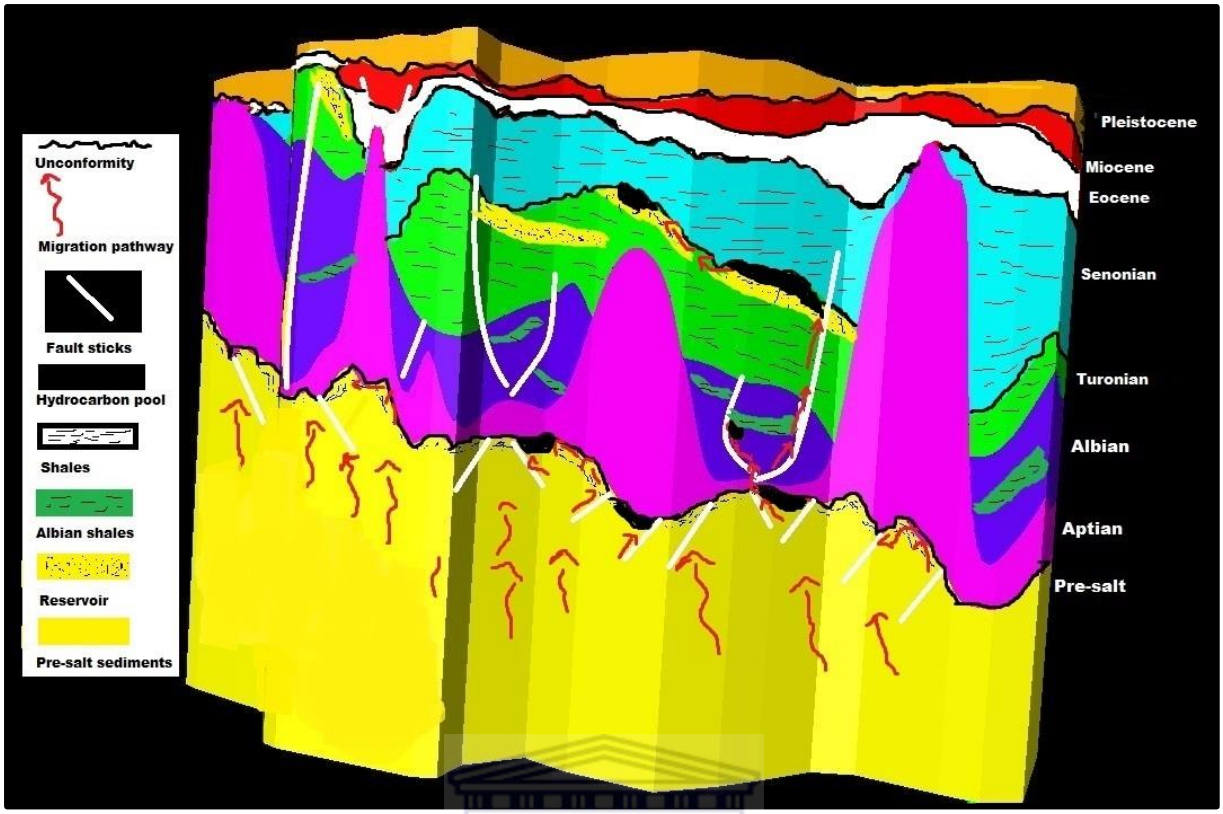

Figure 5.35: Simplified model derived from real data, showing potential post-salt plays in the EMP and how they might accumulate.

For the accumulation of pre-salt sourced hydrocarbons in the post-salt reservoirs, windows in the salt had to serve as migration pathways, allowing communication between the pre-salt and the post-salt sediments. In order to identify such windows in the salt, certain key stratigraphic surfaces were investigated in detail with the aid of Petrel® 3D modeling software. First, the base of the salt reflector (i.e., top of Gamba), and then the top of the salt was selected. Using the structural framework option in Petrel®, the base and the top of the salt geobodies were extracted and finally, the two maps were overlain on top of each other to identify the areas where they are intersecting (Figure 5.36).

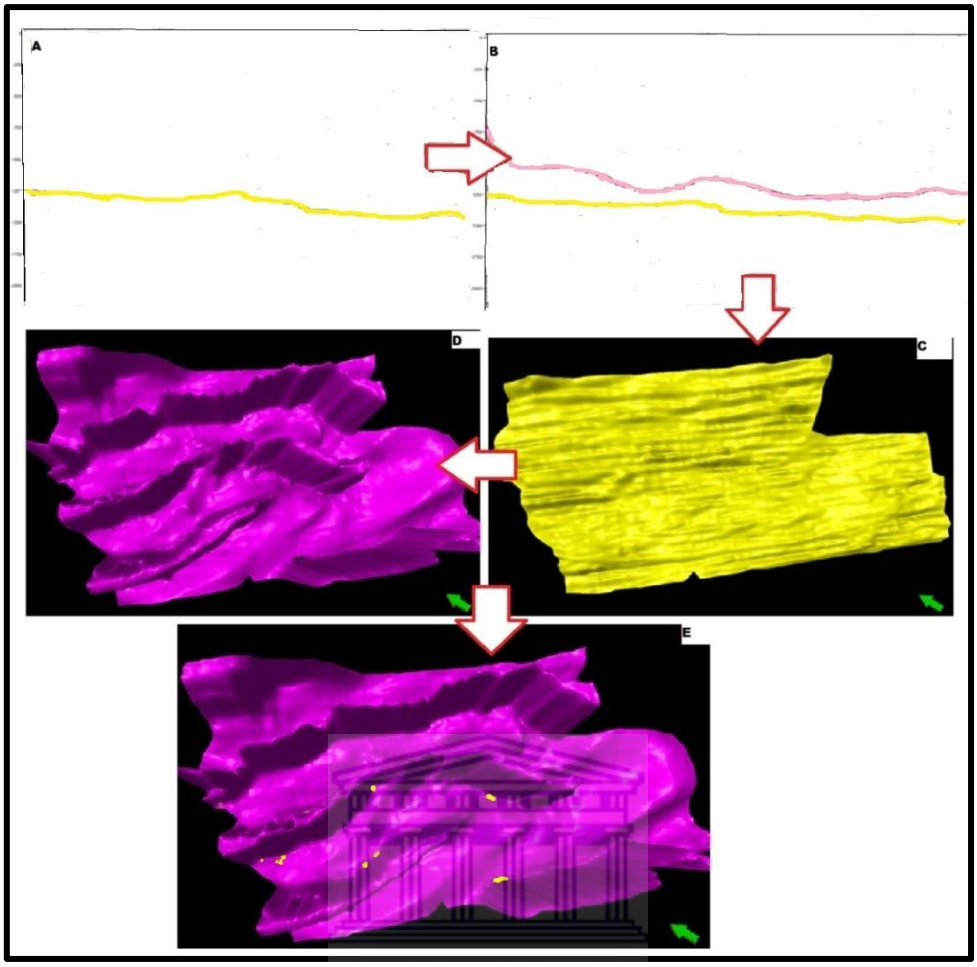

Figure 5.36: Stepwise method in identifying windows in the salt, derived using structural framework in Petrel® . Extracted geobodies for the top (purple) and the base (yellow) of the salt, which were overlain to identify windows within the salt.

Using this method, five windows with a radius ranging from 500-2000 m were delineated on the seismic section (Figure 5.36). In absence of geochemical data, ascertaining whether any hydrocarbons might have passed through these windows is not possible; assumptions were made based on information from the closest well to the windows. Window 1 is situated up dip of well EMP6.2 which is oil producing, and thus there might be the possibility that hydrocarbons could have migrated through this window into the post-salt sediments (Figure 5.37). The closest well to window 2 is the dry EMP11 well, which is down dip from the window, so, it is unlikely that hydrocarbons could have passed through window 2 (Figure 5.37). Window 3 is located up dip of well EMP2 and EMP12, which are dry wells, so similarly with window 2; hydrocarbons are unlikely to have migrated through window 3 (Figure 5.37). Window 4 is located up dip of well EMP13, which is an oil producing well, hence there is some probability for hydrocarbon migration through window 4 (Figure 5.37). There are no wells near window 5, thus assessing it for potential hydrocarbon migration is unjustified (Figure 5.37).

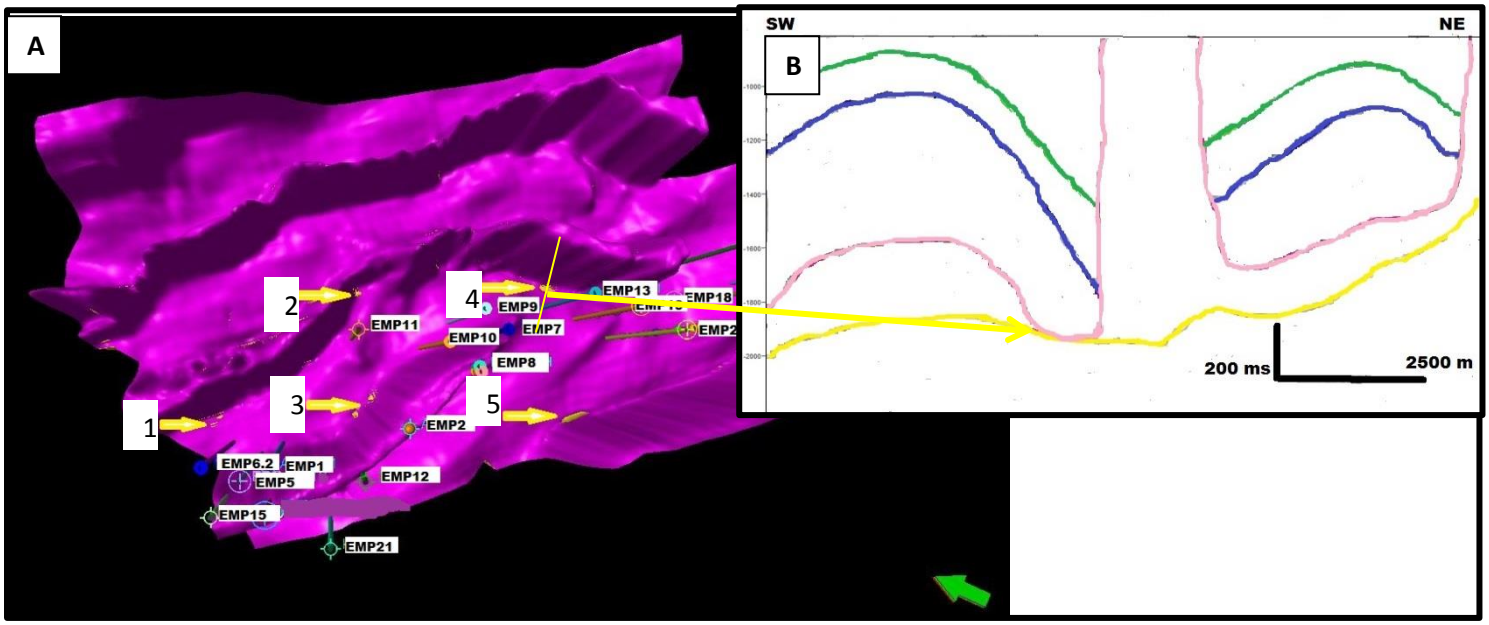

Figure 5.37: Windows in the Ezanga salt, which could act as a migration pathway between pre and post-salt sediments. For each of the 5 windows, a seismic section shows the configuration of the hole and the surrounding wells.

Potential post-salt source rocks are the Albian and Cenomanian shales that were deposited under anoxic conditions and contain an estimated TOC of 3% (Beglinger *et al.*, 2012). Although the Cap Lopez Formation is organic rich and was deposited in anoxic conditions, making it a potential source rock, since heat flow and source rock analysis studies are beyond the scope of this thesis, we cannot say with enough confidence that these shales in the EMP have reached maturity. However, since both Type I (pre-salt lacustrine environment) and Type II (post-salt marine environment) kerogen have been found in the Yombo field reservoirs, there is a possibility that the EMP reservoirs might also be charged with both Type I and II kerogen (Ala and Selley, 1997). However, to reduce uncertainty in our study we will assume that these post-salt shales are immature.

6 DISCUSSION

6.1 Albian to Cenomanian

After deposition of evaporites, relative sea level (RSL) increased, allowing production of thick carbonates to take place at a steady pace in a ramp/platform setting (Hudec and Jackson 2004; Seranne and Anka, 2005; Dupre *et al.*, 2007). This rise in RLS was primarily triggered by the rapid thermal subsidence in the basin. The relatively sudden increase in accommodation space is manifested as syn-depositional normal faults that intersect the carbonate platform succession (Figures 6.1 and 6.2), and which also caused the basin to tilt seawards (Seranne and Anka, 2005; Dupre *et al.*, 2007). Furthermore, the thick pile of platform carbonate accumulation exerted a continued sedimentary loading (probably differential) and triggered the first event of salt tectonics in the Albian, when gravitational gliding moved the salt basinwards (Figure 6.1). According to Seranne and Anka (2005); Dupre *et al.* (2007); Jackson *et al.* (2008), this basinwards movement of the salt indicates that a slope (gliding surface?) must have formed. In the EPM, however, the tabular nature of the platform carbonates suggests that the sediment architecture was primarily influenced by a regionally uniform, thermally driven subsidence rather than salt tectonics.

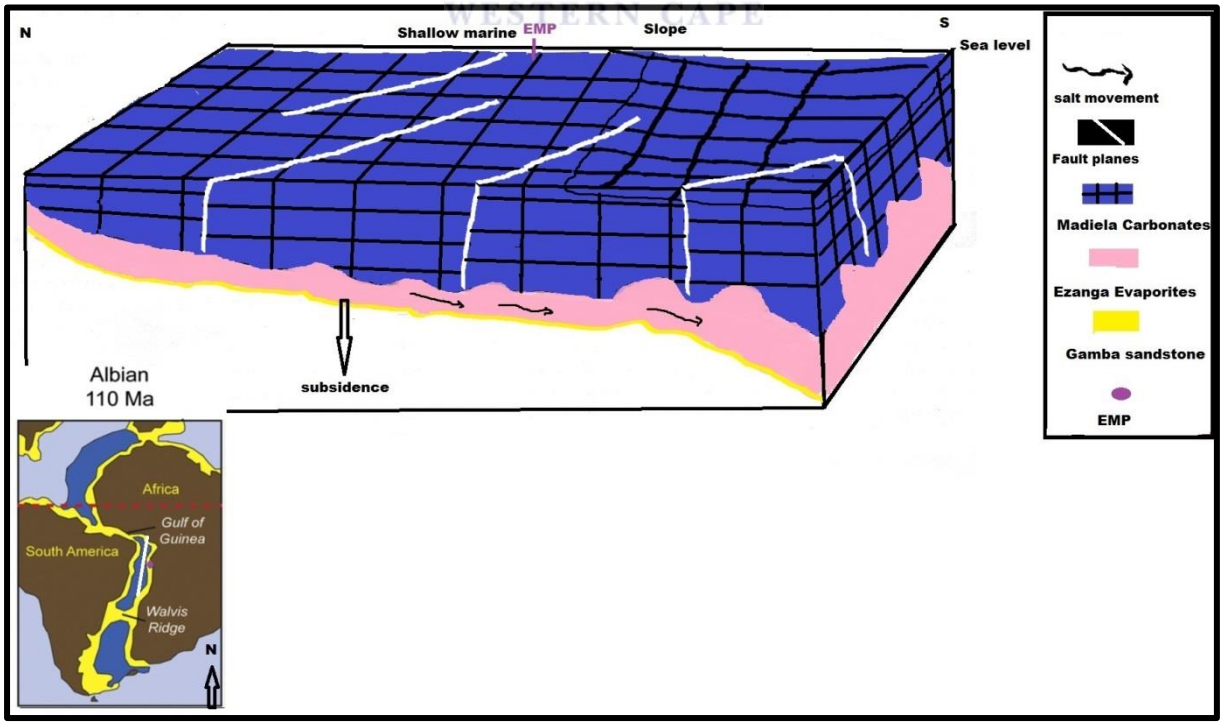

Figure 6.1: Lower Congo Basin during the Albian, indicating a rapid relative sea level rise (TST), which resulted in the production of platform carbonates, and the subsequent basinwards movement of the Ezanga evaporites. The aerial map was modified from Beglinger *et al.* (2012). Images are not to scale.

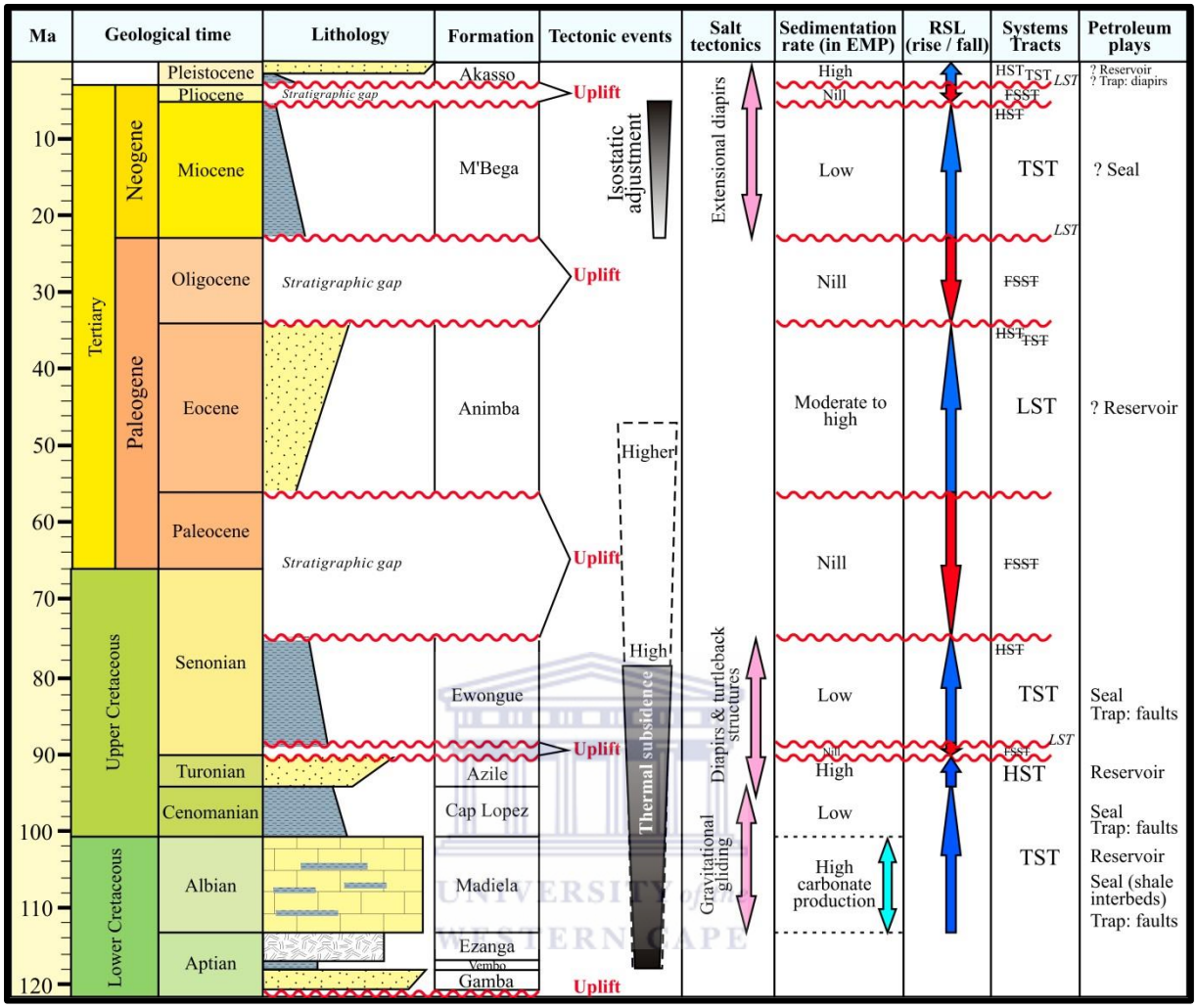

Figure 6.2: EMP stratigraphic column indicating where potential petroleum plays can be expected based on system tracts, the system tracts that has been strikethrough represent system tracts that were deposited by was removed by ersosion, modified after Gill and Cameron (2002).

6.2 Cenomanian to Turonian

At this time, as South America continued to drift away from Africa, the basin continued to thermally subside and tilt seawards (Dupre *et al.*, 2007). Simultenlously, the relative sea level (RSL) increased further and, because the carbonate factory was unable to keep up with the rising RSL (Figures 6.2 and 6.3), the carbonate platfrom drowned (Sarenne and Anka, 2005; Dupre et *al.*, 2007; Jackson *et al.*, 2008). Carbonate sedimentation was replaced by the influx of clastics (shale and shaly sands of the Cap Lopez Formation - see gamma ray logs; Figure 6.3) in the Cenomanian (Sarenne and Anka, 2005; Dupre et *al.*, 2007; Jackson *et al.*, 2008), which could indicates the futher increase in RSL due to ongoing thermal subsidence.

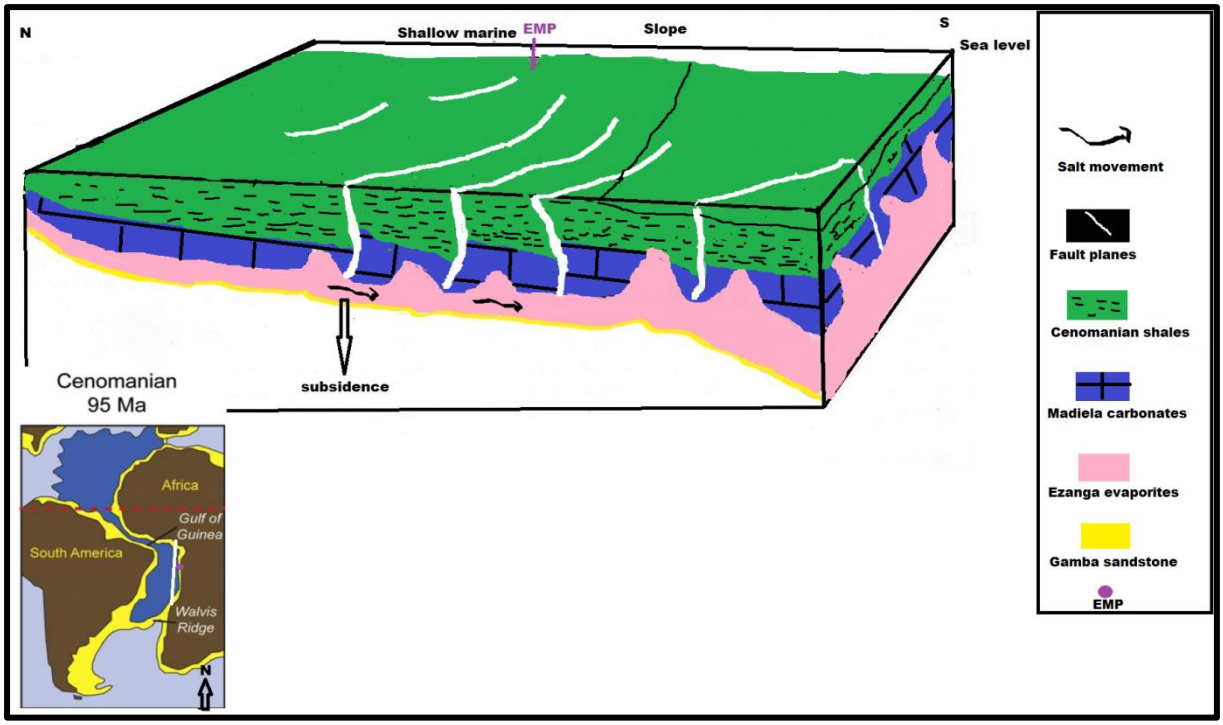

Figure 6.3: Continued RSL rise in the Cenomanian, shutting off carbonates production, which was replaced by clastic sedimentation (Cenomanian shales). The aerial map was modified from Beglinger *et al.* 2012. Images are not to scale.

Coarser Turonian shelf sands over the Conomanian shaly sands indicates a regressieve shoreline in the Turonian. The conformable contact between the shales and sands indicate that the RSL rise eventually slowed down (deccelerated) and was outpaced by the rate of sedimentation which resulted in a normal regressive shoreline in the Turonian and the generation of a high stand system tract (HST). Relatively high sedimentation rates in the Turonian are suggested by the common turtleback structures of the Azile Formation (Figure 5.32d). Dupre *et al.* (2007) also suggest that the Turonian diapirism was initiated by the high sedimentation rates. Truncation at the top of Azile Formation indicate a fall in relative sea level that resulted in the forced regression of the shoreline during the Late Turonian (Figure 6.2). This relative sea level fall could have been driven by a local uplift as explained by Pletsch *et al.* (2001) (Figure 6.4). The presence of incised channels that cut into the Azile Formation are further evidence of a FSST (Figure 6.2). During this uplift, the shelf and shallow marine areas received limited amount of sediments, if any, and consequently, permeable sand bodies (i.e., potential reservoirs) were probably being deposited as LST deposits basinwards (Figure 6.2) (i.e., in the licence blocks south of the EMP).

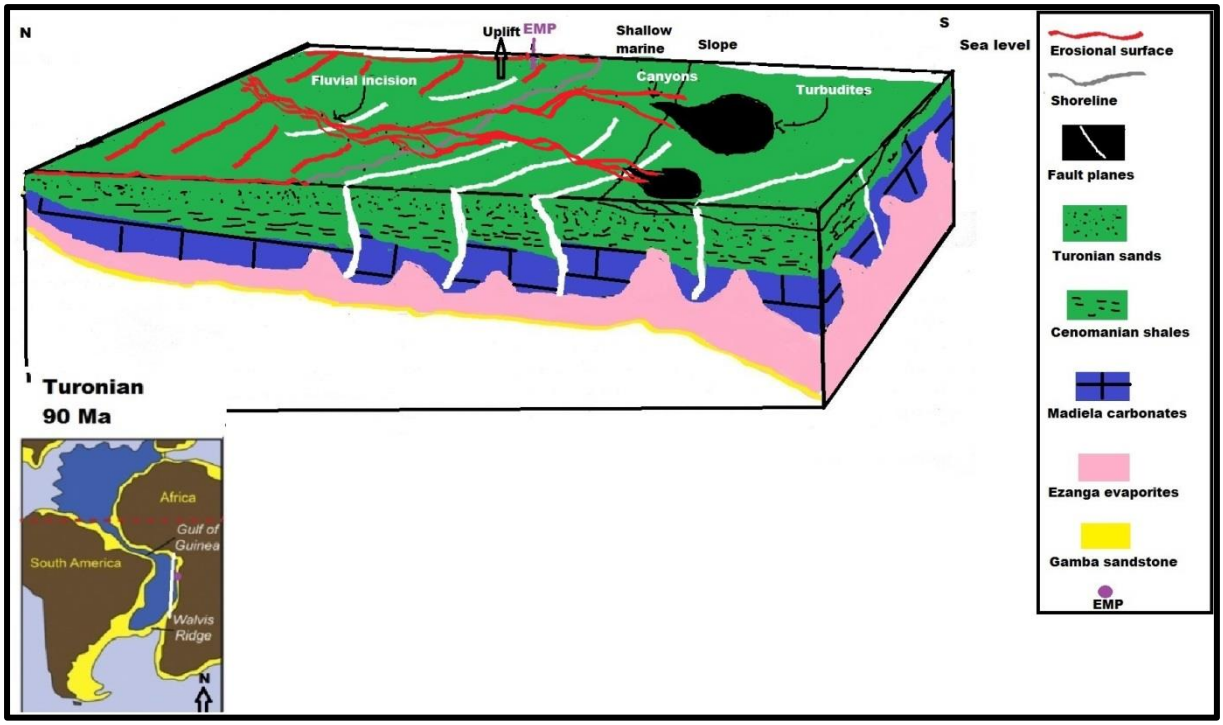

Figure 6.4: Simplified basin reconstruction during the Turonian uplift. The aerial map was modified from Beglinger *et al.* (2007). Images are not to scale.

6.3 Turonian to Senonian (75 Ma)

After the Turonian local uplift, as South America continued to drift away from Africa resulting in a wider and deeper, more established south Atlantic. According to Pletsch *et al.* (2001), the Senonian was a period of rapid eustatic sea level increase, which caused the deepening of all marine settings as well as marine flooding in the nearshore regions. These events on the other hand resulted in the study area becoming more marine dominated and an increase in the RSL within it (Figures 6.2 and 6.5) (Beglinger *et al.*, 2012). Separated from the Turonian sands by a subaerial unconformity is the fining upwards sequence of the Ewongue (Senonian) Formation, which indicates that RSL rise outpaced sedimenatation rates, resulting in a retrogradational stacking pattern that form during transgression. Syn-depositional faults at the base of this sequence suggest that after the Turonian uplift, the subsidence in the basin was renewed, and reactivated the Albian faults (Figure 5.30a.). Within the Senonian sediments, wells EMP16 and EMP22 (Figure 5.11 for the location and 5.21 for gamma ray signature) shows a fining upwards sequence, which is what we would expect in a transgressive system. However, well EMP6.2 (Figure 5.11 for the location and 5.21 for gamma ray signature), shows a coarsening upwards sequence in contrast to the other

wells, this coarsening upwards sequence probably represent the LST coarser Eocene sands channel infill.

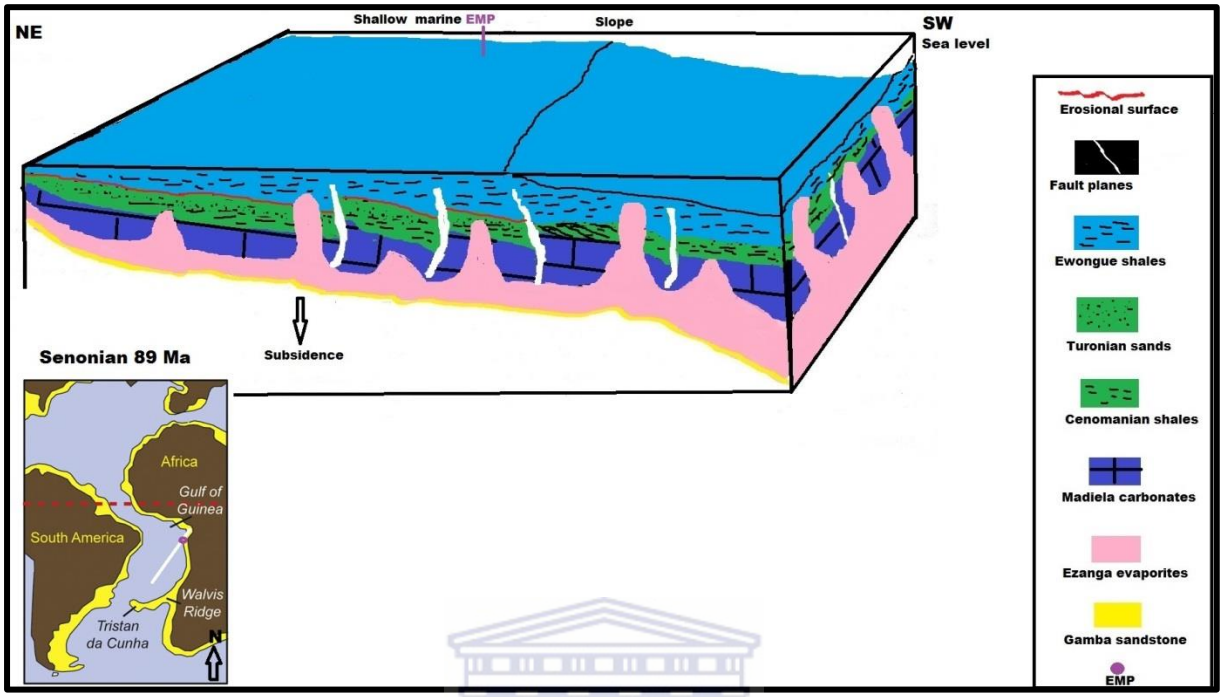

Figure 6.5: Simplified model indicating the rise in RSL during the Senonian. The aerial map was modified from Beglinger *et al.* (2012). Images not drawn to scale.

The end of Cretaceous was marked by a major uplift event along the southwestern margin of Africa, which resulted in what is preserved as truncations at the top of Ewongue Fornation (Figures 5.22, 6.2 and 6.6). This truncated surface probably represent the same Late Senonian (Campanian 75 Ma) major uplift of the African continent that is described in Hudec and Jackson (2004); Seranne and Anka, (2005); Jackson *et al.* (2008); Uluboyo *et al.* (2013) and probably eroded the HST sediments that could have formed in Late Senonian (Figure 6.2 and 6.4).

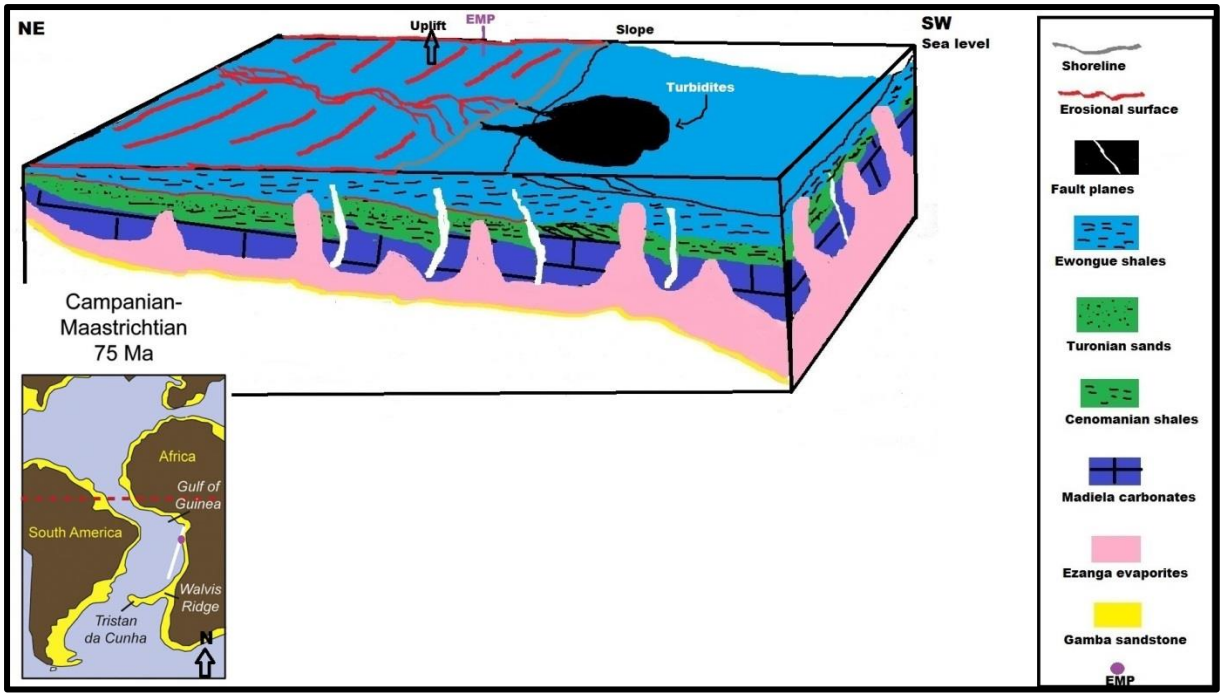

Figure 6.6: Major uplift during the Late Cretaceous that resulted in a drop in RSL. Aerial map was modified from Beglinger *et al.* (2012). Images not to scale.

6.4 Senonian (75 Ma) to Eocene

By this time, South America had completely separated from Africa and the Lower Congo Basin was part of the world ocean circulation (Rasmussen, 1996). Separated from the Senonian deposits by a subaerial unconformity is the Animba (Eocene) Formation. According to Rasmussen (1996), the Eocene was a period of sea level rise; however, our data shows a coarsening upwards sequence (Figure 6.2), indicating a regressive shoreline. A possible explanation for this is that after the Senonian major uplift, the shoreline probably moved all the way to the shelf break, exposing the shelf and depositing sediments basinwards. This would mean that the Animba Formation was deposited during a LST, which would explain the moderate sedimentation rates as calculated in section 5.2 and the coarsening upwards channel fills within the Senonian fining upwards sediments (Figures 6.2 and 6.7). This means that, although sea level was increasing as stated by Rasmussen (1996), it was out-paced by the sediments, which were being deposited basinwards bypassing the shelf. Unlike the previous strata, turtleback structures are not present in the Eocene sediments; and extensional diapirs are dominant. This might be explained by the low sedimentation rates over the shelf, which probably slowed down the rates of salt tectonics in the study area.

The top of the Animba Formation is highly erosional, indicating channelised features (Figure 5.25). According to Seranne and Anka (2005); Jackson *et al.* (2007) and Oluboyo *et al.*

(2013), there was a major uplift during the Late Eocene, which lasted for 10-20 Ma, and hence the Oligocene sediments are not preserved at the shelf. Furthermore, during the Oligocene, there were major changes in climate and sediment supply, and the African continent assumed its current configuration (Rasmussen, 1996; Seranne and Anka, 2005; Dupre *et al.*, 2007; Jackson *et al.*, 2008; Anka *et al.*, 2009; Beglinger *et al.*, 2012; Oluboyo *et al.*, 2013). This Late Eocene-Oligocene uplift caused incision of channels into the shelf as well as sediment bypass over the rest of the shelf and, deposition (probably in form of turbidites) in more offshore, basinwards areas during an LST. Evidence of this basinwards deposition of Oligocene sediments is in the distal (slope setting) Anton and Astrid Martin Permits, where sandy Oligocene sediments are preserved in the slope channels (Jackson *et al.*, 2008).

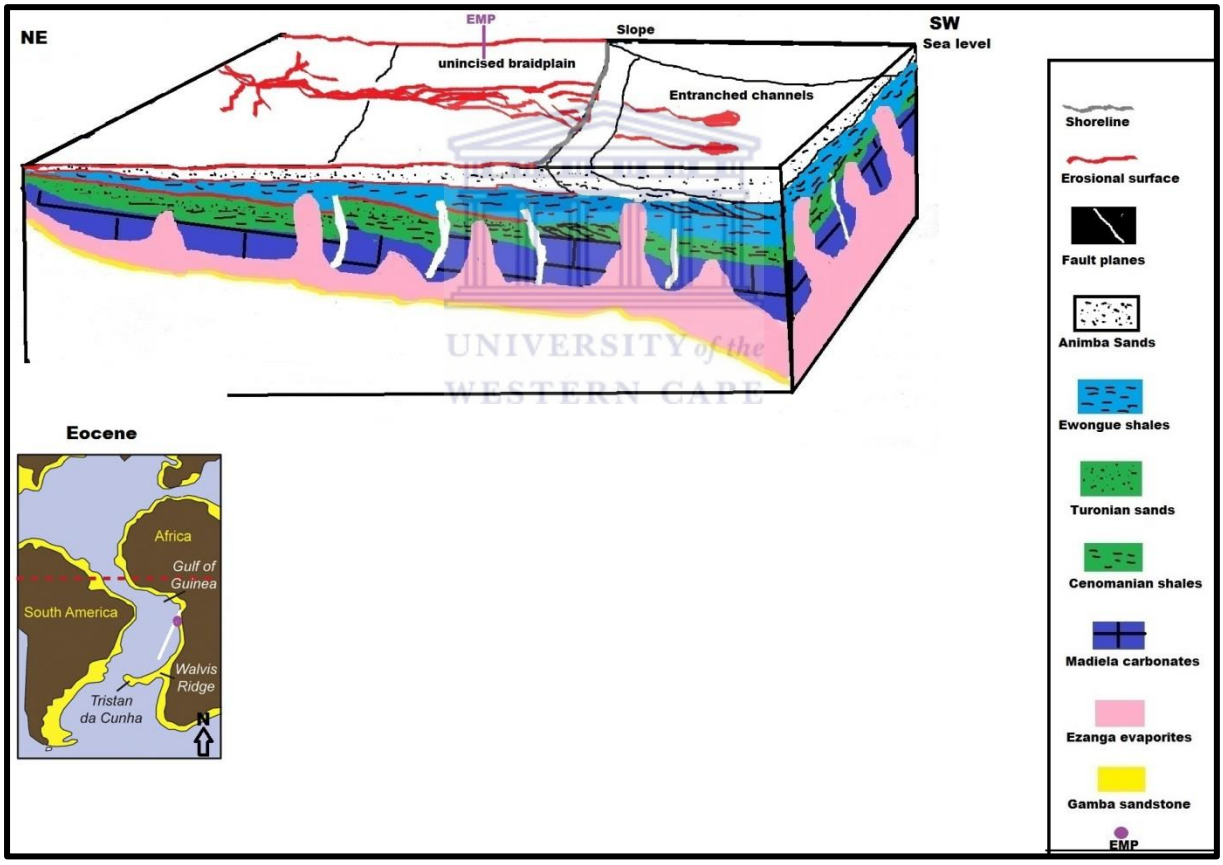

Figure 6.7: Simplified model for the major uplift during the Late Eocene, which cause an erosional surface that can be correlated all the way to the Orange Basin, South Africa. Aerial map was modified from Beglinger *et al.* (2012).

6.5 Miocene

The Miocene M'Bega Formation rests on a subaerial unconformity and predominantly comprises shales and clays (very high gamma ray signatures), suggesting that after the

Eocene/Oligocene uplift, RSL rise eventually outpaced sedimentation and this resulted in a transgressive event that allowed the deposition of the retrogradational sequence (hence the M'Bega Formation is a TST) (Figures 6.1 and 6.8). This TST could have been due to the high subsidence rates which were triggered by a rapidly cooling lithosphere (Rasmussen, 1996). Low sedimentation rates, as calculated in section 5.2, are further evidence that the Miocene was a period of RSL rise in the study area due to the fact that during a TST, most sediments are 'trapped' near shore, resulting in an increasingly thinner sediment package in offshore direction (i.e., basinwards) (Catuneanu, 2006). Onlapping stratal terminations as shown in Figure 5.25 are also further evidence of a TST during the Miocene. Furthermore, the M'Bega Formation also contains evidence for a change in sediment transport direction, which is more from E to W, in contrast to the pre-Miocene sediments, which seem to be transported from a more NW direction. The E to W transport direction during the Miocene could be a result of the continent assuming the current shelf and slope configuration during the major climate change and/or uplift events of the Oligocene (Rasmussen, 1996; Seranne and Anka, 2005; Oluboyo *et al.*, 2013). Furthermore, by this time the West African marine settings were nourished by ancient rivers that transported eroded sediments from the uplifted Central Africa regions (Rasmussen, 1996; Seranne and Anka, 2005; Oluboyo *et al.*, 2013). The top of the M'Bega Formation is erosional; this could be due to the uplift of the shelf during the Late Miocene as a result of isostatic adjustment caused by Eocene and Oligocene basinwards deposition. In addition, according to Martin *et al.* (2009), the Albian and Cenomanian source rocks reached their maturity in distal deeper facies during the Miocene.

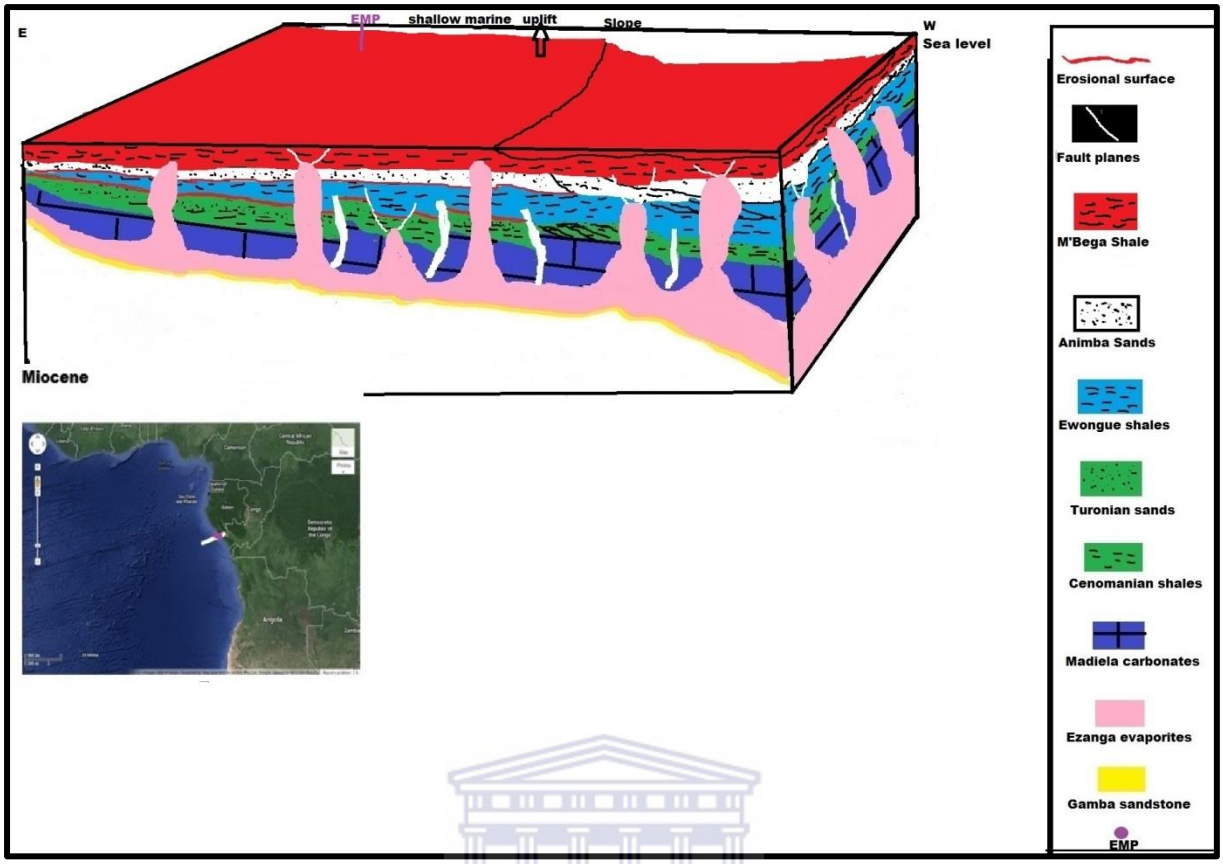

Figure 6.8: Simplified model of the rising RSL during the Miocene. Aerial map is from Google Earth Image 2014.

6.6 Pleistocene to present day

The Pleistocene Akasso Formation is separated from the underlying Miocene sediments by submarine erosion. This Pleistocene to Recent succession is being deposited at high sedimentation rates and is fed by the West African river system (Oluboyo *et al.,* 2013). The base of Pleistocene sediments is made up of shaly sands (high gamma ray - Figure 5.28), which were probably deposited during a TST after the Miocene RSL drop. Coarser Akasso Formation sands then conformably overlie these shaly sands. This coarsening upwards sequence (Figures 6.2 and 5.28) in the shelf indicates that during the Pleistocene, sedimentation rates outpaced relative sea level rise, resulting in a seaward movement of the shoreline, normal regression and progradation of the sedimentary facies forming a HST. The Anton and Astrid Marin Permits which are located westwards (basinwards) of the EMP, contain hemipelagics and distal overbank deposits, which are facies equivalent of the proximal Akasso Formation. Figure 6.9a is a simplified model showing the current configuration of the Lower Congo Basin, with RSL at a highstand. Figure 6.9b shows the current configuration of the stratigraphy of the EMP derived using Petrel® from the current

data. The onlapping stratal terminations of the Pleistocene sediments over the salt are evidence that salt tectonics is still active, and this is most likely due to the continued increase of sediment load over the pre-Albian evaporates.

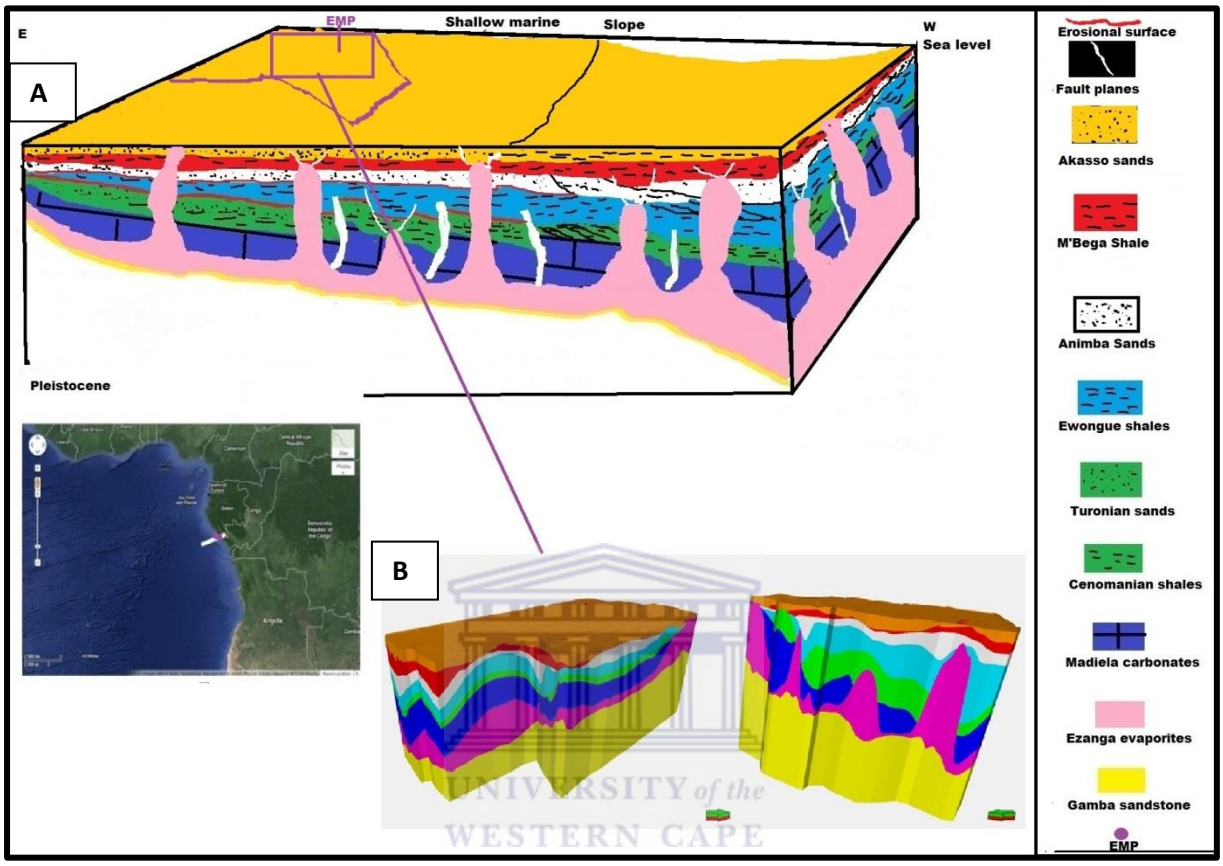

Figure 6.9: (a) Simplified model illustrating the correct stratigraphic configuration of the Lower Congo Basin since the Pleistocene. (b) EMP layered cake stratigraphic model derived from EMP data using Petrel® . Aerial map is from Google Earth Image 2014.

6.7 EMP post-salt hydrocarbon prospectivity

The two potential petroleum plays identified were in the Madiela carbonates and the Turonian sands. Since petrophysical analysis is beyond the scope of this study, and no completion report or composite logs were provided, as is globally accepted that the majory of oil producing reservoirs are carbonates (Reading, 1996), we will assume that the shallow water carbonates are good reservoirs. However, even with this assumption it should be noted that Madiela carbonates have highly variable lateral velocity, meaning that the Madiela Group is made up of different facies, both laterally and vertically. Since the Turonian sands were deposited during a HST in shallow marine setting, they are probably gradationally based shoreface and shelf facies, and hence these shoreline sands would generally make good reservoirs (Table 3.3). Other potential post-salt reservoirs are the silty sands of the Eocene

Animba Formation and also the Pleistocene HST Akasso Formation sands, with the marine M'Bega Formation forming a potential seal. Stratigraphic traps associated with diapirism would be the main trapping mechanism for these post-Cretaceous reservoirs (Figure 6.2). The main traps are fault dependent three way structures in both the carbonates and Turonian sands and the four ways dip structures for the Turonian sand. The Cenomanian and intraformational shales in the Madiela carbonates are seals for the Madiela reservoirs and the thick Senonian shaly sands deposited during a TST act as a seal for the Turonian reservoirs. According to Beglinger *et al.* (2012) and Martin *et al.* (2009) the Albian and Cenomanian shales matured during the Miocene and producing type II kerogen with TOC of up to 3%. However, it is important to note that since source rocks evaluation and migration pathway modeling are beyond the scope of this thesis, we have assumed a simple vertical migration pathway and to reduce further uncertainty in our study, we will assume that post-salt source rocks are immature because heat flow and burial history studies are beyond the scope of this thesis.

This means that, the EMP post-salt reservoirs would rely on the proven pre-salt Melania shale to charge them, on condition that there are windows in the salt, which would serve as a migration pathway for these hydrocarbons. Five windows were identified in the salt, two of which were located up dip of oil wells. As such, there is a possibility that hydrocarbons could have migrated through these windows, however this does not completely write off the other windows, because as shown by Van Balen *et al.* (2000), migration pathways can be very complex. Identifying these windows came with the following uncertainties; due to high acoustic contrast between the carbonates and the salt, the top of the salt can be picked with enough confidence, so there is very little uncertainty for picking the top of the salt. However, as also noted by Dupre *et al.* (2007), there is a large uncertainty in picking the base of the salt, which means that the size, shape or even location of the windows might be slightly different depending on who interpreted the base of the salt and their experience in seismic interpretations. It is for this large uncertainty that the base of the salt (top of Gamba) was interpreted based on the interpretation that was provided with the data. The salt windows ranges from 500-2000 m in diameter, however, although the windows will be laterally resolved, the vertical resolution of the salt (71 m) and the Gamba Formation (44 m), adds another uncertainty to whether these windows exist or not. An easier way of decreasing this uncertainty would be by assembling a number of experienced seismic interpreters to

independently interpret the base and the top of the salt. Furthermore, increasing the resolution of the seismic can help lower the uncertainty in interpreting the base and the top of the salt.

The post-salt play has been proven in the Yombo field as already discussed in section 1.4. However according to Lundin Petroleum reports (2011), most of the Oil in the Yombo field is heavy oil, which could have low API because shallow oil reservoirs are very susceptible to biodegradation. What this means for our case is that, if the post-salt reservoirs are explored in the EMP, there is a risk of the reservoirs containing heavy oils.

7 CONCLUSIONS AND RECOMMENDATIONS

7.1 Conclusions

- Post-salt Lower Congo Basin evolution can be attributed to the interplay between, RSL, sedimentation rates, tectonic and salt tectonics.
- Albian carbonates (Madiela), which immediately overly the Ezanga evaporites were deposited during a period of high thermal subsidence rates and have variable lateral and horizontal velocities due to the presence of intraformational shales. These carbonates were deposited during a TST, which according to Hudec and Jackson (2004) and Durpre *et al.* (2007) to have initiated salt tectonics and are potential post-salt reservoirs.
- Conformably overlaying the Madiela Formation are the Cenomanian Cap Lopez shaly sands, which were deposited during a rapid RSL rise, shutting off carbonates production and favouring deposition of clastic sediments. These shaly sands are potential post-salt source rock and seal.
- RSL rise reached a highstand, followed by deposition of the Turonian Azile shelf sands, the load of these sands together with the Cenomanian shaly sand and the Madiela Group sediments initiated diapirism (Dupre *et al.,* 2007). Salt tectonic became very active as evidence by turtleback structures that are common within the Madiela Formation and the Cenomanian/Turonian sediments in the shelf. These shelf sands are eroded at the top due to a local Turonian uplift and are potential reservoirs.
- RSL increased again, depositing a thick unit of silty sands, which together with the Turonian unconformity are a potential seal and trap for the Azile reservoirs. This load over the salt increased salt tectonics rates, resulting in formation of asymmetric turtleback structure. Thermal cooling of the lithosphere was increasing since the Albian, as evident by syn-depositional normal faults which stretches from the Albian carbonates to the base of Senonian sediments probably stopped sometime during the Early Senonian.
- Truncations at the top of the Senonian sediments indicate a major unconformity during the Late Cretaceous, probably the same uplift as noted by Hudec and

Jackson (2004); Seranne and Anka (2005); Jackson *et al.* (2008) and Oluboyo *et al.* (2013).

- The Senonian uplift pushed the shoreline all the way to the shelf break, resulting in moderate sedimentation rates of Eocene sediments over the shelf because they were being deposited basinwards in a LST.
- The top of Eocene is also very erosional marking another major unconformity, which lasted for 10-20 Myrs (Rasmussen, 1996; Seranne and Anka, 2005; Uluboyo *et al.,* 2013), resulting in Oligocene sediments bypassing the shelf and being deposited basinwards.
- As evident by the onlapping stratal terminations and a fining upwards sequence, the Miocene was a period of RSL rise. However, basinwards deposition of the Eocene and Miocene sediments caused the shelf to be uplifted (isostatic rebound?) during the Late Miocene (Rasmussen, 1996). The top of Miocene sediments is marked by an erosional surface, which could be due to the uplift of the shelf, which outpaced eustatic sea level rise during Late Miocene.
- From the Eocene to Miocene, extensional diapirs become dominant, and there is no turtleback structure after the Cretaceous.
- High sedimentation rates, a normal regressing shoreline and pelagic distal facies (Anton and Astrid Marin Permits) indicate that the Pleistocene to present sediments are being deposited during a HST, following a TST from the Lower Pleistocene (Figure 6.2). Pleistocene sediments onlaps on the diapirs and these diapirs protrude into the seafloor, indicating that salt tectonics is still active to date
- The two plays identified occur in the Madiela carbonates and Turonian shelf sands;
- Both plays can be charged by pre-salt Melania shale, on condition that there are windows within the extensive Ezanga salt.
- Out of the five windows that were identified, two (Window 1 and 4) are located near oil producing wells, and we concluded that there is a possibility that hydrocarbons might have used those windows as migration pathways.
- Based on information of the post-salt Yombo field reservoirs, since the EMP post-salt reservoirs are facies equivalent of the Yombo field and are also very shallow, there is a probability that if these reservoirs contains any hydrocarbons, those hydrocarbons might also be biodegraded.

- If both Type I and II kerogen are to be found in the EMP post-salt reservoirs, we can conclude that Albian and Cenomanian shales reached maturity.

7.2 Technical recommendations

The first drill test well should be in a structural closure near window 4, because in comparison with other windows, this window has less uncertainty due to its size and its location close to an oil well. If this well is successful, the EMP hydrocarbon exploration can also be focused on post-salt reservoirs. Following this study, the top and base of the salt can be reinterpreted in order to confirm the presence and location of the windows. Furthermore, detailed study of heat flow and modeling of possible migration pathways should follow this study. More technical work would include looking out for exceptionally well-exposed, large-scale and structurally undisturbed outcrops onshore to study them and understand better those aspects that the subsurface data is not able to show at this stage due to resolution limitations. Such high-resolution outcrop investigations can assist in documenting and better understanding the abundance and variation in sedimentary facies. Furthermore, if fieldwork is to be conducted on a regional-scale, the outcrop-based information may be scaled up and used to refine the predictive geological framework used for stratigraphic correlation as well as natural resource exploration. High-resolution outcrops-based studies thus may potentially improve the geostatistical modeling of facies architecture (e.g., continuity, geometry) in reservoirs and the estimating of the permeability distribution patterns in depositional systems that may act as petroleum play.

REFERENCES CITED

Ala, M. A and Selley, R.C. 1997. The West African Coastal Basins. In: Selley, R.C. (ed) African Basins. *Sedimentary Basins of the World*, 3, Ch. 8. Elsevier Science B.V., Amsterdam, 173-186.

Anka, Z., Séranne, M,. Lopez, M., Scheck-Wenderoth, M and Savoye, B. 2009. The long-term evolution of the Congo deep-sea fan: A basin-wide view of the interaction between a giant submarine fan and a mature passive margin (ZaiAngo project). *Tectonophysics*, **470**, 42-56.

Beglinger, S. E., Doust, H and Cloetingh, S. 2012. Relative petroleum system and play development to basin evolution: West African South Atlantic basins. *Marine and Petroleum Geology*, **30**, 1-25.

Binks, R. M and Fairhead, J.D. 1991. A plate tectonic setting Mesozoic rifts of West and Central Africa. *Tectonophysics*, **213**, 141-151.

Biddle, K. T and Wielchowsky, C. C. 1994. Hydrocarbon traps. In Magoon,L.B and W.G. Dow,eds. The petroleum system-from source to trap: *AAPG Memoir*, **60,** 219-235.

Boggs, S. 2006. Principles of Sedimentology and Stratigraphy (4th edition). Pearson Prentice Hall, Upper Saddle River, NJ.

Bordy, E. M., Hancox, P.J., Rubidge, B. S. 2004a. Basin development during the deposition of the Elliot Formation (Late Triassic - Early Jurassic), Karoo Supergroup, South Africa. *South African Journal of Geology*, **107**, 395-410.

Bordy, E. M., Hancox, P. J., Rubidge, B. S. 2004b. Fluvial style variations in the Late Triassic - Early Jurassic Elliot Formation, main Karoo Basin, South Africa. *Journal of African Earth Sciences*, **38**, 383–400.

Boyd, D.L. 2010. Seismic interpretation, distribution, and basin modelling of natural gas leakage in Block 2 of the Orange Basin, offshore South Africa. Unpublished MSc thesis, University of Cape Town.

Brown, A. 1999. Interpretation of Three-Dimensional Seismic Data, Fifth Edition. *AAPG Memoir 42 SEG Investigations in Geophysics*, **9**, 355.

Brownfield, M. E and Charpentier, R. R. 2006. Geological and total petroleum system of the West-Central Coastal province (7203), West Africa. *U.S Geological Survey Bulletin* **2207-B.**

Bryant, I,. Herbst, N,. Dailly, P,. Dribus, J. R,. Fainstein, R,. Harvey, N,. McCoss, A. Montaron, B,. Quirk, D and Tapponier, P. 2012. Basin to basin. *Oilfield Review*, **3**, 38-57.

C and C Reservoirs. 2006. Lower Cretaceous Dentale and Gamba Formations: Braided-fluvial and lacustrine fan-delta sandstones, Rabi-Kaunga Field, South Gabon Basin, Gabon. Unpublished *Reservoir Evaluation Report Africa, Digital Analogs*.

Coe, A. L. 2002. The Sedimentary Record of Sea-Level Change. Cambridge, New York: Cambridge University Press. 57–98.

Catuneanu, O. 2002. Sequence stratigraphy of clastic systems: concepts, merits, and pitfalls. *Journal of African Earth Sciences*, **35,** 1–43.

Catuneanu, O. 2006. Principles of Sequence Stratigraphy, Elsevier, Amsterdam 375.

Chopra, S., Castagna, J.P. and Portniaguine, O. 2006. Seismic resolution and thin-bed reflectivity inversion. *CSEG Recorder*, **31**, 19-25.

Cramez, C. and Jackson, M. P. A. 2000. Superposed deformation straddling the continental-oceanic transition in deep-water Angola: *Marine and Petroleum Geology*, **17**, 1095–1109.

Dupre, S., Bertotti, G and Cloetingh, S. 2007. Tectonic history along the south Gabon Basin: Anomalous early post rift subsidence. *Marine and Petroleum Geology*, **24**, 151-172.

Duval, B.C., Cramez, C., Jackson, M.P.A., 1992. Raft tectonics in the Kwanza Basin, Angola. *Marine and Petroleum Geology*, **9**, 389–404.

Eilertsen, H. A. 2010. 3D seismic data indicate potential glide planes for submarine sliding : the mid-Norwegian margin Nyegga area. MSc thesis. University of Tromso.

Emery, D and Myers, K.J. 1996. Sequence Stratigraphy. London: Blackwell Science, 297.

Fossen, H. 2010. Structural geology. Salt tectonics, **19**, 371-392. Cambridge University Press.

Friedman, G. M., Sanders, J. R., and Kopaska-Merkel, D. C. 1992. Principles of Sedimentary Deposits: Stratigraphy and Sedimentology, Macmillan Publishing Co., New York, 717.

Gerry, R.L. 2012. EnerCom Oil and Gas Conference 2012. Denver. Unpublished report NYSE: EGY.

Gottschalk, R.R., Anderson, A. V and Walker, J.D. 2004. Modes of contractional salt tectonics in Angola Block 33, Lower Congo Basin, West Africa. in: Post, P.J., Olson, D.l., Lyons,K. T., Palmes, S.L., Harrison, P. J., and Rosen, N. C. (eds) *salt-sediments interaction and hydrocarbon prospectively: concepts, Application and case studies for the 21st century, 24th Annual research Conference*. SEPM Foundation, 705-734.

Gill, J and Cameron D. 2002. 3D reviews an old play: An Aptian subsalt discovery, Etame field, offshore Gabon, West Africa. *The Leading Edge*, **21**, 1147–1151.

Gray, S. 2000. Velocity Smoothing for Depth Migration: How Much is Too Much? Unpublished, unpaginated Report SEG. CGGVeritas. Permalink: http://dx.doi.org/10.1190/1.1815566

Hampson, D and Galbraith, M. 1981. Wavelet extraction using sonic log correlation. *Canadian Journal of Exploration Geophysics*, **17**, 24-42.

Haq, B.U., Hardenbol, J and Vail, P. R. 1987. Chronology of fluctuating sea levels since the Triassic (250 millionyears ago to present). *Science*, **235,** 1156-1167.

Haq, B.U and Schutter, S. R. 2008. A chronology of Paleozoic sea-level changes. *Science*, **322**, 64-68.

Hart, M.B. 1990. Cretaceous sea level changes and global eustatic curves; evidence from SW England. *Proceedings of the Ussher Society*, **7**, 268-272.

Hubral, P., Schleicher, J., Tygel, M., and Hanitzsch, C. 1993. Determination of Fresnel zones from traveltime measurements. *Geophysics*, **58,** 703–712.

Huc, A.Y. 2004. Petroleum in the south Atlantic. *Oil and Gas Science and Technology*. **59**, 243-253.

Hudec, M. R., and Jackson, M. P. A. 2004. Regional restoration across the Kwanza Basin, Angola: salt tectonics triggered by repeated uplift of a metastable passive margin: *AAPG Bulletin*, **88**, 971–990.

Hudec, M. R., and Jackson, M. P. A. 2007. Terra infirma: understanding salt tectonics: *Earth-Science Reviews*, **82**, 1–24.

Jackson, M.P.A., Cramez, C and Fonck, J.P. 2000. Role of subaerialvolcanic rocks and mantle plumes in creation of South Atlantic margins: implications for salt tectonics and source rocks. *Marine and Petroleum Geology*, **17**, 477 – 498.

Jackson, M. P. A., Hudec, M. R., Jennette, D. C., and Kilby, R. E. 2008. Evolution of the Cretaceous Astrid thrust belt in the ultradeep-water lower Congo Basin, Gabon: *AAPG Bulletin*, **92**, 487–511.

Kendall, A.C., and Harwood, G.M. 1996. Marine evaporites: arid shorelines and basins. In: Reading, H. G,. ed,. Sedimentary Environments: Processes, Facies and Stratigraphy, 3rd ed. Oxford, UK: Blackwell Science, 281-324.

Littau, J.S and Kiremblit, M. 2011. PSDM structural model constraints: Case studies. CGGVeritas, Argentina. Unpublished Report.

Long, A. 2003. Marine acquisition: moving beyond the signal-to-noise ratio. First Break, **21**, 67–70.

Lundin Petroleum. 2011. Blocks Marine XI and XIV, Republic of Congo. *First Energy Capital*.

Mantovani, M and Dugoujard, T. 2010. Simultaneous Joint Inversion as a Salt Detector in South Gabon Land Exploration. 72nd EAGE Conference and Exhibition incorporating SPE EUROPEC, Barcelona, Spain.

Mitchum, R. M. Jr., and Vail, P. R. 1977. Seismic stratigraphy and global changes of sea-level, part 7: stratigraphic interpretation of seismic reflection patterns in depositional sequences. In Seismic Stratigraphy–Applications to Hydrocarbon Exploration (C. E. Payton, Ed.), *American Association of Petroleum Geologists Memoir*, **26**, 135–144.

Merkel, R. H. 1979. Well log formation evaluation. Continuing Education Course Note Series. *American Association of Petroleum Geologists* #14, pp. 82.

Martin, J., Toothill, S., Veritas CGG and Mousavou, R. 2009. Hunting the pre-salt. Geo Expo (http://www.cgg.com/). *Frontier Exploration*, 39-41.

Miall, A. D. 2009. Correlation of sequences and the global eustasy paradigm: A Review of Current Data. *Frontiers + Innovation – 2009 CSPG CSEG CWLS Convention*, 123-126.

Miller, K.G., Sugarman, P.J., Browning, J.V. Hernandez, J. C. Olsson, R.K., Write, J.D., Feigenson and Sickel, M.D. 2003. Late Cretaceous chronology of large, rapid sea-level changes: Glacioeustasy during the greenhouse world. *Geological Society of America*, **31**, 585–588.

Neal, J., Risch, D and Vail, P. 1993. Sequence Stratigraphy-a Global Theory for Local Success. *Oil Field Review*, **5**, 51-62.

Nance, R.D., Murphy, B. J and Santosh, M. 2014. The supercontinent cycle: A retrospective essay. *Gondwana Research*, **25**, 4–29.

Oluboyo, A. P.,. Gawthorpe, R. L., Bakke, K and Hadler-Jacobsen, F. 2013. Salt tectonic controls on deep-water turbidite depositional systems: Miocene, southwestern Lower Congo Basin, offshore Angola. *Basin Research,* **26**, 1–24.

Pletsch, T.,Erbacherb, J., Holbourna, A.E.L., Kuhnta W., Moulladec, M Oboh-Ikuenobeded, F.E., Södinge, E and Wagnerf, T. 2001. Cretaceous separation of Africa and South America: the view from the West African margin (ODP Leg 159). *Journal of South American Earth Sciences*, **14**, 147-174.

Quirk, D. G and Pilcher, R.S. 2012. Flip-flop salt tectonics, *Geological Society of London, Special Publications*, **363**, 245-264.

Rasmussen, E. S. 1996. Structural evolution and sequence formation offshore South Gabon during the Tertiary. *Tectonophysics*, **266**, 509-523.

Reading, H.G. 1996. Sedimentary environment and facies, Blackwell Sci. Pub. pp. 615.

Richards, B.C. 1989. Uppermost Devonian and Lower Carboniferous stratigraphy, sedimentation, and diagenesis, southwestern District of Mackenzie and southeastern Yukon Territory. *Bulletin of the Geological Survey of Canada*, **390**, 135.

Séranne, M and Anka, Z. 2005. South Atlantic continental margins of Africa: a comparison of the tectonic vs climate interplay on the evolution of equatorial West Africa and SW Africa margins. *Journal of African Earth Sciences*, **43**, 283–300.

Schlumberger, 1989. Log Interpretation Principles/Applications. https://www.slb.com

Shanmugam, G. 1988. Origin, recognition and imprudence of erosional unconformities in sedimentary basins. In: K. Kleinspehn, C Paola (editors): New Perspectives in Basin Analysis, Springer Verlag, New York, 83-108.

Sheriff, R.E. 1977. Limitations on resolution of seismic reflections and geologic detail derivable from them. In: Payton (Ed.), Seismic Stratigraphy: Application to Hydrocarbon Exploration. *Memoir of the American Association of Petroleum Geologists*, **26**, 3–14.

Spasojevic, S and Gurnis, M. 2012. Sea level and vertical motion of continents from dynamic earth models since the Late Cretaceous. *American Association of Petroleum Geologists Bulletin*, **96**, 2037–2064.

Tucker, M.E. 2001. Sedimentary Petrology (third edition), Blackwell Science, Oxford, 166 p., ISBN: 0632057351.

Vaalco Energy (Gabon) inc. 2005. Forage du puits et-5h&developpement Etame phase ii. *Vaalco Energy internal reports*.

Van Balen, R.T., Bergen, G.v., Leeuw, C.d., Pagnier, H.J.M., Simmelink, H., VanWees, J.-D and Verweij, J.M. 2000. Modeling the hydrocarbon generation and migration in the West Netherlands Basin, the Netherlands. Netherlands, *Journal of Geosciences*, **79**, 29-44.

Vendeville, B. C., and Jackson, M. P. A. 1992. The rise and fall of diapirs during thin-skinned extension: The University of Texas at Austin, *Bureau of Economic Geology Report of Investigations*, **209**, 60.

Van Horn, J. 2001. Sendji Formation reservoir delineation based on 2-D and 3-D inversion, Yombo Field, offshore Congo. *The Leading Edge*, **20**, 435-441.

Veeken, P.C.H. 2007. Handbook of geophysical exploration – seismic stratigraphy, basin analysis and reservoir characterization. *Elsevier*, **37**, 523.

http://www.cambridge.org/resources/emods/Chapter%2019/19%20Salt%20tectonics.html [date accessed 13/03/13]

http://www.addaxpetroleum.com/operations/gabon [date accessed 22/04/13]

http://www.nexttraining.net/Sessions/Details/Petrel®___Structural_Modeling.aspx?sessionid=12731 [date accessed 26/04/13]

https://www.slb.com/~/media/Files/software/product_sheets/Petrel®_2012_geology_and_modeling.pdf [date accessed 29/04/13]

http://sepmstrata.org/page.aspx?&pageid=15&2 [date accessed 15/05/13]

http://www.slb.com/~/media/Files/resources/oilfield_review/ors12/aut12/3_basin_basin.pdf [date accessed 27/07/13]

http://www.aapg.org/slide_resources/schroeder/6/index.cfm [date accessed 31/03/14]